Systems & Control: Foundations & Applications

Luis T. Aguilar
Igor Boiko
Leonid Fridman
Rafael Iriarte

Self-Oscillations in Dynamic Systems

A New Methodology via Two-Relay Controllers

Birkhäuser

Birkhäuser

Systems & Control: Foundations & Applications

More information about this series at http://www.springer.com/series/4895

Luis T. Aguilar • Igor Boiko • Leonid Fridman
Rafael Iriarte

Self-Oscillations in Dynamic Systems

A New Methodology via Two-Relay Controllers

Birkhäuser

Luis T. Aguilar
CITEDI
Instituto Politecnico Nacional
Tijuana, BC, Mexico

Igor Boiko
Department of Electrical Engineering
The Petroleum Institute
Abu Dhabi, UAE

Leonid Fridman
Division de Ingenieria Electrica
Universidad Nacional
Autonoma de Mexico
Mexico City, DF, Mexico

Rafael Iriarte
Division de Ingenieria Electrica
Universidad Nacional
Autonoma de Mexico
Mexico City, DF, Mexico

ISSN 2324-9749 ISSN 2324-9757 (electronic)
Systems & Control: Foundations & Applications
ISBN 978-3-319-23302-4 ISBN 978-3-319-23303-1 (eBook)
DOI 10.1007/978-3-319-23303-1

Library of Congress Control Number: 2015953028

Mathematics Subject Classification (2010): 93B12, 93C10, 93C80, 34D20, 34C25

Springer Cham Heidelberg New York Dordrecht London

Printed on acid-free paper

Springer International Publishing AG Switzerland is part of Springer Science+Business Media (www.springer.com)

We dedicate this book with love and gratitude to
Luis's wife Erica, his son Gabriel, and his daughter Elisa,
Igor's wife Natasha,
Leonid's wife Millie,
Rafael's family: his son Rafa, his daughter Erika, and his wife Judith

Preface

This book began with a question asked by Professor Luis T. Aguilar to Professor Leonid Fridman in 2005: How can I generate oscillations of low frequency and particular amplitude using variable structure control?

Coincidentally, this question was asked in the right place and at the right time, because in 2005, Professors Igor Boiko and Leonid Fridman completed their research on the second-order sliding mode control algorithms in frequency domain [13, 14, 16–18], resulting in the possibility of calculating the amplitude and frequency of chattering in systems with second-order sliding mode controllers. They discovered that describing functions (DF) of the second-order sliding mode control algorithms could shift the point characterizing the oscillatory mode resulting from chattering to the second and third quadrants of the complex plane. With the discovery of this property, a straightforward logical conclusion could be made that the problem of generation of self-oscillations (SO) with desired amplitude and frequency could be defined as an inverse problem with respect to the one previously studied. Motivated by this question, Professor Rafael Iriarte found his subject of research in this area too.

Usually, the DF of a single-valued nonlinearity is located on the negative part of the real axis of the complex plane. So for the design of SO in such a situation, only dynamic compensators can be employed, but the possibility of compensators to shape the Nyquist plot of the plant is very limited.

Therefore, the idea that *the controller itself could be designed in such a way that its DF (negative reciprocal of the DF) might be placed in any desired point of the complex plane* was conceived. This idea serves as the basis for the main subject of this book.

In this book, the two-relay controller (TRC) is proposed, which is intended for the generation of SO in dynamic systems. A remarkable feature of this controller is the possibility, with a simple change of controller gains, for one to produce the DF in every phase angle between 0 and 360°, which corresponds to the crossing of the Nyquist plot of the plant and the negative reciprocal of the DF of the controller in any desired point. This point would define the SO produced in the system containing the plant and the controller. The design procedures for TRC are proposed using three different methodologies based on the following: DF, Poincaré maps, and locus of a perturbed relay system (LPRS) method. Three strategies of robustification of generated SO are also proposed. The theoretical results are illustrated by experiments on SO generation in four underactuated systems: wheel pendulum, Furuta pendulum, three-link robot, and three-degrees-of-freedom (3-DOF) helicopter. The experiments are recorded with available video recordings presented in the following web links:

– https://www.youtube.com/watch?v=t_1DcUdwFGE
– https://www.youtube.com/watch?v=MwXVQXlbJMQ

Acknowledgments

We wish to thank our friends and colleagues Professors Leonid Freidovich, Luis Martínez-Salamero, and Iván Castellanos and Drs. Alejandra Ferreira and Antonio Estrada.

The work was partially supported by CONACYT under grant 132125, SIP-IPN Grants, PAPIIT under Grant IN113613 and IN112915, DGAPA PASPA Program, and RIFP Project No. 12310 of the Petroleum Institute.

Tijuana, Mexico — Luis T. Aguilar
Abu Dhabi, UAE — Igor Boiko
Mexico City, Mexico — Leonid Fridman
June 2015 — Rafael Iriarte

Notations and Acronyms

TRC	Two-relay control
SO	Self-oscillation
DF	Describing function
SOSM	Second-order sliding modes
HOSM	High-order sliding modes
LPRS	Locus of a perturbed relay system
DOF	Degree(s) of freedom
AOS	Asymptotic orbital stability

$\mathbb{R}$	The set of real numbers
$\mathbb{R}^n$	The set of all n-dimensional vector with real numbers
$\mathbb{R}^{m\times n}$	The set of all $m \times n$ matrices with real elements
$\mathbb{C}$	The set of complex numbers
j	Imaginary unit
$d(p, S)$	Distance between the point p and the set S ($\inf_{x\in S} \lvert p - x\rvert$)
$q \in \mathbb{R}^n$	Joint position vector
$\dot{q} \in \mathbb{R}^n$	The time derivative of the joint position vector
c_1, c_2	Two-relay controller gains
$\boldsymbol{A}_1$	Amplitude of the oscillation
ω	Frequency of the oscillation
$\boldsymbol{\Omega}$	Particular or desired value of frequency of the oscillation
t	Time
$N(A, \omega)$	Describing function depending on the amplitude and frequency of the oscillation
s	Frequency domain complex variable $s = j\omega$
$W(s)$	Transfer function
ξ	Ratio of the two-relay controller gains
T	Period of a signal
η	Actuated states vector
ν	Unactuated states vector
$\eta_1^\star,\ \nu^\star$	Fixed point of Poincaré map

t_2, $\bar{t}_2$	Hypothetical boundary crossing times in Poincaré map construction
σ_0	Constant term in the error signal
σ_p	Sum of periodic terms of Fourier series of the error signal
u_0	Constant term in the control signal
u_p	Sum of periodic terms of Fourier series of the control signal
y_0	Constant term in the output signal
y_p	Sum of periodic terms of Fourier series of the output signal
θ	Asymmetric duty in two-relay controller
$L(\omega, \theta)$	Operative function for LPRS computation
$J(\omega)$	LPRS complex function
$A_L(\omega)$	Modulus of the transfer function $\|W(j\omega)\|$
A_u	Amplitude of the control signal (first harmonic)
γ	Constant value that provides a fraction of the period T of a signal $t = \gamma T$, $\gamma \in [-0.5; 0.5]$
a_u	Amplitude of the control signal

Contents

1 Introduction 1
- 1.1 State of the Art 1
  - 1.1.1 Overview 1
  - 1.1.2 Tools for Generation of Self-Oscillations Used in this Book 2
  - 1.1.3 Generation Methods Self-Oscillations 3
- 1.2 Generation of Self-Excited Oscillations: A Describing Function Approach 5
  - 1.2.1 Analysis of Van der Pol Equation 6
  - 1.2.2 The Problem of Self-Oscillations in Systems Containing Double Integrator 9
  - 1.2.3 Why Not Tracking? 11
- 1.3 Organization of the Book 14
  - 1.3.1 Contents of the Book 14
  - 1.3.2 How to Read the Book? 15

Part I Design of Self-Oscillations Using Two-Relay Controller

2 Describing Function-Based Design of TRC for Generation of Self-Oscillation 19
- 2.1 Introduction 19
- 2.2 The Two-Relay Controller 19
- 2.3 Describing Function of the Two-Relay Control 20
- 2.4 Describing Function as Design Method 22
- 2.5 Orbital Asymptotic Stability 24
- 2.6 The Inertia Wheel Pendulum: An Example 30
  - 2.6.1 Linearization of IWP dynamics 31
  - 2.6.2 Gains Adjustment 32
  - 2.6.3 Bounded Input Problem 34
  - 2.6.4 Simulation Results 36
- 2.7 Concluding Remarks 37

3 Poincaré Map-Based Design 39
3.1 Introduction 39
3.2 Poincaré Map-Based Design of the Gains of the TRC for Linearized Model 40
3.3 General Poincaré Map Approach Generated by TRC 43
3.4 The Inertia Wheel Pendulum—TRC Gains Tuning for Generating SO 46
3.5 Comments 52

4 Self-Oscillation via Locus of a Perturbed Relay System Design (LPRS) 53
4.1 Introduction 53
4.2 LPRS-Based Analysis of a System with TRC 54
4.3 Computation of LPRS for the Two-Relay Controller Based on Infinite Series 57
4.4 LPRS as Design Method 60
4.5 The Inertia Wheel Pendulum: Gain Tuning Based on LPRS Design 61
4.6 Linearized Poincaré Map-Based Analysis of Orbital Stability 62
4.7 Comments 64

Part II Robustification of Self-Oscillations Generated by Two-Relay Controller

5 Robustification of the Self-Oscillation via Sliding Modes Tracking Controllers 67
5.1 Introduction 67
5.2 Idea for Robustification 68
5.3 Inertia Wheel Pendulum Under Disturbances and Friction 69
5.4 Generation of Nominal Trajectories 69
5.5 Tracking of the SO Generated by the TRC 71
5.5.1 Twisting Tracking Control 71
5.5.2 HOSM Tracking Controller 76
5.6 Experimental Study 77
5.6.1 Experimental Setup 77
5.6.2 Experimental Results 78
5.7 Comments and Remarks 79

6 Output-Based Robust Generation of Self-Oscillations via High-Order Sliding Modes Observer 81
6.1 Introduction 81
6.2 HOSM Observation and Uncertainties Compensation 82
6.2.1 Generation of SO in a Nominal System 84
6.2.2 Uncertainties Compensation 85
6.3 Application to the Inertia Wheel Pendulum 85

6.4 Simulation Results 87
6.5 Comments 88

Part III Applications

7 Generating Self-Oscillations in Furuta Pendulum 91
7.1 Introduction 91
7.2 Description of the Plant and Problem Formulation 92
7.3 Linearization 94
7.4 Experimental Study 95
7.4.1 Experimental Setup 95
7.4.2 Experimental Results 95
7.5 Conclusion and Remarks 97

8 Three Link Serial Structure Underactuated Robot 99
8.1 Introduction 99
8.2 Description of the 3-DOF Underactuated Robot and Problem Statement 99
8.3 The TRC Gains Computation 102
8.4 Simulation Results 103
8.5 Comments and Remarks 105

9 Generation of Self-Oscillations in Systems with Double Integrator 109
9.1 Introduction 109
9.2 Dynamic Model of 3-DOF Helicopter and Problem Statement 110
9.3 Main Result 112
9.3.1 Periodic Motion of the Elevation Angle 112
9.3.2 Periodic Motion of Rotation and Direction Angles 114
9.4 Simulation Results 116
9.5 Conclusions 116

10 Fixed-Phase Loop (FPL) 121
10.1 Introduction 121
10.2 Design of TRC for FPL 122
10.2.1 Synthesis of TRC under Input Saturation 123
10.2.2 Upper Bound Estimates 124
10.2.3 Experimental Results 126
10.3 Analogue Realization of Fixed-Phase Loop (FPL) 127
10.3.1 Simulations and Experiments 132
10.4 Conclusions 135

A Describing Function 137
A.1 Describing Function of a Single-Relay 139

B The locus of a perturbed relay system (LPRS) 141
B.1 Asymmetric oscillations in relay feedback systems 141

B.2 Computation of the LPRS 142
B.2.1 Computeation of LPRS from matrix state space description 142
B.2.2 Computation of the LPRS from transfer function 144
B.2.3 Some properties of the LPRS 144

C Poincaré map 147
C.1 Basic concepts in Poincaré maps 147

D Output Feedback 149
D.1 State observer design 149

References 153

Index 157

Chapter 1
Introduction

Oscillations play an important role in many areas of life and science. Many technical and biological systems involve modes that can be considered as self-excited oscillations. Various types of periodic motions can usually be considered as oscillations. Examples range from the planetary motion to internal combustion engine work and oscillations used in radio technology. Walking gait being a kind of functional motion under some simplifying conditions can also be considered as a specific oscillation. The given examples show that some of these periodic motions occur naturally, and some—in engineering systems—require specific methods of generation.

1.1 State of the Art

1.1.1 Overview

Researchers have been investigating and applying limit cycle behavior to many different engineering fields since a long time ago. We can find several research works on this subject (see, e.g., [74]), but in the present book, we will focus on limit cycles induced by relay feedback systems only. In this monograph, we consider generation of one of the simplest types of a functional motion: a periodic motion. The systems that we consider in the book are underactuated and non-minimum-phase systems that are a challenging object for the stated task. Current representative works on periodic motions and orbital stabilization of underactuated systems involve finding and using a reference model as a generator of limit cycles (see, e.g., [10, 68]), in which the problem of obtaining a periodic motion is considered as a servo problem. Orbital stabilization of underactuated systems finds applications in the coordinated motion of biped robots [23, 45, 70], gymnastic robots, electrical

L.T. Aguilar et al., *Self-Oscillations in Dynamic Systems*, Systems & Control: Foundations & Applications, DOI 10.1007/978-3-319-23303-1_1

converters [2, 66], and others (see, e.g., [41, 81] and references therein). On the other hand, we can find a lot of systems where self-oscillations can be produced within the system itself, such as biological systems [21, 27], chemical processes [43, 91], solid-state electronics [72, 75], nuclear systems [50, 56], among others [6, 60].

In power electronics applications, the idea of self-oscillating switching is used in dc–dc inverters [22, 59, 66]. This allows one to ensure nearly zero sensitivity to load changes and high performance. Such inverters are attractive to operate in dc–ac converters since two buck–boost dc–dc inverters are commonly used. Several topologies were proposed for these converters, for example, a buck–boost dc–ac inverter using a double-loop control for a buck–boost dc–dc converter was designed in [76]. In [94] a self-sustained oscillating controller for power factor correction circuits was presented.

In particular, one of the most interesting applications of self-oscillation is to develop motion planning algorithms which allow an underactuated robot to execute reliable maneuvers under small-amplitude and high-frequency control which is a challenge in mechanical systems. The formulation is different from typical formulation of the output tracking control problem for fully actuated mechanical systems [89] where the reference trajectories can be arbitrarily given. This difficulty comes from the complexity of underactuated systems that are neither feedback nor input-state linearizable. In this problem, special attention to the selection of the desired trajectory is required too. Different approaches to orbital stabilization are available in the literature that are discussed below.

1.1.2 Tools for Generation of Self-Oscillations Used in this Book

In this book, we will use traditional methods of analysis of periodic solutions of relay systems and chattering in sliding mode control systems [13, 14, 16, 36–38, 88].

They could be divided in two groups: the *frequency-domain approach* and the *state-space approach*.

The main method we will use in this book is a describing function method (see, e.g., [8, 31, 42, 87, 90]). From the DF method, we discovered the idea of the TRC (Section 2.4). The DF method is used to find the approximate value of TRC parameters of desired SO. Loeb criteria based on DF is used for stability analysis of generated oscillations.

Traditionally Poincaré maps (point mappings) (see [36–38, 49, 64, 90] and references therein) are used as the sufficient and/or necessary conditions for existence and stability of periodic motions. In Chapter 3 of this book, Poincaré maps are firstly used for generation of SO with desired period and amplitude. Poincaré maps gives the formulas for exact values of parameters for TRC together with sufficient and necessary conditions for existence and sufficient conditions for stability of generated SO.

In Chapter 4 locus of a perturbed relay system (LPRS)[13, 14, 16] is used to find theoretically exact values of TRC parameters and investigate stability of generated periodic solutions LPRS.

1.1.3 Generation Methods Self-Oscillations

There are several methods for generation of SO. For example, in [80] a constructive tool for generation and orbital stabilization of periodic motion in underactuated nonlinear system through virtual constraint approach was introduced. In [41] asymptotic tracking for an unactuated link by finding conditions for the existence of a set of outputs that yield a system with a one-dimensional exponentially stable zero dynamics was demonstrated. In [69] and [78], an asymptotic harmonic generator was introduced through a modified Van der Pol equation tested on a friction pendulum to solve the swing-up problem for an inverted pendulum. In [10], a set of exact trajectories of the nonlinear equations of motion, which involve inverted periodic motions, was derived. There are several applications of the abovementioned procedures in the literature (see, e.g., [10, 20, 82, 83] and references therein). In [1], a method for SO based on a two-relay controller interconnected to a linear system applied to an underactuated system was proposed.

The research given in [13, 14, 16–18], where analysis of the second-order sliding mode algorithms in frequency domain was made, provides means for computations of the amplitude and frequency of chattering in systems governed by the second-order sliding mode controllers. It was discovered in the above-noted research that the negative reciprocal DF of the second-order sliding mode algorithms can be placed in the second and third quadrants of the complex plane—depending on the controller parameters. Usually, negative reciprocal of the DF of a single-valued nonlinearity is located on the negative part of the real axis of complex plane. So for the design of the SO in such situation, only dynamic compensators can be used. But the possibility of shaping the Nyquist plot of the plant through the use of compensators is very limited. The possibility of placement of the negative reciprocal DF using the control algorithm parameters to have it cross the Nyquist plot of the plant in any desired point is an idea that lies in the foundation of the presented SO design.

The present monograph provides a study of such situations, where conventional methods of exciting oscillations are unsuitable, and proposed a new method named the *two-relay controller* (TRC) . The main purpose of the book is to demonstrate the capabilities of the two-relay controller to induce SO in dynamic systems with wide range of desired amplitudes and frequencies. With respect to the problem of analysis of oscillations, the problem of generation of self-oscillations (SO) with desired amplitude and frequency is an inverse problem. Still, solution is nontrivial, and knowledge of analysis does not answer the question of how to design a controller producing SO with desired amplitude and frequency.

The specific feature of the TRC is that one can rotate its negative reciprocal DF within 360 degrees range through a simple change of controller gains, which allows for obtaining the intersection point with the Nyquist plot of the plant in any desired location. Therefore, the central contribution of the book is related to the design procedures of self-oscillation with desired frequency and amplitude using TRC. This design is done through three different methodologies DF, Poincaré maps, and locus of a perturbed relay system (LPRS) method. It should be pointed out that standard methods for design of SO usually rely on the plant being a double integrator.

In this book, underactuated systems are considered as systems with internal (unactuated) dynamics with respect to the actuated variables. It allows us to propose a method of generating a self-oscillation in underactuated systems where the same behavior can be seen via second-order sliding mode (SOSM) algorithms, that is, generating self-excited oscillations using the same mechanism as the one that produces chattering. However, the generalization of the SOSM algorithms and the treatment of the unactuated part of the plant as additional dynamics result in the oscillations that may not necessarily be fast and of small amplitude.

The main results of the book are summarized as follows:

- A two-relay controller is used to generate self-excited oscillations in linear closed-loop systems. The required frequencies and amplitudes of periodic motions are produced without tracking of precomputed trajectories. It allows for generating a wider (than the original twisting algorithm with additional dynamics) range of frequencies and encompassing a variety of plant dynamics.
- An approximate approach based on the describing function is proposed to find the values of the controller parameters allowing one to obtain the desired frequencies and the output amplitudes.
- A design methodology based on LPRS that gives exact values of controller parameters for the linear plants is developed.
- An algorithm that uses Poincaré maps and provides the values of the controller parameters ensuring the existence of the locally orbitally stable periodic motions is proposed.
- Necessary conditions for orbital asymptotic stability of desired self-oscillations are given.
- The theoretical results are validated numerically and experimentally via the tests on the laboratory underactuated pendulums such as inertia wheel pendulum and Furuta pendulum. The computed gains of the TRC allow for the existence of a periodic motion of the required frequency and amplitude around the pendulum upright position (which gives the non-minimum-phase system case) in wide ranges of frequencies and amplitudes.

1.2 Generation of Self-Excited Oscillations: A Describing Function Approach

Self-excited oscillations can occur only in nonlinear systems. A system $\dot{x} = f(x)$ oscillates when it has a nontrivial periodic solution $x(t + T) = x(t)$ for some $T > 0$. A periodic motion that may arguably occur in a marginally stable linear system cannot be stable: due to the scalability of solutions in linear systems, there is no unique periodic solution in a marginally stable system; every disturbance would drive the process to a different periodic motion. Despite the theoretical existence of periodic solutions, marginally stable linear systems cannot have limit cycles—isolated closed-loop trajectories with certain domains of attraction.

Normally, for the possibility of producing oscillations by a system, the following conditions must be satisfied:

- The system must have a dynamic part that can be linear or nonlinear
- The system must have a nonlinear part (nonlinearity), which may be static (single-valued or hysteretic) or dynamic nonlinearity
- The system must have a feedback between the dynamic part and the nonlinearity ensuring their connections in a loop (Fig. 1.1)

If the dynamic part does not contain nonlinearities and, therefore, can be described by a transfer function, then oscillations in the system can be found from the harmonic balance equation:

$$W(j\Omega_0)N(a_0, \Omega_0) = -1, \tag{1.1}$$

where $W(s)$ is the transfer function of the dynamic part, N is the DF of the nonlinear part, Ω_0 is the frequency, and a_0 is the amplitude of the oscillations.

However, not all self-oscillating systems are usually given by the diagram of Fig. 1.1. There are some that are formally designed using different principles. One of them is presented in the following section.

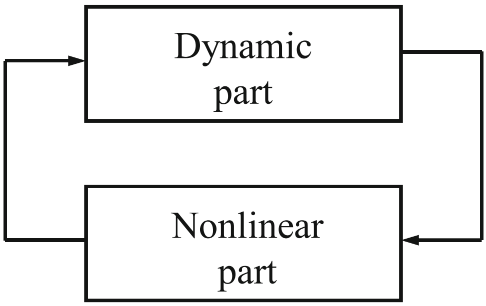

Fig. 1.1 Feedback loop with dynamic and nonlinear part

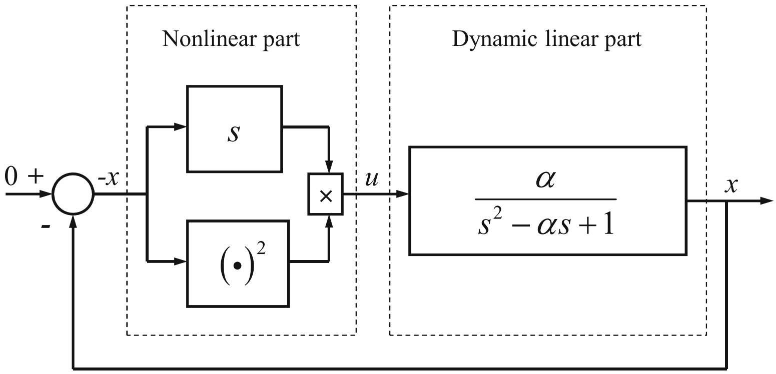

Fig. 1.2 Transformed Van der Pol system

1.2.1 Analysis of Van der Pol Equation

The Van der Pol oscillator is an example of such a system whose equation is given by

$$\ddot{x} + \alpha(x^2 - 1)\dot{x} + x = 0. \tag{1.2}$$

However, the following transformation (adopted from [44]) allows us to present the dynamic system (1.2) in the format given by Fig. 1.1. The transformed system is presented in Fig. 1.2. We further assume that a symmetric oscillation exists in system (1.2), and signal $x(t)$ is close to a sinusoid:

$$x(t) = a_0 \sin(\Omega_0 t). \tag{1.3}$$

The time derivative of the output signal is

$$\dot{x}(t) = a_0 \Omega_0 \cos(\Omega_0 t).$$

Therefore, the output of the nonlinear part is

$$\begin{aligned} u = -x^2\dot{x} &= -a_0^2 \sin^2(\Omega_0 t) a_0 \Omega_0 \cos(\Omega_0 t) \\ &= -\frac{a_0^3 \Omega_0}{2}(1 - \cos(2\Omega_0 t))\cos(\Omega_0 t) \\ &= -\frac{a_0^3 \Omega_0}{4}(\cos(\Omega_0 t) - \cos(3\Omega_0 t)). \end{aligned} \tag{1.4}$$

One can see from (1.4) that $u(t)$ contains the third harmonic. Let us analyze now the frequency response properties of the linear dynamic part. The magnitude frequency response (magnitude Bode plot) of the dynamic part is the same as that of the better known transfer function $\alpha/(s^2 + \alpha s + 1)$ because the two poles are complex conjugate:

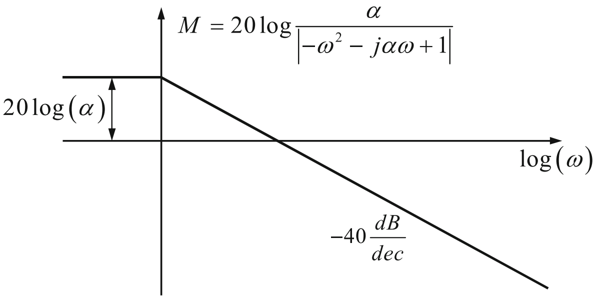

Fig. 1.3 Magnitude Bode plot of the Van der Pol system

$$\begin{aligned} M(\omega) &= 20\log\frac{\alpha}{|(j\omega)^2 - j\omega\alpha + 1|} \\ &= 20\log\frac{\alpha}{\sqrt{(1-\omega^2)^2 + \omega^2\alpha^2}}. \end{aligned} \tag{1.5}$$

The magnitude Bode plot of the linear part is given in Fig. 1.3. One can see that the linear part has low-pass filtering properties. Thus, we might expect that the third harmonic term in (1.4), when propagated through the linear part, would be attenuated, so that the output signal $x(t)$ would be close to a sinusoid. Therefore, our initial assumption about the sinusoidal shape of signal $x(t)$ makes sense, and we can disregard the third harmonic in analysis of signals propagation for the considered system.

We can define the DF of the relay nonlinearity as the complex gain that describes the propagation of the first harmonic in $x(t)$ through the nonlinearity. Disregarding the third harmonic in $u(t)$, we can write for the control signal

$$u(t) \approx -\frac{a_0^3 \Omega_0}{4}\cos(\Omega_0 t).$$

Considering the fact that $x(t) = a_0 \sin(\Omega_0 t)$ and $\dot{x}(t) = a_0 \Omega_0 \cos(\Omega_0 t)$, we rewrite $u(t)$ as follows:

$$u(t) \approx -\frac{a_0^2}{4}\dot{x}(t).$$

Recalling that $s = j\omega$ in the Laplace domain represents differentiation, we write for the DF:

$$N(a,\omega) = j\frac{a^2}{4}\omega, \tag{1.6}$$

where a and ω are arbitrary amplitude and frequency (arguments of the DF).

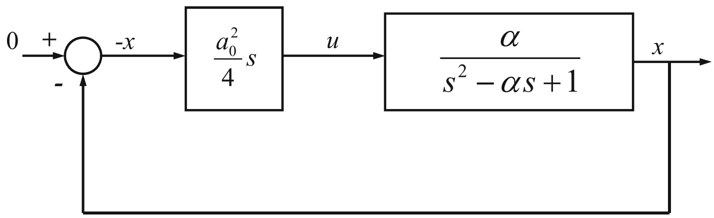

Fig. 1.4 Equivalent Van der Pol system

Amplitude and frequency in Van der Pol equation can be found from the harmonic balance condition (1.1):

$$j\frac{a_0^2}{4}\Omega_0\frac{\alpha}{-\Omega_0^2-j\alpha\Omega_0+1}=-1. \tag{1.7}$$

Block diagram of the equivalent dynamics of the system under the assumption of the sinusoidal shape of $x(t)$ due to the low-pass filtering properties of the linear part is presented in Fig. 1.4. Solution of (1.7) provides the following results: $a_0 = 2$, $\Omega_0 = 1$.

One can see from the analysis given above that the original Van der Pol equations can be transformed into the format that satisfies the three conditions mentioned above. The transformed model includes a nonlinearity represented by the DF (1.6), a linear part, and their connections in a loop.

Through the analysis of the self-excited oscillations in Van der Pol equation, the harmonic balance (see (1.1)) application was illustrated. It allows for another form of the equation (1.1) that is convenient in many practical computations and which we are going to use below:

$$-\frac{1}{N(a_0,\Omega_0)}=W(j\Omega_0). \tag{1.8}$$

The function that appears in the left-hand side of this equation is the negative reciprocal of the DF. The solution of equation (1.8) has a simple graphical interpretation, especially if the DF depends only on the amplitude ($N = N(a)$). If the frequency response of the dynamic (linear) part is depicted as a Nyquist plot in the complex plane and the negative reciprocal is depicted as a function of amplitude a, then the point of intersection of the two curves yields the periodic solution (approximately—because only the first harmonic is accounted for). Many practically important nonlinearities encountered in oscillatory systems are single-valued or hysteretic nonlinearities.

Formula (1.8) can also be a foundation of a method of exciting periodic motions in mechanical and other physical systems, when the plant is available, and oscillations can be excited by including nonlinearities in the controller. For the single-valued nonlinearities, negative reciprocal DF coincides with the real axis of the complex plane. For hysteretic nonlinearities, negative reciprocal DF is usually located in the third quadrant (for positive hysteresis) or second quadrant (for negative hysteresis) of the complex plane.

1.2.2 The Problem of Self-Oscillations in Systems Containing Double Integrator

There are some "difficult" systems, in which the use of feedback having a single-valued nonlinearity (e.g., relay) may not produce a desirable result. Let us illustrate it by the following example.

Consider the double integrator closed by the relay feedback:

$$\ddot{x} = -\operatorname{sign}(x). \tag{1.9}$$

Assume that a periodic motion may exist in system (1.9) and find parameters (amplitude and frequency) of this periodic motion. Assume that a periodic solution of frequency ω (period $T = 2\pi/\omega$) exists. In this case the second derivative if the output is given as a square wave:

$$\ddot{x} = \begin{cases} 1 & \text{if} \quad 0 < t \le T/2 \\ -1 & \text{if} \quad T/2 < t \le T. \end{cases} \tag{1.10}$$

In formula (1.10), we associate initial time with the switch of the relay control from -1 to $+1$. The symmetric solution for $\dot{x}$ is found via integration of (1.10) on each interval, with proper constant term selection:

$$\dot{x} = \begin{cases} t - T/4 & \text{if} \quad 0 < t \le T/2 \\ 3T/4 - t & \text{if} \quad T/2 < t \le T, \end{cases} \tag{1.11}$$

and in the same way, we find the symmetric periodic solution for $x(t)$—via taking an integral of (1.11):

$$x = \begin{cases} t^2/2 - Tt/4 & \text{if} \quad 0 < t \le T/2 \\ 3Tt/4 - t^2/2 - T^2/4 & \text{if} \quad T/2 < t \le T. \end{cases} \tag{1.12}$$

We can now check the switching conditions for the relay from formula (1.12). One can see that $x(0) = x(T) = 0$ and $x(T/2) = 0$. Therefore, the switching of the relay (right-hand side of (1.10)) is ensured at time $t = 0$ and $t = T/2$. Thus, a periodic motion of period T, indeed, exists in this system. However, we also see that this periodic motion may exist for any value of period T, because for every given

T equations (1.11), (1.12) remain valid. In fact, the frequency that will be actually produced in the system would depend on the initial conditions $x(0)$, $\dot{x}(0)$ (note: time $t = 0$ is not the same time as in formulas (1.11), (1.12)).

We can see that relay control cannot produce a stable periodic motion in the double integrator system. Instead, we have infinite number of periodic solutions, each of those depend on initial conditions.

Consider another example—also containing a double integrator. The following model represents the vertical channel of a helicopter dynamics (height control in the autonomous application):

$$\begin{aligned} \ddot{x} &= \frac{1}{m}(v - F_g) \\ \dot{v} &= \frac{1}{T_a}(K_a u - v) \end{aligned} \tag{1.13}$$

where $x(t)$ is the height, m is the helicopter mass, $v(t) = F_t$ is the thrust, $F_g = mg$ is the gravity force, K_a and T_a are gain and time constant of motor-propeller dynamics, respectively, and $u(t)$ is the controller command. We attribute the dynamics given by the transfer function $K_a/(T_a s + 1)$ to motor-propeller dynamics, and the whole dynamic model of the helicopter height channel can be presented as the block diagram in Fig. 1.5. Nyquist plot of the helicopter dynamics is schematically presented in Fig. 1.6. One can see that the plot begins in the second quadrant for zero

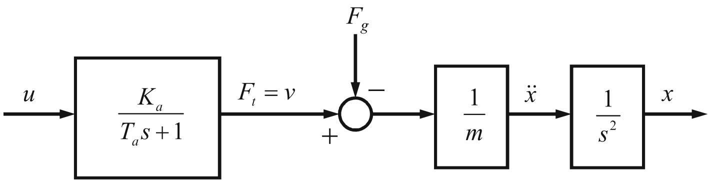

Fig. 1.5 Block diagram of helicopter dynamics

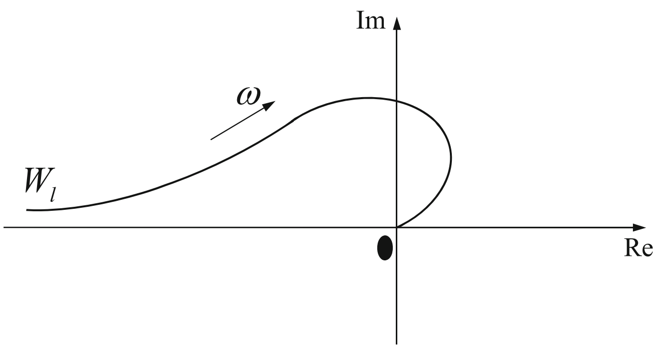

Fig. 1.6 Nyquist plot of helicopter dynamics

frequency and then with frequency increase continues to the first quadrant and ends in the origin with infinite frequency. The plot does not have points of intersection with the real axis. Thus, generation of self-excited oscillations by means of inclusion of a single-valued nonlinearity in the feedback is impossible. The question that may arise is: how one could excite self-oscillations in this system. These oscillations may be used for controller auto-tuning or as a part of a maneuvering motion (we review below application of the tracking principle for this purpose). One possible way of doing this would be through the use of a relay with negative hysteresis. However, with application of this approach, there may be issues in finding a proper hysteresis value that would ensure the existence of self-excited periodic motions. And also, there may be issues with stability of these periodic motions.

The present monograph provides a study of such situations, where conventional methods of exciting oscillations are unsuitable, and proposes a new method named the *two-relay controller*.

1.2.3 Why Not Tracking?

Another quite obvious method of producing periodic motions in a physical system would be through tracking. For this purpose, a closed-loop system must be organized, which should include a feedback controller, so that the system might track external signals. With this arrangement, the system may track not only periodic but any external signal that is applied to its input. This looks like an advantage over the method of exciting self-oscillations. Let us, however, analyze and compare these two methods in some detail.

We shall consider that the dynamic part is linear and attributed to the plant, and the nonlinear part is attributed to the controller. Therefore, in the considered option, the nonlinear part is simply not present, because the selected method of generating oscillations is through the use of tracking, that is, the use of a linear controller. The presence of some nonlinearities in the dynamic part is possible and may only insignificantly change the situation if these nonlinearities are relatively small.

We consider the following example of generating oscillation through the use of the relay feedback having an ideal (non-hysteretic) relay as the first option and a tracking system having the same dynamic linear part as the second option. Assume that the system has the dynamic linear part given by the transfer function $W_l(s)$. Nyquist plot of this transfer function is presented in Fig. 1.7. Consider the design of the simplest type of a feedback controller—the proportional one. The controller is characterized by only one parameter—proportional gain K_c. Due to the requirement of the closed-loop stability, we must design controller with gain K_c that satisfies the following inequality:

$$K_c|W_l(j\omega_\pi)| < 1, \tag{1.14}$$

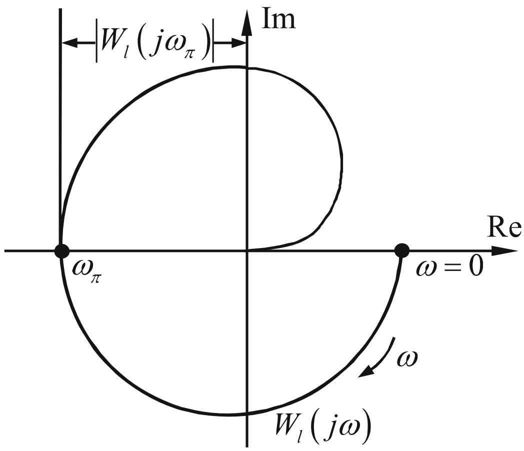

Fig. 1.7 Nyquist plot

where ω_π is the phase crossover frequency of the linear part, that is, the frequency corresponding to 180 deg of the phase lag of the linear part.

In fact, for providing proper performance, not only the above constraint must hold, but a certain gain margin must be ensured. Normally, the gain margins used in practice are always larger than two. Therefore, if we assume this minimum value, we can rewrite formula (1.14) as follows:

$$K_c|W_l(j\omega_\pi)| = 0.5. \tag{1.15}$$

Therefore, the proportional gain K_c can be chosen simply as

$$K_c = 0.5/|W_l(j\omega_\pi)|.$$

As a result of the use of the formula for finding the closed-loop transfer function

$$W_{cl}(j\omega) = \frac{K_c W_l(j\omega)}{1 + K_c W_l(j\omega)}, \tag{1.16}$$

which can be rewritten considering (1.15) as

$$W_{cl}(j\omega) = \frac{0.5W_l(j\omega)/|W_l(j\omega_\pi)|}{1 + 0.5W_l(j\omega)/|W_l(j\omega_\pi)|}, \tag{1.17}$$

such characteristics of tracking quality as the phase lag and the closed-loop system gain at the frequency of the input signal can be considered:

$$\phi_{cl}(\omega) = \arg W_{cl}(j\omega)$$

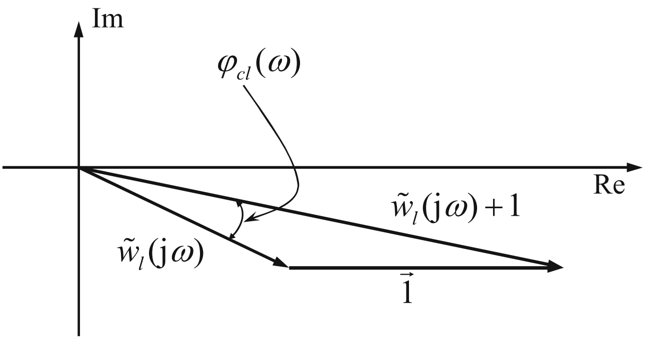

Fig. 1.8 Closed-loop characteristics at low frequencies

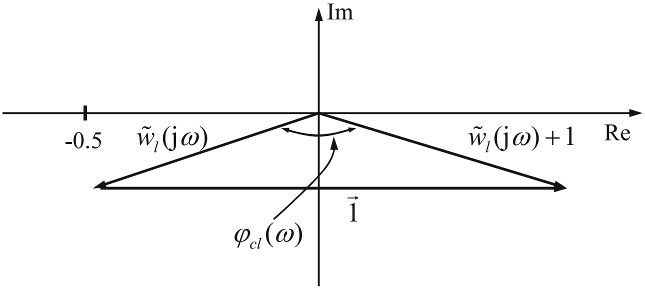

Fig. 1.9 Closed-loop characteristics at high frequencies

and

$$M_{cl}(\omega) = |W_{cl}(j\omega)|.$$

Good tracking quality would be characterized by the following values of ϕ_{cl} and $M_{cl}(\omega)$: $\phi_{cl} \approx 0$ ($\phi_{cl} < 0$), that is having small phase lag, and $M_{cl}(\omega) \approx 1$, i.e., having nearly unity closed-loop gain. We can illustrate by vector diagrams the mechanism of producing the closed-loop characteristics at different frequencies (Figs. 1.8 and 1.9). We should note that at low frequencies ω of the input signal, the ratio $|W_l(j\omega)|/|W_l(j\omega_\pi)|$ is greater than one and of the order of a few units (for non-integrating dynamic linear part), whereas at frequencies close to the phase crossover frequency (high frequencies), this ratio is close to one. Figure 1.8 illustrates the mechanism of producing the closed-loop system phase lag at low frequencies and Fig. 1.9 at high frequencies. The closed-loop gain can also be estimated using Figs. 1.8 and 1.9 as a ratio of the lengths of vectors $\tilde{W}_l(j\omega) = 0.5W_l(j\omega)/|W_l(j\omega_\pi)|$ and $1 + 0.5W_l(j\omega)/|W_l(j\omega_\pi)| = 1 + \tilde{W}_l(j\omega)$. One can see that the angle $|\phi_{cl}|$ in Fig. 1.8 can be small, but this angle in Fig. 1.9 can never be small. Therefore, while fairly good tracking property is possible for low-frequency input signals, it is absolutely impossible for high-frequency signals (frequency close to the phase crossover frequency).

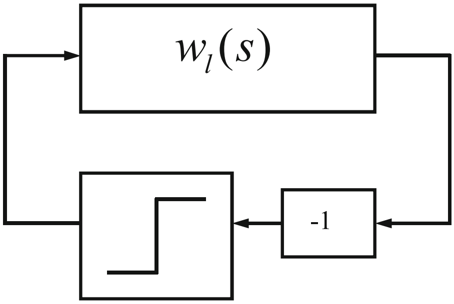

Fig. 1.10 Single-valued relay dynamics

On the other hand, we can consider generation of self-excited oscillations through the use of a nonlinear (relay in the considered example) feedback (Fig. 1.10). Again, we shall consider the same dynamic linear part having the transfer function $W_l(s)$. According to the harmonic balance equation (1.1), oscillations are generated at the frequency, where the phase lag of the linear part is equal to 180 deg, because the DF of the ideal relay is $N(a) = 4h/(\pi a)$, where h is the relay amplitude, that is at the phase crossover frequency! Whatever is practically impossible with the use of the tracking principle can be easily achieved with the self-oscillation. Frequencies other than ω_π can also be generated through self-oscillations if proper values of hysteresis are selected in the relay. This monograph, in particular, considers methods of producing self-oscillations of various frequencies. The tracking principle has its own advantages, of course, with the main one being the possibility of tracking different shapes, whereas with the self-oscillation, the shape is hardly controllable. But in the aspect of achieving high frequencies of produced oscillations, the principle of self-excited oscillation is advantageous.

Some systems, in particular those containing double integrators, require oscillations in a wide bandwidth corresponding to the third quadrant of the Nyquist plane. So it becomes difficult or practically impossible with tracking to reach the set of desired frequencies. This book describes how one can generate self-oscillations in a wide range of frequencies using TRC.

1.3 Organization of the Book

1.3.1 Contents of the Book

The book consists of an introduction and three parts, and it is organized as follows.

- *Part I*. In this part, we focused in the design of SO using the two-relay controller. In Chapter 2, we use the describing function method to obtain a set of equations for the values of controller parameters, which provide the required amplitude and frequency of SO. Additionally, stability of the periodic solution is analyzed through the Loeb-like criterion. In Chapter 3, the Poincaré method, which is a recognized tool for analysis of the existence of limit cycles, is used as a design of the TRC that would ensure specified SO. A set of algebraic equations is presented, and a theorem on stability of a limit cycle is formulated as well. The last method for the design, the locus of a perturbed relay system (LPRS), that is normally used for conventional relay systems, is extended to the TRC in Chapter 4 and is used to compute the exact values of the controller parameters. An example for the inertia wheel pendulum is presented through Part I in Chapters 2–4.

- *Part II*. This part is focused on robustification of generation of periodic motions. Two approaches are presented: (a) by using the sliding mode control and (b) through disturbance identification. They are given in Chapters 5 and 6, respectively. Chapter 5 presents an alternative strategy in the problem of generating SO with disturbances rejected. Such strategy includes generation of SO using the TRC and the model of the plant as external generator of trajectories injected to a robust closed-loop system using a variable structure controller. In particular, second-order and high-order sliding mode controls are used in Chapter 5. In Chapter 6, the problem of robust output-based generation of self-oscillations in nonlinear uncertain underactuated systems is addressed. Disturbance identification vector is used as a part of the control input to exactly reject matched disturbances.
- *Part III*. This part is concerned with applications to underactuated systems. The results of the first six chapters are summarized in illustrative applications from Chapters 7 through 9. The Furuta pendulum is under study in Chapter 7. In Chapter 8, we illustrate the methodology using a 3-DOF underactuated robot with two control inputs. In Chapter 9, we illustrate the capability of the TRC to generate SO in a system containing a double integrator. We use an application of a 3-DOF helicopter to demonstrate the results. Finally, in Chapter 10 is devoted to the use of TRC in electronics.

This monograph is complemented with four appendices providing additional material about DF, LPRS, Poincaré map, and output feedback control.

1.3.2 How to Read the Book?

The intended audiences of this book are researchers and graduated students interested in the problems of tracking and generation of self-excited periodic motion of electromechanical systems including non-minimum-phase systems, such as underactuated robots.

We try to make the book self-contained with respect to the following subjects:

- Describing function method,
- LPRS,
- Poincaré maps.

We assume that there might be four different categories of readers:

- Readers having a good knowledge of all above-listed topics, who can start reading the book from Chapter one.
- Readers well familiar with frequency-domain methods (describing function and LPRS), who can start reading the book from Appendix C containing basic concepts of Poincaré maps (see, e.g., [49, Ch. 7]) to better understand Chapter three.
- Readers having also a good knowledge of Poincaré maps, who can start reading the book from Appendices A and B concerned with basics material about describing function method and LPRS (the interested reader can consult [14, 35, 57] for a comprehensive study on the matter).
- We strongly recommend the beginner readers to start reading the book from Appendices.

Readers interested in the output feedback control might find it useful to review Appendix D. Interested readers can also review supplementary material about underactuated mechanical systems in [24, 30, 41], in particular about modeling and linearization methods. Basic knowledge of sliding mode control is required for Chapter five (see [84, 89], for instance).

Enjoy reading!

Part I
Design of Self-Oscillations Using Two-Relay Controller

Chapter 2
Describing Function-Based Design of TRC for Generation of Self-Oscillation

Abstract The TRC for the design of a self-excited oscillation of a desired amplitude and frequency in linear plants is presented. An approximate approach based on the DF method aimed at finding the TRC gains is given. The proposed approach is illustrated by experiments on an inertia wheel pendulum.

2.1 Introduction

The describing function (DF) method is a convenient method of finding approximate values of the frequency and the amplitude of periodic motions in the systems with linear plants driven by relay controllers. In this chapter, DF will be used as a tool for the design of self-excited oscillations of a desired amplitude and frequency in linear plants by means of the variable structure controller named the *two-relay controller (TRC)*.

The proposed approach is based on the fact that all relay algorithms (see, e.g., [14]) produce periodic motions. In this Chapter, we aim to use this property for the purpose of generating a relatively slow motion with a significantly high amplitude.

This chapter is organized as follows. We present the TRC in Section 2.2. In Section 2.3, we develop the DF-based analysis for a linear plant with the two-relay control. Section 2.4 provides formulas for computation of the two-relay controller parameters. In Section 2.5, we proceed with the analysis of orbital stability of oscillations in the closed-loop system. In Section 2.6, we illustrate the design methodology through an example of the inertia wheel pendulum, which is a two-degrees-of-freedom underactuated mechanical system.

2.2 The Two-Relay Controller

Consider the following nonlinear system:

$$\dot{x} = f(x, u) \tag{2.1}$$

L.T. Aguilar et al., *Self-Oscillations in Dynamic Systems*, Systems & Control: Foundations & Applications, DOI 10.1007/978-3-319-23303-1_2

where $x(t) \in \mathbb{R}^n$ is the state and $u(t) \in \mathbb{R}$ is the control input. Let us introduce the following control, which will be further referred to as the two-relay control (TRC):

$$u = -c_1 \operatorname{sign}(y) - c_2 \operatorname{sign}(\dot{y}). \tag{2.2}$$

It is proposed in this book for the purpose of excitation of a periodic motion. The constants c_1 and c_2 are parameters chosen in such a way that the scalar output of the system

$$y = h(x) \tag{2.3}$$

has a steady periodic motion with the desired frequency and amplitude. The output $h(x)$ is assumed at least twice differentiable.

Let us assume that the two-relay controller has two independent parameters $c_1 \in \mathscr{C}_1 \subset \mathbb{R}$ and $c_2 \in \mathscr{C}_2 \subset \mathbb{R}$, so that the changes to those parameters result in the respective changes of the frequency $\Omega \in \mathscr{W} \subset \mathbb{R}$ and the amplitude $A_1 \in \mathscr{A} \subset \mathbb{R}$ of the self-excited oscillations. Then we can note that there exist two mappings $F_1 : \mathscr{C}_1 \times \mathscr{C}_2 \mapsto \mathscr{W}$ and $F_2 : \mathscr{C}_1 \times \mathscr{C}_2 \mapsto \mathscr{A}$, which can be rewritten as $F : \mathscr{C}_1 \times \mathscr{C}_2 \mapsto \mathscr{W} \times \mathscr{A} \subset \mathbb{R}^2$. Assume that mapping F is unique. Then there exists an inverse mapping $G : \mathscr{W} \times \mathscr{A} \mapsto \mathscr{C}_1 \times \mathscr{C}_2$. The objective is, therefore, (a) to obtain mapping G using a frequency-domain method for deriving the model of the periodic process in the system, (b) to prove the uniqueness of mappings F and G for the selected controller, and (c) to find the ranges of variation of Ω and A_1 that can be achieved by varying parameters c_1 and c_2.

The *analysis and design objectives* lead to the two mutually inverse problems that correspond to the mappings F and G, respectively. The design problem is formulated as follows: find the parameter values c_1 and c_2 in (2.2) such that the system (2.1) has a periodic motion with the desired frequency $\boldsymbol{\Omega}$ and desired amplitude of the output signal $\boldsymbol{A} = A_1$. Therefore, the main objective of this research is to find mapping G to be able to select (tune) c_1 and c_2 values. In the following section, we will investigate the periodic solution through the DF method for the two-relay controller.

2.3 Describing Function of the Two-Relay Control

Consider the linear or linearized plant be given by

$$\begin{array}{l} \dot{x} = Ax + Bu \\ y = Cx \end{array}, \qquad x \in \mathbb{R}^n, \quad y \in \mathbb{R} \tag{2.4}$$

which can be represented in the transfer function form as follows:

$$W(s) = C(sI - A)^{-1}B.$$

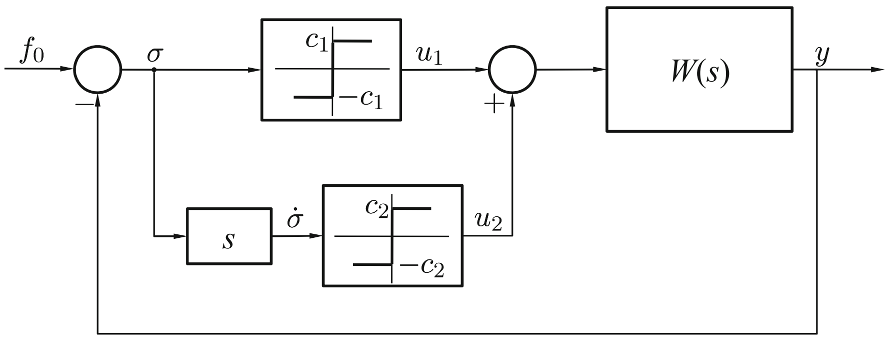

Fig. 2.1 Relay feedback system using two-relay controller

Let us assume that matrix A has no eigenvalues at the imaginary axis and the relative degree of (2.4) is greater than 1.

Let us consider the variable structure controller (2.2) named above as the *two-relay controller*. The describing function, N, of the variable structure controller (2.2) is the first harmonic of the periodic control signal divided by the amplitude of the harmonic signal $y(t)$:

$$N(A,\omega) = \frac{\omega}{\pi \boldsymbol{A}_1}\int_0^{2\pi/\omega} u(t)\sin(\omega t)dt + j\frac{\omega}{\pi \boldsymbol{A}_1}\int_0^{2\pi/\omega} u(t)\cos(\omega t)dt \tag{2.5}$$

where $\boldsymbol{A}_1$ is the amplitude of the input to the nonlinearity (of $y(t)$ in our case) and ω is the frequency of $y(t)$. However, the analysis of the TRC can utilize the fact that it is a combination of two relay nonlinearities, for which the DFs are known. The TRC can be viewed as the parallel connection of two ideal relays where the input to the first relay is the output variable and the input to the second relay is the derivative of the output variable (see Fig. 2.1). For the first relay, the DF is

$$N_1(\boldsymbol{A}_1) = \frac{4c_1}{\pi \boldsymbol{A}_1},$$

and for the second relay, it is

$$N_2(A_2) = \frac{4c_2}{\pi A_2},$$

where A_2 is the amplitude of dy/dt. Also, let us take into account the relationship between y and dy/dt in the Laplace domain, which gives the relationship between the amplitudes $\boldsymbol{A}_1$ and A_2: $A_2 = \boldsymbol{A}_1\boldsymbol{\Omega}$. Hereinafter, $\boldsymbol{\Omega}$ denotes the desired frequency of the oscillation. Using the notation of the TRC algorithm (2.2), we can rewrite this equation as follows:

Taking the magnitude of both sides of the above equation, we get

$$|W(j\boldsymbol{\Omega})| = \pi \boldsymbol{A}_1 \frac{\sqrt{-c_1^2 + c_2^2}}{4(c_1^2 + c_2^2)} = \frac{\pi \boldsymbol{A}_1}{4} \frac{1}{\sqrt{(c_1^2 + c_2^2)}}. \tag{2.12}$$

Finally, we obtain an expression for the amplitude of the oscillations as follows:

$$\boldsymbol{A}_1 = \frac{4}{\pi} |W(j\boldsymbol{\Omega})| \sqrt{c_1^2 + c_2^2}. \tag{2.13}$$

Therefore, the c_1 and c_2 values can be computed as follows:

$$c_1 = \begin{cases} \frac{\pi}{4} \frac{\boldsymbol{A}_1}{|W(j\boldsymbol{\Omega})|} \left(\sqrt{1+\xi^2}\right)^{-1} & \text{if } \boldsymbol{\Omega} \in Q_2 \cup Q_3 \\ -\frac{\pi}{4} \frac{\boldsymbol{A}_1}{|W(j\boldsymbol{\Omega})|} \left(\sqrt{1+\xi^2}\right)^{-1} & \text{elsewhere} \end{cases} \tag{2.14}$$

$$c_2 = \xi \cdot c_1. \tag{2.15}$$

2.5 Orbital Asymptotic Stability

To begin, let us recall the concepts of orbital stability and asymptotical orbital stability. First, let us define

$$O^+(x_0, t_0) = \{x \in \mathbb{R}^n | x = \bar{x}(t), t \geq 0, \bar{x}(t_0) = x_0\} \tag{2.16}$$

as a positive orbit through the point x_0 for $t \geq t_0$.

According to [93], the concepts of orbital stability and asymptotical orbital stability read as follows:

Definition 2.1 (Orbital stability). $\bar{x}$ is said to be orbitally stable if, given $\varepsilon > 0$, there exists a $\delta = \delta(\varepsilon) > 0$ such that, for any other solution, $y(t)$, of (2.1) satisfying $|\bar{x}(t_0) - y(t_0)| < \delta$ then $d(y(t), O^+(x_0, y_0)) < \varepsilon$, for $t > t_0$.

Definition 2.2 (Asymptotic orbital stability). $\bar{x}$ is said to be asymptotically orbitally stable if it is orbitally stable and for any other, $y(t)$, of (2.1), there exists a constant $b > 0$ such that, if $|\bar{x}(t_0) - y(t_0)| < b$, then $\lim_{t\to\infty} d(y(t), O^+(x_0, y_0)) = 0$.

The conditions of the existence of a periodic solution in a system with the TRC can be derived from analysis of Nyquist plot (see Fig. 2.2). Obviously, every system with a plant of relative degree three and higher would have a point of intersection with the negative reciprocal of the DF of the TRC, and therefore, a periodic solution would exist. The stability of the solution can be proven through the Loeb-like criterion [8, 39].

Proposition 2.1. *If the following inequality holds:*

$$\operatorname{Re} \frac{h_1}{h_2 + N \left. \frac{\partial \ln W(s)}{\partial s} \right|_{s=j\Omega}} < 0 \tag{2.17}$$

where

$$h_1 = \frac{4}{\pi \boldsymbol{A}_1^2}(c_1 + jc_2), \qquad h_2 = \frac{4c_2}{\pi \boldsymbol{A}_1 \boldsymbol{\Omega}}$$

then the periodic solution of (2.2), (2.4) is locally orbitally asymptotically stable.

Proof. To investigate the stability of the solution of the system (2.2), (2.4), we consider the system transients due to small perturbations of this solution when $\boldsymbol{A}_1$ is quasi-statically varied to $(\boldsymbol{A}_1 + \Delta \boldsymbol{A}_1)$. As in the proof of Loeb criterion, we assume that the harmonic balance equation still holds for slight perturbations, so a damped oscillation of the complex frequency $j\boldsymbol{\Omega} + (\Delta\sigma + j\Delta\Omega)$ corresponds to the modified amplitude $(\boldsymbol{A}_1 + \Delta A)$

$$N(\boldsymbol{A}_1 + \Delta A, j\boldsymbol{\Omega} + (\Delta\sigma + j\Delta\Omega)) \cdot W(j\boldsymbol{\Omega} + (\Delta\sigma + j\Delta\Omega)) = -1 \tag{2.18}$$

where the DF $N(\boldsymbol{A}_1, \boldsymbol{\Omega})$ is given by formula (2.6). The nominal solution is determined by zero perturbations: $\Delta\sigma = \Delta\Omega = \Delta A = 0$. Considering the variations around the nominal solution defined by $\boldsymbol{\Omega}$ and $\boldsymbol{A}_1$, we follow the idea of the proof of Loeb criterion: if ΔA is positive, it is expected that the oscillation must be converging, which is equivalent to $\sigma < 0$, and vice versa, if ΔA is negative then $\sigma > 0$. This can be summarized in the value of $\Lambda = \Delta\sigma/\Delta A$ being negative. For that purpose, take the derivative of (2.18) with respect to ΔA as follows:

$$\begin{aligned} &\left\{ \left. \frac{dN(\Delta A, \Delta\sigma, \Delta\Omega)}{d\Delta A} \right|_{\Delta A=0} \cdot W(j\Omega) \right. \\ &\left. + \left. \frac{dW(\Delta\sigma, \Delta\Omega)}{d\Delta A} \right|_{\Delta A=0} \cdot N(A, \boldsymbol{\Omega}) \right\} \Delta A = 0. \end{aligned} \tag{2.19}$$

Take the derivatives of $N(\boldsymbol{A}_1, \boldsymbol{\Omega})$ and $W(j\boldsymbol{\Omega})$ considering them composite functions

$$\left. \frac{dN}{d\Delta A} \right|_{\Delta A=0} = -\frac{4}{\pi A_1^2}(c_1 + jc_2) + \left[\frac{d\sigma}{d\Delta A} + j\frac{d\Delta\Omega}{d\Delta A} \right] \frac{4c_2}{\pi A_1 \boldsymbol{\Omega}} \tag{2.20}$$

$$\left. \frac{dW}{d\Delta A} \right|_{\Delta A=0} = \left. \frac{dW}{ds} \right|_{s=j\Omega} \left(\frac{d\Delta\sigma}{d\Delta A} + j\frac{d\Delta\Omega}{d\Delta A} \right). \tag{2.21}$$

Solving (2.19) for $((d\Delta\sigma)/(d\Delta A) + j(d\Delta\Omega)/(d\Delta A))$ with the account of (2.20) and (2.21), we can obtain an analytical formula. Considering only the real part of this formula, we obtain (2.17). ■

In the above-given proof, as well as in the proof of the theorem given below, we assume that the harmonic balance condition still holds for small perturbations of the amplitude and the frequency. This is a certain idealization of the actual process, which, however, allows us to obtain an important result in a very simple way. Under this assumption, the oscillation can be described as a damped one, with the following logical construction: if the damping parameter is negative at a positive increment of the amplitude and positive at a negative increment of the amplitude, then the perturbation will vanish, and the oscillations converge to the limit cycle, and limit cycle is OAS. We formulate and prove the following theorem, which would be more convenient in a practical analysis of orbital stability of the periodic motion and design the TRC.

Theorem 2.1. *Suppose that for the values of the c_1 and c_2 given by (2.14)–(2.15), there exists a corresponding periodic solution to the system (2.2)–(2.4). If*

$$\left.\frac{d \arg W}{d \ln \omega}\right|_{\omega=\boldsymbol{\Omega}} \leq -\frac{c_1 c_2}{c_1^2 + c_2^2} \tag{2.22}$$

then the abovementioned periodic solutions to the system (2.2)–(2.4) are OAS.

Proof. The approach for the stability analysis of the periodic motions is similar to the one proposed in [57]. Let us write the harmonic balance equation for the perturbed motion:

$$\begin{aligned}\{N_1(A_1 + \Delta A_1) + [j\boldsymbol{\Omega} + (\Delta\sigma + j\Delta\boldsymbol{\Omega})]N_2(A_2 + \Delta A_2)\}\\ \times W(\Delta\sigma + j(\boldsymbol{\Omega} + \Delta\boldsymbol{\Omega})) = -1\end{aligned}$$

where $A_2 = \boldsymbol{\Omega A}_1$. The Laplace variable for the damped oscillation is $s = j\boldsymbol{\Omega} + (\Delta\sigma + j\Delta\boldsymbol{\Omega})$. Take the derivative of both sides of this equation with respect to $\Delta\boldsymbol{A}_1$:

$$\begin{aligned}&\left.\frac{\partial N_1}{\partial \Delta \boldsymbol{A}_1}\right|_{\Delta \boldsymbol{A}_1=0} \cdot W(j\boldsymbol{\Omega}) + \left.\frac{\partial N_2}{\partial \Delta \boldsymbol{A}_1}\right|_{\Delta \boldsymbol{A}_1=0} \cdot j\boldsymbol{\Omega}\, W(j\boldsymbol{\Omega})\\
&\quad + \left.\frac{dW}{dS}\right|_{s=j\boldsymbol{\Omega}} \left(\frac{d\Delta\sigma}{d\Delta A_1} + j\frac{d\Delta\boldsymbol{\Omega}}{d\Delta A_1}\right) \cdot N_1(\boldsymbol{A}_1)\\
&\quad + N_2(A_2)\left(\frac{d\Delta\sigma}{d\Delta \boldsymbol{A}_1} + j\frac{d\Delta\boldsymbol{\Omega}}{d\Delta \boldsymbol{A}_1}\right) W(j\boldsymbol{\Omega})\\
&\quad + N_2(A_2)\left[j\boldsymbol{\Omega}\left.\frac{dW}{ds}\right|_{s=j\boldsymbol{\Omega}} \left(\frac{d\Delta\sigma}{d\Delta \boldsymbol{A}_1} + j\frac{d\Delta\boldsymbol{\Omega}}{d\Delta \boldsymbol{A}_1}\right)\right] = 0\end{aligned}$$

where

$$\frac{\partial N_1}{\partial \Delta \boldsymbol{A}_1} = -\frac{4c_1}{\pi \boldsymbol{A}_1^2}; \quad \text{and} \quad \frac{\partial N_2}{\partial \Delta \boldsymbol{A}_1} = -\frac{4c_2}{\pi A_2^2}\boldsymbol{\Omega} = -\frac{4c_2}{\pi \boldsymbol{\Omega} \boldsymbol{A}_1^2}.$$

Thus, the following equation is obtained

$$-\frac{4c_1}{\pi \boldsymbol{A}_1^2} W(j\boldsymbol{\Omega}) - j\frac{4c_2}{\pi \boldsymbol{A}_1^2} W(j\boldsymbol{\Omega}) = \left(\frac{d\Delta\sigma}{d\Delta \boldsymbol{A}_1} + j\frac{d\Delta\sigma}{d\Delta \boldsymbol{A}_1}\right) \times$$
$$\left\{ -N_1(\boldsymbol{A}_1) \left.\frac{dW}{ds}\right|_{s=j\boldsymbol{\Omega}} - N_2(A_2)\left[W(j\boldsymbol{\Omega}) + j\boldsymbol{\Omega} \left.\frac{dW}{ds}\right|_{s=j\boldsymbol{\Omega}} \right] \right\}.$$

Express the quantity $\frac{d\Delta\sigma}{d\Delta \boldsymbol{A}_1} + j\frac{d\Delta\boldsymbol{\Omega}}{d\Delta \boldsymbol{A}_1}$ from that equation

$$\frac{d\Delta\sigma}{d\Delta \boldsymbol{A}_1} + j\frac{d\Delta\boldsymbol{\Omega}}{d\Delta \boldsymbol{A}_1} = \frac{W(j\boldsymbol{\Omega})[c_1 + jc_2]}{\boldsymbol{A}_1 \left\{ c_1 \left.\frac{dW}{ds}\right|_{s=j\boldsymbol{\Omega}} + c_2 \left[\frac{1}{\boldsymbol{\Omega}} W(j\boldsymbol{\Omega}) + j \left.\frac{dW}{ds}\right|_{s=j\boldsymbol{\Omega}} \right] \right\}}$$
$$= \frac{1}{\boldsymbol{A}_1 \underbrace{\left\{ \left.\frac{d\ln W}{ds}\right|_{s=j\boldsymbol{\Omega}} + \frac{c_2}{\boldsymbol{\Omega}} \frac{c_1 - jc_2}{c_1^2 + c_2^2} \right\}}_{\Lambda}}.$$

Then for the inequality

$$\frac{d\Delta\sigma}{d\Delta \boldsymbol{A}_1} < 0 \tag{2.23}$$

to be true, the following should hold:

$$\mathrm{Re}\frac{1}{\boldsymbol{A}_1 \Lambda} < 0 \quad \text{or} \quad \mathrm{Re}\Lambda < 0. \tag{2.24}$$

Then for the real part of Λ, we can write

$$\mathrm{Re}\left.\frac{d\ln W}{ds}\right|_{s=j\boldsymbol{\Omega}} + \frac{c_1 c_2}{\boldsymbol{\Omega}(c_1^2 + c_2^2)} < 0. \tag{2.25}$$

Representation of the transfer function in the exponential format and differentiation with respect to s yield

$$\left.\frac{d\arg W}{d\omega}\right|_{\omega=\boldsymbol{\Omega}} < -\frac{c_1 c_2}{\boldsymbol{\Omega}(c_1^2 + c_2^2)} \tag{2.26}$$

or finally

$$\left.\frac{d \arg W}{d \ln \omega}\right|_{\omega=\boldsymbol{\Omega}} < -\frac{\xi}{\xi^2+1}. \tag{2.27}$$

Therefore, the stability of the periodic motion is determined just by the slope of the phase characteristic of the plant, which must be steeper than a certain value for the oscillation to be asymptotically stable. ■

In the example considered below, we illustrate the use of the DF method for design.

Example 2.1. Consider the following linear system:

$$\begin{aligned}\dot{x}_1 &= x_2\\ \dot{x}_2 &= -x_1 - 3x_2 + u\\ y &= x_1\end{aligned} \tag{2.28}$$

where $x_1(t), x_2(t)$ are the states and $y(t)$ is the output, in which we are interested to induce self-oscillation with amplitude $\boldsymbol{A}_1 = 0.1$ and frequency $\boldsymbol{\Omega} = 4$ rad/s via the TRC $u(t)$ given by (2.2). Formulas (2.14), (2.15) provide the values of the controller parameters that must be used. In these formulas, the transfer function corresponding to the equations of the above system is given by

$$W(s) = \frac{1}{s^2+3s+1}. \tag{2.29}$$

The magnitude of the above transfer function and its real and imaginary parts are, respectively,

$$\begin{aligned}|W(j\omega)| &= \frac{1}{\sqrt{(1-\omega^2)^2+9\omega^2}},\\ \mathrm{Re}\{W(j\omega)\} &= \frac{1-\omega^2}{(1-\omega^2)^2+9\omega^2},\\ \mathrm{Im}\{W(j\omega)\} &= \frac{-3\omega}{(1-\omega^2)^2+9\omega^2}.\end{aligned} \tag{2.30}$$

For the desired frequency and amplitude, we can explicitly get values of the plant frequency response: $\mathrm{Re}\{W(j4)\} = -0.0407$ and $\mathrm{Im}\{W(j4)\} = -0.0325$. From the fact that the desired frequency of oscillations is located in the third quadrant and the computed value of $\xi = -0.80$, we find through (2.14)–(2.15), the values of controller parameters: $c_1 = 1.1781$ and $c_2 = -0.9425$. The periodic output signal

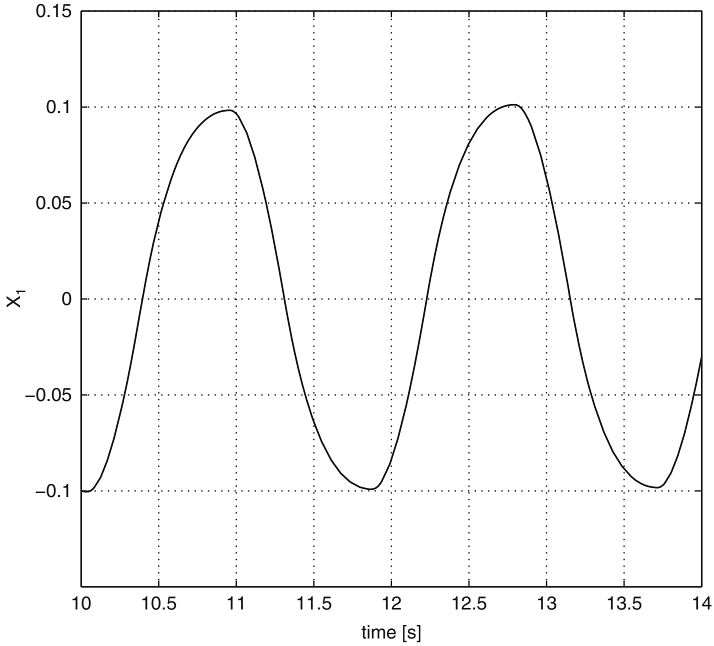

Fig. 2.3 Period output response of the example linear system (2.28) enforced by the TRC (2.2)

is plotted in Fig. 2.3, where the amplitude of the system output produced through simulations matches the desired amplitude, whereas the frequency of this signal shows some deviation from the desired value: $\boldsymbol{\Omega} = 3.6$ rad/s. This discrepancy is expected due to the approximate nature of the DF method.

To check if the periodic solution is stable, we need to find the derivative of the phase characteristic of the plant with respect to the frequency

$$\left.\frac{d \arg W(j\omega)}{d \ln \omega}\right|_{s=j\Omega} = -\frac{3\boldsymbol{\Omega}^2 + 3}{\boldsymbol{\Omega}^4 + 7\boldsymbol{\Omega}^2 + 1}. \tag{2.31}$$

The stability condition (2.27) for the system becomes

$$-\frac{3\boldsymbol{\Omega}^2 + 3}{\boldsymbol{\Omega}^4 + 7\boldsymbol{\Omega}^2 + 1} \le -\frac{\xi}{\xi^2 + 1}. \tag{2.32}$$

We note that the left-hand side of (2.32) is −0.1382 and the right-hand side is 0.1220. Therefore, the system (2.2), (2.28), with $c_1 = 1.1781$ and $c_2 = -0.9425$, is orbitally asymptotically stable.

2.6 The Inertia Wheel Pendulum: An Example

The inertia wheel pendulum (IWP) is a pendulum that has a rotating inertia wheel (see Fig. 2.4). The pendulum itself is not actuated but the wheel is, so that the system is controlled via the wheel. For experimental verification of the presented theoretical results, an inertia wheel pendulum manufactured by Quanser, Inc., is used. The dynamics of IWP (see [12]) is given as follows:

$$\begin{bmatrix} J_1 & J_2 \\ J_2 & J_2 \end{bmatrix} \begin{bmatrix} \ddot{q}_1 \\ \ddot{q}_2 \end{bmatrix} + \begin{bmatrix} h \sin q_1 \\ 0 \end{bmatrix} = \begin{bmatrix} 0 \\ 1 \end{bmatrix} \tau. \tag{2.33}$$

In the above equation, $q_1(t) \in \mathbb{R}$ is the absolute angle of the pendulum, counted clockwise from the vertical downward position; $q_2(t) \in \mathbb{R}$ is the absolute angle of the disk; $t \in \mathbb{R}$ is the time; J_1, J_2, and h are positive physical parameters, which depend on the geometric dimensions and the inertia–mass distribution; and $\tau \in \mathbb{R}$ is the controlled torque applied to the disk (see Fig. 2.4).

The *design objective* is formulated as follows: find parameter values of c_1 and c_2 (2.2) of the TRC using the algorithm provided in Subsection 2.4, such that the output

$$y = q_1 \tag{2.34}$$

Fig. 2.4 Inertia wheel pendulum

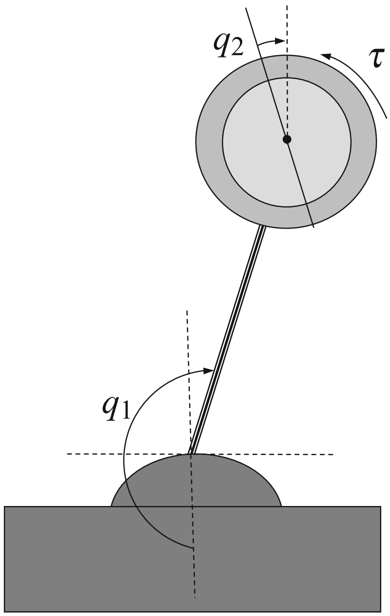

of system (2.33) produces a periodic motion with the desired frequency $\boldsymbol{\Omega}$ and desired amplitude $\boldsymbol{A}_1$. Notice that the model of the plant is nonlinear, while the method for gain adjustment requires that the plant should be linear. Therefore, linearization of plant dynamics (2.33) is required, which is the subject of the following subsection.

2.6.1 Linearization of IWP dynamics

The inertia wheel pendulum has underactuation degree one, and according to [41], it is locally exact linearizable through a change of variable that is also aimed at ensuring local stability of its zero dynamics. Let us note that the zero dynamics describes the internal dynamics of a system $\dot{x} = f(x)$, with vector $x \in \mathbb{R}^n$, when its output y is identically equal to zero (cf. [47, p. 162]).

Let us consider the following change of variable

$$\begin{aligned} p_1 &= q_1 - \pi + J_1^{-1} J_2 q_2 \\ \eta &= J_1 \dot{q}_1 + J_2 \dot{q}_2 + K p_1 \end{aligned}$$

where $K > 0$ is a constant. It is easy to verify that

$$J_1 \dot{p}_1 = \eta - K p_1$$

while

$$\begin{aligned} \dot{\eta} &= K J_1^{-1} J_2 \dot{q}_2 - h \sin(q_1) + K \dot{q}_1, \\ \ddot{\eta} &= -h \cos(q_1) \dot{q}_1 - K J_1^{-1} h \sin(q_1), \\ \dddot{\eta} &= R(q_1, \dot{q}_1) + H(q_1) \tau \end{aligned}$$

where

$$\begin{aligned} H(q_1) &= \frac{h \cos(q_1)}{J_1 - J_2}, \\ R(q_1, \dot{q}_1) &= \left(\dot{q}_1^2 + H(q_1)\right) h \sin(q_1) - \frac{hK}{J_1} \dot{q}_1 \cos(q_1). \end{aligned} \tag{2.35}$$

Hence, we can consider

$$\tau = H^{-1}(q_1) \left(u - a_0 \eta - a_1 \dot{\eta} - a_2 \ddot{\eta} - R(q_1, \dot{q}_1)\right), \tag{2.36}$$

where $H(q_1)$ is nonsingular about the equilibrium point $[q_1^\star \ \dot{q}_1^\star]^T = [\pi \ 0]^T$ and a_0, a_1, and a_2 are positive constants. Introducing the new state coordinates $x = [x_1 \ x_2 \ x_3]^T = [\eta \ \dot{\eta} \ \ddot{\eta}]^T$, we obtain

$$\begin{bmatrix} \dot{x}_1 \\ \dot{x}_2 \\ \dot{x}_3 \end{bmatrix} = \begin{bmatrix} 0 & 1 & 0 \\ 0 & 0 & 1 \\ -a_0 & -a_1 & -a_2 \end{bmatrix} \begin{bmatrix} x_1 \\ x_2 \\ x_3 \end{bmatrix} + \begin{bmatrix} 0 \\ 0 \\ 1 \end{bmatrix} u, \tag{2.37}$$

$$\dot{p}_1 = -\frac{K}{J_1} p_1 + \frac{1}{J_1} y, \qquad y = \begin{bmatrix} 1 & 0 & 0 \end{bmatrix} x. \tag{2.38}$$

The corresponding transfer function of (2.37) is

$$W_p(s) = \frac{1}{s^3 + a_2 s^2 + a_1 s + a_0}, \qquad s = j\omega \tag{2.39}$$

where ω is the frequency. The magnitude of the above transfer function is

$$\begin{aligned} |W_p(j\omega)| &= \left| \frac{1}{(j\omega)^3 + a_2 (j\omega)^2 + a_1 (j\omega) + a_0} \right| \\ &= \frac{1}{\sqrt{(a_0 - a_2\omega^2)^2 + \omega^2 (a_1 - \omega^2)^2}}. \end{aligned} \tag{2.40}$$

For plant parameters $a_0 = 350$, $a_1 = 155$, and $a_2 = 22$, the desired frequency $\boldsymbol{\Omega} = 2$ and the desired amplitude $\boldsymbol{A}_1 = 0.007$, we explicitly obtain $|W_p(j2)| = 0.0025$.

2.6.2 *Gains Adjustment*

Since we are interested in presenting the final results for the original coordinates q_1 and q_2, we start with computing of an approximation for the amplitude of oscillation of the pendulum. From the equality $\dot{p}_1 + J_1^{-1} K p_1 = J_1^{-1} \eta(t)$, we know that p_1 exponentially converges to a periodic function, with convergence rate regulated by varying K.

Taking into account only the first harmonic and letting the steady value for $\eta(t)$ be $\eta(t) \approx \boldsymbol{A}_1 \sin(\boldsymbol{\Omega} t)$, we can compute the approximate value for $p_1(t)$ in the steady periodic motion in the form

$$p_1(t) \approx \frac{\boldsymbol{A}_1}{\sqrt{J_1^2 \boldsymbol{\Omega}^2 + K^2}} \sin\left(\boldsymbol{\Omega} t + \arg\left\{ \frac{1}{jJ_1 \boldsymbol{\Omega} + K} \right\} \right).$$

Now using the equation $\dot{\eta}(t) \approx \boldsymbol{\Omega} \boldsymbol{A}_1$ and the equation $h \sin(q_{1r}) = \dot{\eta} - K\dot{p}_1$, one can conclude that q_1 exponentially converges to a steady periodic motion—provided the oscillations are small.

Finally, for q_1 close enough to π, we have $\sin(q_1) \approx \pi - q_1$, so that

$$q_1(t) \approx \pi - \frac{\boldsymbol{\Omega} \boldsymbol{A}_1}{h} \cos(\boldsymbol{\Omega} t) - \frac{\boldsymbol{\Omega} \boldsymbol{A}_1}{h\sqrt{J_1^2 \boldsymbol{\Omega}^2 + K^2}} \sin\left(\boldsymbol{\Omega} t + \arg\left\{\frac{1}{jJ_1 \boldsymbol{\Omega} + K}\right\}\right). \tag{2.41}$$

This expression gives us an estimate of the amplitude of the oscillations of the pendulum established around the point of π:

$$A \approx \frac{\boldsymbol{\Omega} \boldsymbol{A}_1}{h} h \sqrt{1 + \frac{1}{J_1^2 \boldsymbol{\Omega}^2 + K^2}}. \tag{2.42}$$

Since $q_2 = J_1(p_1 - (\pi - q_1))/J_2$, the amplitude of the steady periodic motion of q_2 can be estimated as well.

The gains c_1 and c_2 of the TRC algorithm (2.2) are found using the procedure given in Section 2.4 for $\boldsymbol{\Omega} = 2$ rad/s and $\boldsymbol{A}_1 = 0.007$ being the desired frequency and amplitude, respectively. The results of the computation through equations (2.14) and (2.15) are $c_1 = 2$ and $c_2 = -0.1$. Figure 2.5 shows also that the frequency of the oscillations is located in the third quadrant. Block diagram of the controller is presented in Figure 2.6.

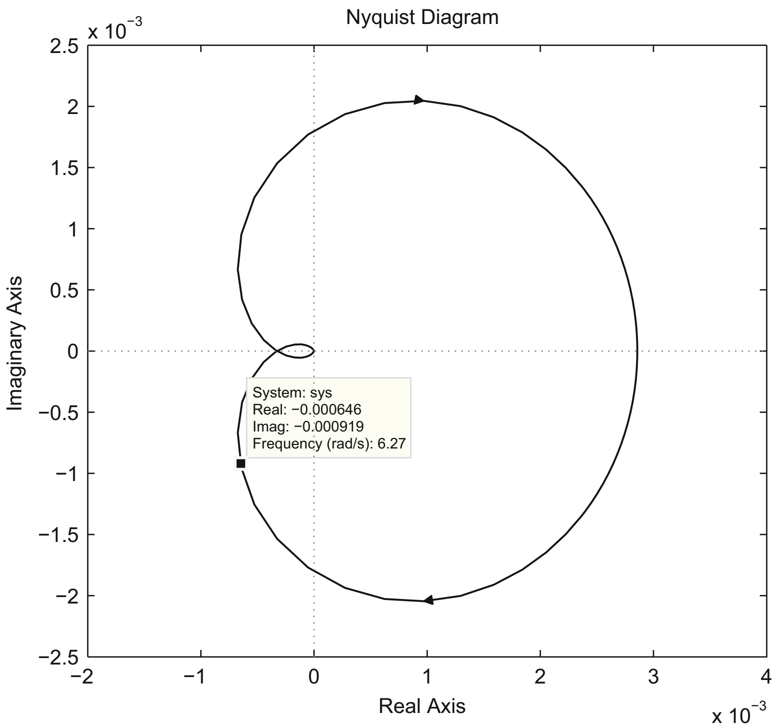

Fig. 2.5 Nyquist plot of the linearized model of the inertia wheel pendulum

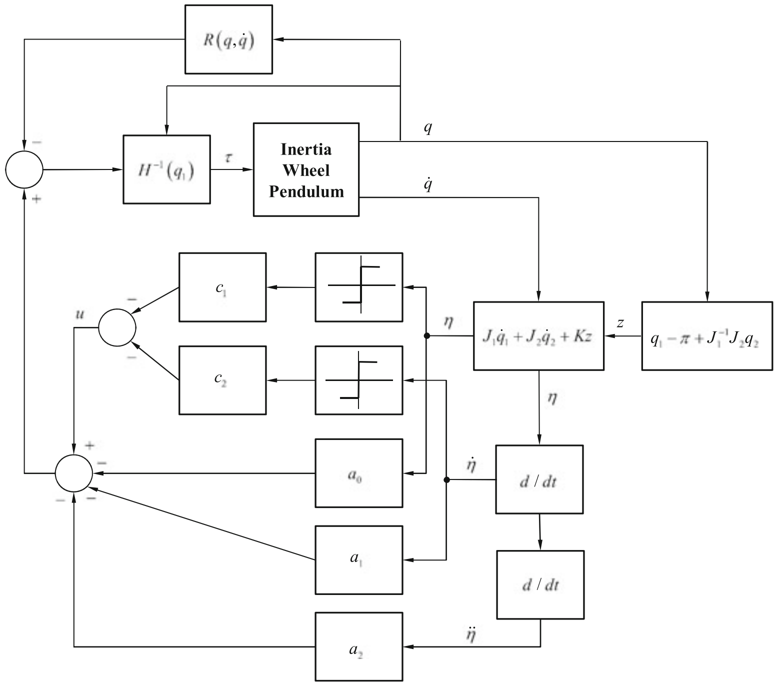

Fig. 2.6 Block diagram to generate the auto-oscillation using the TRC controller with the linearized IWP model

2.6.3 Bounded Input Problem

Due to the necessity use of various actuators that feature limited power, the aspect of constrained control is of practical interest in the considered problem. Let us assume that the actuator has limitations on the developed torque, with maximum torque being $u^{\max}$, therefore leading to

$$|u| \le u^{\max}. \tag{2.43}$$

Formulas (2.14)–(2.15) may give relatively large values of c_1 and c_2, which exceed the maximum allowable torque $u^{\max}$. To take into account the lower and upper bounds on the torques, we can use equations (2.14)–(2.15), (2.43), to write the following inequality:

$$\begin{aligned}|u| &= |c_1(\boldsymbol{A}_1, \boldsymbol{\Omega}) + c_2(\boldsymbol{A}_1, \boldsymbol{\Omega})|\\ &= |(1+\xi)c_1(\boldsymbol{A}_1, \boldsymbol{\Omega})|\\ &= \left|(1+\xi)\left[\frac{\pi}{4}\frac{\boldsymbol{A}_1}{\|W(j\boldsymbol{\Omega})\|}\left(\sqrt{1+\xi^2}\right)^{-1}\right]\right|\end{aligned}$$

$$
\begin{aligned}
&= \left| \frac{\mathrm{Re}\{W(j\boldsymbol{\Omega})\} + \mathrm{Im}\{W(j\boldsymbol{\Omega})\}}{\|W(j\boldsymbol{\Omega})\|^2} \right| \frac{\boldsymbol{A}_1 \pi}{4} \\
&\leq u^{\max}.
\end{aligned} \tag{2.44}
$$

From the above equation, it is possible to find a range of frequencies $\boldsymbol{\Omega}_{\min} \leq \boldsymbol{\Omega} \leq \boldsymbol{\Omega}_{\max}$ corresponding to a particular desired amplitude $\boldsymbol{A}_1$ that would satisfy (2.44). The values of $\boldsymbol{\Omega}_{\min}$ and $\boldsymbol{\Omega}_{\max}$ are the minimum and maximum desired frequency that can chosen for the system (2.33) without saturating the actuator power. In fact, only in this range simultaneous requirements to the frequency and the amplitude can be satisfied.

For the linearized model of the inertia wheel pendulum (2.39), we obtain

$$
\begin{aligned}
\mathrm{Re}\{W(j\boldsymbol{\Omega})\} &= \frac{a_0 - a_2\boldsymbol{\Omega}^2}{(a_0 - a_2\boldsymbol{\Omega}^2)^2 + (a_1\boldsymbol{\Omega} - \boldsymbol{\Omega}^3)^2} \\
\mathrm{Im}\{W(j\boldsymbol{\Omega})\} &= \frac{\boldsymbol{\Omega}^3 - a_1\boldsymbol{\Omega}}{(a_0 - a_2\boldsymbol{\Omega}^2)^2 + (a_1\boldsymbol{\Omega} - \boldsymbol{\Omega}^3)^2}.
\end{aligned} \tag{2.45}
$$

Therefore, it is possible to select from equations (2.44)–(2.45) a range of the desired amplitudes $\boldsymbol{A}_1$ and frequencies $\boldsymbol{\Omega}$, such that the inequality (2.44) holds. By considering the formula

$$
\underbrace{\left(\frac{\mathrm{Re}\{W(j\boldsymbol{\Omega})\} + \mathrm{Im}\{W(j\boldsymbol{\Omega})\}}{\|W(j\boldsymbol{\Omega})\|^2} \right) \frac{\boldsymbol{A}_1 \pi}{4}}_{h(\boldsymbol{\Omega})} = u^{\max} \tag{2.46}
$$

we find that the upper bound $\boldsymbol{\Omega}_{\max}$ can be obtained from the following equation:

$$
\pi \boldsymbol{A}_1 F_1(\boldsymbol{\Omega}_{\max}) + 4u^{\max} F_2(\boldsymbol{\Omega}_{\max}) = 0, \tag{2.47}
$$

where

$$
\begin{aligned}
F_1(\boldsymbol{\Omega}) &= \left[(a_0 - a_2\boldsymbol{\Omega}^2)^2 + (a_1\boldsymbol{\Omega} - \boldsymbol{\Omega}^3)^2\right] \cdot \left[a_0 - a_1\boldsymbol{\Omega} - a_2\boldsymbol{\Omega}^2 + \Omega^3\right] \\
F_2(\boldsymbol{\Omega}) &= (a_0 - a_2\boldsymbol{\Omega}^2)^2 + (\boldsymbol{\Omega}^3 - a_1\boldsymbol{\Omega})^2.
\end{aligned}
$$

Similarly, the lower bound $\boldsymbol{\Omega}_{\min}$ can be obtained by considering the following equation:

$$
\pi \boldsymbol{A}_1 F_1(\boldsymbol{\Omega}_{\min}) - 4u^{\max} F_2(\boldsymbol{\Omega}_{\min}) = 0. \tag{2.48}
$$

For example, choosing $\boldsymbol{A}_1 = 1.0$ and $u^{\max} = 10$ and solving the set of algebraic equations (2.47)–(2.48), we find that $\boldsymbol{\Omega}_{\min} = 8.2$ rad/s and $\boldsymbol{\Omega}_{\max} = 9.5$ rad/s are the minimum and maximum frequency that should be chosen in order to not

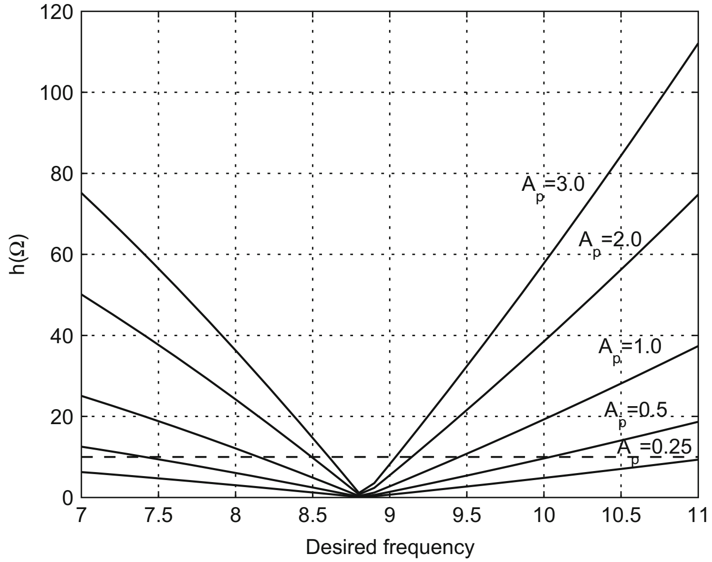

Fig. 2.7 Attainable desired frequencies for several amplitudes, DF-based design where dotted line corresponds to the $h(\Omega)$ value where $u_{\max}$ level can be reached

saturate the control input. The range of attainable desired frequencies, for a set of possible desired output amplitudes, is depicted in Figure 2.7. Dotted line in the same figure indicates the $h(\Omega)$ value where $u_{\max}$ level can be reached, that is, for the same desired amplitude, it can be seen from the figure that the frequency to be chosen is $\boldsymbol{\Omega} = 9.25$ rad/s.

2.6.4 Simulation Results

The simulation was done for the model of the laboratory inertia wheel pendulum from Mechatronics Control Kit, prototype manufactured by Quanser, Inc., shown in Fig. 2.4. The parameter values used in simulations are as follows: $J_1 = 4.572\times10^{-3}$, $J_2 = 2.495 \times 10^{-5}$, $h = 0.3544$. Parameters of the linearized system are $K = 1 \times 10^{-4}$, $a_0 = 350$, $a_1 = 155$, and $a_2 = 22$. Figure 2.6 shows the block diagram of the overall controller (2.36).

For simulations, the initial conditions for the IWP were set to $q_1(0) = 3.1$ rad and $q_2(0) = 0$ rad, and all the velocity initial conditions were set to $\dot{q}_1(0) = \dot{q}_2(t) = 0$ rad/s. Figure 2.8 shows the self-excited periodic motion of the pendulum (state q_1). Some discrepancy between the desired and actual values of frequency and amplitude can be attributed to the approximate nature of the DF method.

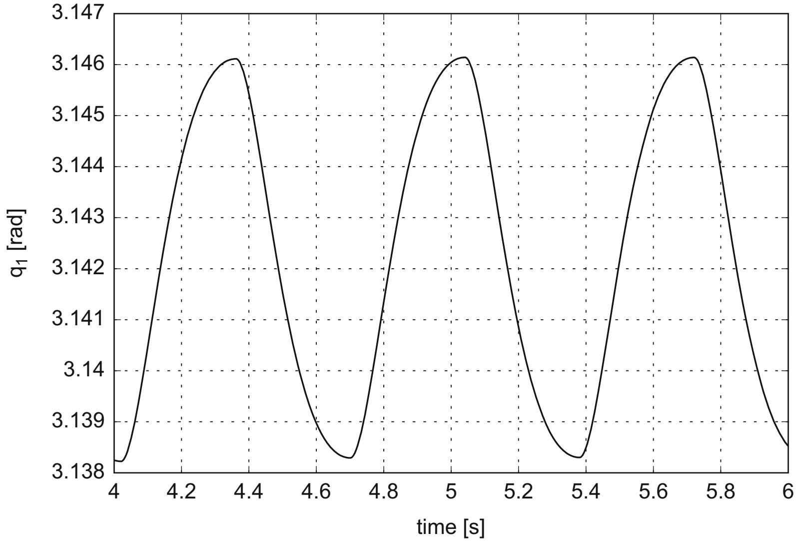

Fig. 2.8 Oscillation motion generated at $\boldsymbol{\Omega} = 2\pi$ rad/s and $\boldsymbol{A}_1 = 0.007$ generated by the two-relay controller with the linearized IWP plant under parameters $c_1 = 2$, $c_2 = -0.1$, $K = 1 \times 10^{-4}$, $a_0 = 350$, $a_1 = 155$, and $a_2 = 22$

2.7 Concluding Remarks

A two-relay controller is proposed for generation of self-excited oscillations with a desired amplitude and frequency of the system output signal. A methodology of the TRC design that ensures generation of oscillations of the desired frequency and amplitude in the system is proposed. The developed methodology is illustrated by an example of controller design for an inertia wheel pendulum. Values of the controller parameters are approximately computed through application of the DF method and verified through simulations. Another important issue for implementation purposes was covered in this chapter that is to find the set of desired frequencies were the computed parameters avoids the input saturation.

Chapter 3
Poincaré Map-Based Design

Abstract In this chapter, Poincaré maps were used, to the best knowledge of the authors, for the first time as a design tool: to find controller parameters that provide the desired amplitude and frequency of the periodic motion of in systems having nonlinear plants, through the use of the TRC. We present application to an underactuated mechanical system via generating a self-excited oscillation of a desired amplitude and frequency of the unactuated position variable. Poincaré map design provides values of the TRC parameters and ensures local orbital stability of the periodic motions, for an arbitrary mechanical plant. The proposed approach is illustrated by the controller design for and experiments on the inertia wheel pendulum.

3.1 Introduction

The Poincaré maps are successfully used to ensure the existence and stability of periodic motions. In this chapter, an algorithm that provides the values of the controller parameters and guarantees the local asymptotic orbital stability of periodic motions for an arbitrary mechanical plant through the use Poincaré maps is presented.

In Appendix C, readers can find basic definitions and theorems concerning Poincaré maps. In Section 3.2, we provide the Poincaré map-based design for a linear system. Section 3.3 gives the Poincaré map analysis for an arbitrary two-degrees-of-freedom underactuated system where orbital asymptotical stability of the limit cycle is provided. In particular, we describe the procedure of finding the coefficients of the two-relay controller, from the given amplitude and frequency, using the linearized Euler–Lagrange dynamic model. In Section 3.4 an example of controller design for the inertia wheel pendulum is provided. We conclude the chapter with providing comments and remarks in Section 3.5.

L.T. Aguilar et al., *Self-Oscillations in Dynamic Systems*, Systems & Control: Foundations & Applications, DOI 10.1007/978-3-319-23303-1_3

3.2 Poincaré Map-Based Design of the Gains of the TRC for Linearized Model

The *design objectives* considered in this chapter are formulated as finding the values of parameters c_1 and c_2 of the two-relay controller (3.12) that ensure a self-excited periodic motion $y(t)$ in the closed-loop system comprising a linear plant, with a desired frequency $\boldsymbol{\Omega}$ and amplitude $\boldsymbol{A}_1$.

$$\begin{aligned}\dot{x} &= Ax + Bu \\ y &= Cx\end{aligned}, \qquad x \in \mathbb{R}^n, \quad y \in \mathbb{R}. \tag{3.1}$$

To construct the Poincaré map, one has to choose a surface of section S in the state space $\mathbb{R}^n$ and consider the points of successive intersections of a given trajectory with this surface. Switching occurs on the level surfaces defined by

$$\begin{aligned} S_1 &= \{x : y > 0, \dot{y} = 0\}, \qquad & S_2 &= \{x : y = 0, \dot{y} < 0\} \\ S_3 &= \{x : y < 0, \dot{y} = 0\}, \qquad & S_4 &= \{x : y = 0, \dot{y} > 0\}. \end{aligned} \tag{3.2}$$

The space $\mathbb{R}^n$ is divided into four regions by $R_1, \dots, R_4$ defined as

$$\begin{aligned} R_1 &= \{x : y > 0, \dot{y} > 0\}, \qquad & R_2 &= \{x : y > 0, \dot{y} < 0\}, \\ R_3 &= \{x : y < 0, \dot{y} < 0\}, \qquad & R_4 &= \{x : y < 0, \dot{y} > 0\}. \end{aligned} \tag{3.3}$$

Depending on the state, the system is governed by one of the four models defined by

$$\begin{aligned} M_1 &: \dot{x} = Ax + B(c_1 + c_2), \\ M_2 &: \dot{x} = Ax + B(c_1 - c_2), \\ M_3 &: \dot{x} = Ax - B(c_1 + c_2), \\ M_4 &: \dot{x} = Ax + B(-c_1 + c_2). \end{aligned}$$

The solution of M_1 on the time interval $[0; t_1]$, where t_1 is the transition time from S_1 to S_2, subject to the initial condition of $x(0) = \rho_p$, where "$(\cdot)_p$" stands for "periodic", such that (without loss of generality)

$$\begin{aligned} y(0) &= C\,x(0) = C\,\rho_p = 0, \\ \dot{y}(0) &= C\,(A\,x(0) + B\,u) = C\,A\,\rho_p < 0, \end{aligned} \tag{3.4}$$

is given by

$$x(t) = e^{At}x(0) + \int_0^t e^{A\tau} d\tau B u.$$

Integral of the exponent of the state matrix is given by

$$\int_0^t e^{A\tau} d\tau = \sum_{i=1}^{\infty} A^{i-1} t^i / i! = A^{-1}(e^{At} - I)$$

The control in (3.4) is given by $u = c_1 + c_2$. The transition to S_2 and switching to $u = c_1 - c_2$ is ensured under the technical transversality condition

$$\ddot{y}(t_1) = CA^2 \eta_k > 0. \tag{3.5}$$

Under this condition, the trajectory will enter the region R_2, and since the matrix A is Hurwitz, it will reach either S_3 or return back to S_2. We will assume for now that the latter does not happen.

Analogously, the four state transitions initiated at $\rho_k = \rho_p$ are given by

$$\begin{aligned} \eta_k &= e^{At_1} \rho_k + A^{-1}(e^{At_1} - I)B(c_1 + c_2), \\ \rho_k^- &= e^{At_2} \eta_k + A^{-1}(e^{At_2} - I)B(c_1 - c_2), \\ \eta_k^- &= e^{At_3} \rho_k^- - A^{-1}(e^{At_3} - I)B(c_1 + c_2), \\ \rho_{k+1} &= e^{At_4} \eta_k^- - A^{-1}(e^{At_4} - I)B(c_1 - c_2), \end{aligned} \tag{3.6}$$

where t_2 is the time interval between S_2 and S_3, t_3 is the time interval between S_3 and S_4, and t_4 is the time interval between S_4 and S_1.

The fixed point of the Poincaré map, corresponding to an isolated periodic solution of system (3.1) driven by the two-relay controller, is determined by equation $\rho_{k+1} = \rho_k = \rho_p$. Skipping the sequential numbers of switching in (3.6) and using the principle of symmetry, one can write the following: $\rho_p^- = -\rho_p$. For the T-periodic (symmetric) solution, we will use the following notation: $t_1 = t_3 = \theta_1$, $t_2 = t_4 = \theta_2 = T/2 - \theta_1$.

The equation for the fixed point together with the switching conditions can be rewritten as follows:

$$-\rho_p = e^{A\theta_2} \eta_p + A^{-1}(e^{A\theta_2} - I)B(c_1 - c_2) \tag{3.7}$$

and, with the help of $y(0) = \dot{y}(\theta_1) = 0$ and $CB = 0$,

$$\begin{gathered} \eta_p = e^{A\theta_1} \rho_p + A^{-1}(e^{A\theta_1} - I)B(c_1 + c_2) \\ C\rho_p = 0, \quad CA\eta_p = 0, \quad CA\rho_p < 0, \quad CA^2\eta_p > 0. \end{gathered} \tag{3.8}$$

We assume in (3.7) and (3.8) that there are no additional switches on intervals $t \in (0; t_1)$ and $t \in (t_1; t_2)$, respectively, since $\dot{y} < 0$ initially and y monotonically decreases from zero and cannot cross zero before $\dot{y}$ changes sign at $t = t_1$. This condition can be easily verified after parameters θ_1 and θ_2 are determined.

We need now to formalize the condition ensuring transition from S_2 to S_3 without leaving R_2. Defining two hypothetical (for the fixed control input $u = c_1 - c_2$) boundary crossing times as $\bar{t}_2$ and t_2, we can write for them:

$$t_2 = \min\left\{t > 0 : C\left(e^{At}\eta_p + A^{-1}(e^{At} - I)B(c_1 - c_2)\right) = 0\right\}$$

and

$$\bar{t}_2 = \min\left\{t > 0 : CA\left(e^{At}\eta_p + A^{-1}(e^{At} - I)B(c_1 - c_2)\right) = 0\right\}.$$

Hence, we require that the following condition holds

$$t_2 < \bar{t}_2 \tag{3.9}$$

to ensure that our analysis of the limit cycle with exactly four switches is correct. In the case when the transition time is sufficiently small, dropping smaller-order terms in the definitions of t_2 and $\bar{t}_2$, one can derive the following simplified approximate algebraic assumption[1]

$$0 < t_2 \approx -\frac{2CA^2\eta_p}{CA^3\eta_p + c_2 - c_1} < \sqrt{\frac{2C\eta_p}{-CA^2\eta_p}} \approx \bar{t}_2.$$

Let us now proceed with defining the amplitude and frequency of the oscillations.

Formulas (3.7) and (3.8) can be considered as a system of algebraic equations for design of the two-relay controller providing for the system (3.1) the desired periodic solution of a given frequency $\boldsymbol{\Omega}$ and amplitude $\boldsymbol{A}_1$. Taking into account that

$$y(\theta_1) = C\eta_p = \boldsymbol{A}_1, \quad \theta_1 + \theta_2 = \pi/\boldsymbol{\Omega} = T/2 \tag{3.10}$$

we can reduce (3.7), (3.8), and (3.10) to a system of five nonlinear algebraic equations with five unknown variables: c_1, c_2, θ_1, and the first and the second coordinates of the vector ρ_p. Once the system of equations is solved, the two-relay controller gains that are found from this solution would provide the desired periodic motion of the system (3.1), unless the corresponding solution encounters singularity of the control transformation. This can be summarized as follows.

Theorem 3.1. *If the system of equations (3.7), (3.8), and (3.10) has an isolated solution satisfying (3.9), the desired amplitude* $\boldsymbol{A}_1$ *is sufficiently small, and there are no additional switches on intervals* $t \in (0; t_1)$ *and* $t \in (t_1; t_2)$*, then the closed-loop system (3.1), (3.12) has the desired periodic solution.*

[1] Here we have used the identities $CA\eta_p = 0$, $CB = CAB = 0$, and $CA^2B = 1$ and dropped the third-order terms in the series expansions for the matrix exponents.

Note, however, that (3.7), (3.8), and (3.10) is a system of nonlinear algebraic equations that might be hard to solve. It may not even have any solutions for particular values of $\boldsymbol{A}_1$ and $\boldsymbol{\Omega}$. This issue requires a special treatment.

It turns out that the linearity of the (transformed) plant and the fact that the control in the periodic motion can be represented as a sum of two relay controls, in which the response of the plant can be found as a linear combination (sum) of the two periodic relay controls of amplitudes c_1 and c_2, allow for a reduction of the complexity of the original problem.

3.3 General Poincaré Map Approach Generated by TRC

Consider the Euler–Lagrange equation [5]

$$M(q)\ddot{q} + N(q, \dot{q}) = Bu, \tag{3.11}$$

where $q(t) \in \mathbb{R}^n$ is the vector of joint positions; $B = [0_{(n-1)} \;\; 1]^T$; $M(q)$ is the $n \times n$ inertia matrix which is symmetric positive definite for all q (see, e.g., [5, p. 67]); $N(q, \dot{q})$ is the $n \times 1$ vector that contains the Coriolis, centrifugal, and gravitational torques; and $u(t) \in \mathbb{R}$ is the two-relay control (TRC) given by

$$u = -c_1 \operatorname{sign}(y) - c_2 \operatorname{sign}(\dot{y}), \tag{3.12}$$

where c_1 and c_2 are parameters designed such that the scalar output of the system

$$y = h(q) \tag{3.13}$$

has a steady periodic motion with desired amplitude and frequency. Here, the parameters c_1 and c_2 are constants to be found via Poincaré maps. It is assumed that velocities $\dot{q}(t) \in \mathbb{R}^n$ of the joints can be measured.

Let us assume without loss of generality that the actuated degrees of freedom are represented by the elements of $\eta = [\eta_1 \;\; \eta_2]^T \in \mathbb{R}^2$ and the unactuated degrees of freedom are represented by the elements of $\nu = [\nu_1 \;\; \nu_2]^T \in \mathbb{R}^{2n-2}$ and let us define the output $y = \eta_1$. Then, system (3.11) can be represented in the state-space form by

$$\begin{bmatrix} \dot{\eta}_1 \\ \dot{\eta}_2 \\ \dot{\nu}_1 \\ \dot{\nu}_2 \end{bmatrix} = \begin{bmatrix} \eta_2 \\ \left\{ \begin{array}{c} \Delta_m^{-1}\{M_{22}(\eta_1, \nu_1)[u - N_1(\eta, \nu)] \\ + M_{12}(\eta_1, \nu_1)N_2(\eta, \nu)\} \end{array} \right\} \\ \nu_2 \\ \left\{ \begin{array}{c} \Delta_m^{-1}\{-M_{12}(\eta_1, \nu_1)[u - N_1(\eta, \nu)] \\ - M_{11}(\eta_1, \nu_1)N_2(\eta, \nu)\} \end{array} \right\} \end{bmatrix} = \begin{bmatrix} \eta_2 \\ f_1(\eta, \nu, u) \\ \nu_2 \\ f_2(\eta, \nu, u) \end{bmatrix} \tag{3.14}$$

where $\Delta_m = M_{11}(\eta_1, \nu_1)M_{22}(\eta_1, \nu_1) - M_{12}(\eta_1, \nu_1)M_{12}(\eta_1, \nu_1)$.

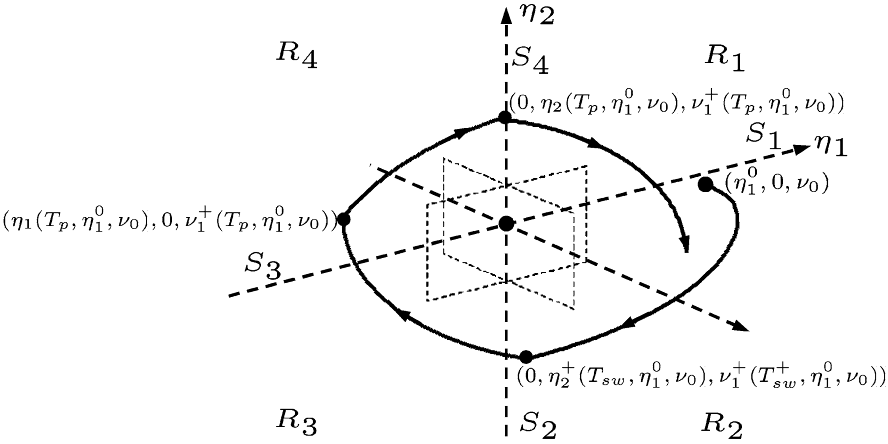

Fig. 3.1 Partitioning of the state space and the Poincaré map

Control law (3.12) exhibits switches on the surface $\eta_1 = 0$ and $\eta_2 = 0$. Let us consider the sets (see Fig. 3.1):

$$\begin{aligned} S_1 &= \{(\eta_1, \eta_2, \nu_1, \nu_2) : \eta_1 > 0, \eta_2 = 0\} \\ S_2 &= \{(\eta_1, \eta_2, \nu_1, \nu_2) : \eta_1 = 0, \eta_2 < 0\} \\ S_3 &= \{(\eta_1, \eta_2, \nu_1, \nu_2) : \eta_1 < 0, \eta_2 = 0\} \\ S_4 &= \{(\eta_1, \eta_2, \nu_1, \nu_2) : \eta_1 = 0, \eta_2 > 0\}. \end{aligned} \tag{3.15}$$

The space $\mathbb{R}^n$ is divided by $S_1, \ldots, S_4$, into four regions $R_1, \ldots, R_4$, as follows:

$$\begin{aligned} R_1 &= \{(\eta_1, \eta_2, \nu_1, \nu_2) : \eta_1 > 0, \eta_2 > 0\}, \\ R_2 &= \{(\eta_1, \eta_2, \nu_1, \nu_2) : \eta_1 > 0, \eta_2 < 0\}, \\ R_3 &= \{(\eta_1, \eta_2, \nu_1, \nu_2) : \eta_1 < 0, \eta_2 < 0\}, \\ R_4 &= \{(\eta_1, \eta_2, \nu_1, \nu_2) : \eta_1 < 0, \eta_2 > 0\} \end{aligned} \tag{3.16}$$

with $f_1 < 0$ for all $\eta_1, \eta_2, \nu, \in R_1 \cup R_2$ and $f_1 > 0$ for all $\eta_1, \eta_2, \nu \in R_3 \cup R_4$. Assume that f_1 and f_2 are differentiable in the set R_i, $i = 1, \ldots, 4$. Moreover, suppose that the values of the functions of f_k, $(k = 1, 2)$ in the sets R_i could be smoothly extended till their closures $\bar{R}_i$. Considering $[\eta_1 \;\; \eta_2]^T$, let us derive the Poincaré map from $\varphi_1(\cdot) = (\eta_1, 0)$, where $\eta_1 > 0$, into $\varphi_2(\cdot) = (0, \eta_2)$, where $\eta_2 < 0$ (see region R_2 in Fig. 3.1). Let $\eta_1^0 > 0$ and denote as

$$\begin{aligned} &\eta_1^+(t, \eta_1^0, \nu^0, c_1, c_2), \; \eta_2^+(t, \eta_1^0, \nu^0, c_1, c_2) \\ &\nu_1^+(t, \eta_1^0, \nu^0, c_1, c_2), \; \nu_2^+(t, \eta_1^0, \nu^0, c_1, c_2) \end{aligned} \tag{3.17}$$

the solution of the system (3.14) with the initial conditions

$$\eta_1^+(0, \eta_1^0, \nu^0, c_1, c_2) = \eta_1^0, \ \eta_2^+(0, \eta_1^0, \nu^0, c_1, c_2) = 0,$$
$$\nu^+(0, \eta_1^{\cdot} \nu^0, c_1, c_2) = \nu^0. \tag{3.18}$$

Let $T_{sw}(\eta, \nu, c_1, c_2)$ be the smallest positive root of the equation

$$\eta_1^+(T_{sw}, \eta_1^0, \nu^0, c_1, c_2) = 0 \tag{3.19}$$

and such that $d\eta_1^+(T_{sw}, \eta_1^0, \nu^0, c_1, c_2)/dt = \eta_2^+(T_{sw}, \eta_1^0, \nu^0, c_1, c_2) < 0$, that is, the functions

$$T_{sw}(\eta_1^0, \nu^0, c_1, c_2), \quad \eta_1^+(T_{sw}, \eta_1^0, \nu^0, c_1, c_2),$$
$$\eta_2^+(T_{sw}, \eta_1^0, \nu^0, c_1, c_2), \quad \nu^+(T_{sw}, \eta_1^0, \nu^0, c_1, c_2),$$

are smooth functions of their arguments.

Now, let us derive the Poincaré map from the sets $\varphi_2(\cdot) = (0, \eta_2, \nu_1^0)$, where $\eta_2 < 0$, into the sets $\varphi_3(\cdot) = (\eta_1, 0, \nu_1^0)$ where $\eta_1 < 0$ (see region R_3 in Fig. 3.1). To this end, denote as

$$\eta_{1p}^+(t, \eta_1^0, \nu^0, c_1, c_2), \ \eta_{2p}^+(t, \eta_1^0, \nu^0, c_1, c_2), \ \nu_p^+(t, \eta_1^0, \nu^0, c_1, c_2), \tag{3.20}$$

the solution of the system (3.14) with the initial conditions

$$\begin{aligned}
&\eta_{1p}^+(T_{sw}^+(\eta_1^0, \nu^0, c_1, c_2), \eta^0, \nu^0, c_1, c_2) = 0,\\
&\eta_{2p}^+(T_{sw}^+(\eta_1^0, \nu^0, c_1, c_2), \eta^0, \nu^0, c_1, c_2) = \eta_2^+(T_{sw}^+(\eta_1^0, \nu^0, c_1, c_2), \eta_1^0, \nu^0, c_1, c_2),\\
&\nu_p^+(T_{sw}^+(\eta_1^0, \nu^0, c_1, c_2), \eta^0, \nu^0, c_1, c_2) = \nu_1^+(T_{sw}^+(\eta_1^0, \nu^0, c_1, c_2), \eta_1^0, \nu^0, c_1, c_2).
\end{aligned} \tag{3.21}$$

Let $T_p^+(\eta, \nu, c_1, c_2)$ be the smallest root satisfying the restrictions $T_p^+ > T_{sw}^+ > 0$ of the equation

$$\eta_{2p}^+(T_p^+, \eta_1^0, \nu^0, c_1, c_2) = 0 \tag{3.22}$$

and such that $d\eta_2^+(T_p^+)/dt = f_1(T_p^+, \eta_1, \eta_2, \nu, c_1, c_2) < 0$, that is, the functions

$$\begin{aligned}
&T_p(\eta_1^0, \nu^0, c_1, c_2), && \eta_1^+(T_p, \eta_1^0, \nu^0, c_1, c_2),\\
&\eta_2^+(T_p, \eta_1^0, \nu^0, c_1, c_2), && \nu_1^+(T_p, \eta_1^0, \nu^0, c_1, c_2),\\
&\nu_2^+(T_p, \eta_1^0, \nu^0, c_1, c_2)
\end{aligned}$$

smoothly depend on their arguments. Therefore, we have designed the map

$$\Xi^{+}(\eta_1^0, \nu^0, c_1, c_2) = \begin{bmatrix} \eta_1^{+}(T_p^{+}(\eta_1^0, \nu^0, c_1, c_2), \eta_1^0, \nu^0, c_1, c_2) \\ \nu^{+}(T_p^{+}(\eta_1^0, \nu^0, c_1, c_2), \eta_1^0, \nu^0, c_1, c_2) \end{bmatrix}. \tag{3.23}$$

The map $\Xi^{-}(\eta_1^0, \nu^0, c_1, c_2)$ of $\varphi_3(\cdot) = (\eta_1, 0, \nu^0)$, $\eta_1 < 0$ together with the time constant $T_p^{+} < T_{sw}^{-} < T_p^{-}$ can be defined by the similar procedure.

Therefore the desired periodic solution corresponds to the fixed point of the Poincaré map

$$\begin{bmatrix} \eta_1^{\star} \\ \nu^{\star} \end{bmatrix} - \Xi^{-}(T_p^{-}, \eta_1^{\star}, \nu^{\star}, c_1, c_2) = 0. \tag{3.24}$$

Finally, to complete the design of periodic solution with desired period $T_p^{-} = 2\pi/\boldsymbol{\Omega}$ and amplitude $\eta_1^{\star} = \boldsymbol{A}_1$, one needs to solve the set of algebraic equations with respect to c_1, c_2, and ν^0:

$$\begin{aligned} \begin{bmatrix} \boldsymbol{A}_1 \\ \nu^{\star} \end{bmatrix} - \Xi^{-}(2\pi/\boldsymbol{\Omega}, \boldsymbol{A}_1, \nu^{\star}, c_1, c_2) &= 0, \\ \eta_{2p}^{-}(2\pi/\boldsymbol{\Omega}, \boldsymbol{A}_1, \nu^{\star}, c_1, c_2) &= 0, \end{aligned} \tag{3.25}$$

where c_1 and c_2, are unknown parameters. Stability of the designed periodic motion can be verified through the following theorem.

Theorem 3.2. *Suppose that for the given value of amplitude $\boldsymbol{A}_1$ and value of frequency $\boldsymbol{\Omega}$, there exist c_1 and c_2 such that the Poincaré map $\Xi(\eta_1^0, \nu^0, c_1, c_2)$ has a fixed point $[\eta_1^{\star}, \nu^{\star}]$, where $T_p^{-} = 2\pi/\boldsymbol{\Omega}$, $\eta_1^{\star} = \boldsymbol{A}_1$, and the condition*

$$\left\| \left. \frac{\partial \Xi^{-}(\eta_1, \nu, c_1, c_2)}{\partial(\eta_1, \nu)} \right|_{(\boldsymbol{A}_1, \nu^{\star})} \right\| < 1 \tag{3.26}$$

holds. Then, the system (3.14) has an orbitally asymptotically stable limit cycle with a desired period $2\pi/\boldsymbol{\Omega}$ and amplitude $\boldsymbol{A}_1$.

3.4 The Inertia Wheel Pendulum—TRC Gains Tuning for Generating SO

Let us consider the dynamic model of the inertia wheel pendulum

$$\begin{bmatrix} J_1 & J_2 \\ J_2 & J_2 \end{bmatrix} \begin{bmatrix} \ddot{q}_1 \\ \ddot{q}_2 \end{bmatrix} + \begin{bmatrix} h \sin q_1 \\ 0 \end{bmatrix} = \begin{bmatrix} 0 \\ 1 \end{bmatrix} \tau. \tag{3.27}$$

As we explain in Subsection 2.6.1, the linearization of the above dynamics results in

$$\begin{bmatrix} \dot{x}_1 \\ \dot{x}_2 \\ \dot{x}_3 \end{bmatrix} = \begin{bmatrix} 0 & 1 & 0 \\ 0 & 0 & 1 \\ -a_0 & -a_1 & -a_2 \end{bmatrix} \begin{bmatrix} x_1 \\ x_2 \\ x_3 \end{bmatrix} + \begin{bmatrix} 0 \\ 0 \\ 1 \end{bmatrix} u, \tag{3.28}$$

$$\dot{p}_1 = -\frac{K}{J_1} p_1 + \frac{1}{J_1} y, \qquad y = \begin{bmatrix} 1 & 0 & 0 \end{bmatrix} x \tag{3.29}$$

where $p_1 = q_1 - \pi + J_1^{-1} J_2 q_2$ and $x_1 = J_1 \dot{q}_1 + J_2 \dot{q}_2 + K p_1$.

Let us begin with the mapping from φ_1 into the set φ_2 where the linearized system (3.28) takes the form

$$\begin{aligned} \frac{dx_1}{dt} &= x_2 \\ \frac{dx_2}{dt} &= x_3 \\ \frac{dx_3}{dt} &= -a_0 x_1 - a_1 x_2 - a_2 x_3 - c_1 + c_2. \end{aligned} \tag{3.30}$$

Solution of (3.30) on the time interval $[0, T_{sw}]$ subject to the initial conditions

$$x_1^+(x^0, c_1, c_2) = x_1^0 > 0, \quad x_2^+(x^0, c_1, c_2) = 0, \quad x_3^+(x^0, c_1, c_2) = x_3^0$$

is given by the following formulas:

$$\begin{aligned} x_1^+ = & \underbrace{-\frac{1}{350} c_1 + \frac{1}{350} c_2}_{\gamma_1} + \underbrace{\left(\frac{1}{150} c_1 - \frac{1}{150} c_2 + \frac{7}{3} x_1^0 + \frac{1}{15} x_3^0 \right)}_{\gamma_2(x_1^0, x_3^0, c_1, c_2)} e^{-10t} \\ & + \underbrace{\left(-\frac{1}{42} c_1 + \frac{1}{42} c_2 - \frac{25}{3} x_1^0 - \frac{1}{6} x_3^0 \right)}_{\gamma_3(x_1^0, x_3^0, c_1, c_2)} e^{-7t} + \underbrace{\left(\frac{1}{50} c_1 - \frac{1}{50} c_2 + 7 x_1^0 + \frac{1}{10} x_3^0 \right)}_{\gamma_4(x_1^0, x_3^0, c_1, c_2)} e^{-5t} \end{aligned} \tag{3.31}$$

$$\begin{aligned} x_2^+ = & -10 \gamma_2(x_1^0, x_3^0, c_1, c_2) e^{-10t} - 7 \gamma_3(x_1^0, x_3^0, c_1, c_2) e^{-7t} \\ & - 5 \gamma_4(x_1^0, x_3^0, c_1, c_2) e^{-5t} \end{aligned} \tag{3.32}$$

$$\begin{aligned} x_3^+ = & \ 100 \gamma_2(x_1^0, x_3^0, c_1, c_2) e^{-10t} + 49 \gamma_3(x_1^0, x_3^0, c_1, c_2) e^{-7t} \\ & + 25 \gamma_4(x_1^0, x_3^0, c_1, c_2) e^{-5t}, \end{aligned} \tag{3.33}$$

where

$$T_{sw}(x_1^0, x_3^0, c_1, c_2) = \ln z \quad (z = e^t) \tag{3.34}$$

is obtained as the smallest positive root of the equation

$$x_1^+(T_{sw}, x_1^0, x_3^0, c_1, c_2) = \gamma_1 z^{10} + \gamma_4 z^5 + \gamma_3 z^3 + \gamma_2 = 0, \tag{3.35}$$

where $\gamma_2 = \gamma_2(x_1^0, x_3^0, c_1, c_2)$, $\gamma_3 = \gamma_3(x_1^0, x_3^0, c_1, c_2)$, and $\gamma_4 = \gamma_4(x_1^0, x_3^0, c_1, c_2)$. Let us proceed with the mapping from φ_2 into φ_3 where the system (3.28) takes the form

$$\begin{aligned} \frac{dx_1}{dt} &= x_2 \\ \frac{dx_2}{dt} &= x_3 \\ \frac{dx_3}{dt} &= -a_0 x_1 - a_1 x_2 - a_2 x_3 + c_1 + c_2. \end{aligned} \tag{3.36}$$

Solution of (3.36) on the time interval $[T_{sw}, T_p]$ subject to the initial conditions

$$\begin{aligned} x_{1sw}^+ &= x_{1p}^+ = 0 \\ x_{2sw}^+ &= x_{2p}^+ = -10\gamma_2 e^{-10T_{sw}} - 7\gamma_3 e^{-7T_{sw}} - 5\gamma_4 e^{-5T_{sw}} \\ x_{3sw}^+ &= x_{3p}^+ = 100\gamma_2 e^{-10T_{sw}} + 49\gamma_3 e^{-7T_{sw}} + 25\gamma_4 e^{-5T_{sw}} \end{aligned}$$

is given by

$$\begin{aligned} x_{1p}^+ = {} & \underbrace{\frac{1}{350}c_1 + \frac{1}{350}c_2}_{\gamma_{1p}} \\ & + \underbrace{\left(-\frac{1}{150}c_1 - \frac{1}{150}c_2 + \frac{4}{5}x_{2sw}^+ + \frac{1}{15}x_{3sw}^+\right)}_{\gamma_{2p}(x_1^0, x_3^0, c_1, c_2)} e^{-10(t-T_{sw})} \\ & + \underbrace{\left(\frac{1}{42}c_1 + \frac{1}{42}c_2 - \frac{5}{2}x_{2sw}^+ - \frac{1}{6}x_{3sw}^+\right)}_{\gamma_{3p}(x_1^0, x_3^0, c_1, c_2)} e^{-7(t-T_{sw})} \\ & + \underbrace{\left(-\frac{1}{50}c_1 - \frac{1}{50}c_2 + \frac{17}{10}x_{2sw}^+ + \frac{1}{10}x_{3sw}^+\right)}_{\gamma_{4p}(x_1^0, x_3^0, c_1, c_2)} e^{-5(t-T_{sw})} \end{aligned} \tag{3.37}$$

$$x_{2p}^+ = -10\gamma_{2p} e^{-10(t-T_{sw})} - 7\gamma_{3p} e^{-7(t-T_{sw})} - 5\gamma_{4p} e^{-5(t-T_{sw})} \tag{3.38}$$

$$x_{3p}^+ = 100\gamma_{2p} e^{-10(t-T_{sw})} + 49\gamma_{3p} e^{-7(t-T_{sw})} + 25\gamma_{4p} e^{-5(t-T_{sw})}, \tag{3.39}$$

where $\gamma_{2p} = \gamma_{2p}(x^0, c_1, c_2)$, $\gamma_{3p} = \gamma_{3p}(x^0, c_1, c_2)$, $\gamma_{4p} = \gamma_{4p}(x^0, c_1, c_2)$, and

$$T_p(x^0, c_1, c_2) = \ln z_p + T_{sw} \quad (z_p = e^{(t-T_{sw})}) \tag{3.40}$$

results are obtained as the smallest positive root of equation

$$x_{2p}^{+}(T_p, x^0, c_1, c_2) = -5\gamma_{4p} z_p^5 - 7\gamma_{3p} z_p^3 - 10\gamma_{2p} = 0. \tag{3.41}$$

Then, the Poincaré map can be written as

$$\begin{aligned} &\Xi_1^{+}(T_p(x^0, c_1, c_2), x^0, c_1, c_2) \\ &= \begin{bmatrix} \gamma_1 + \gamma_2 e^{-10T_p} + \gamma_3 e^{-7T_p} + \gamma_4^{-5T_p} \\ 100\gamma_2 e^{-10T_p} + 49\gamma_3 e^{-7T_p} + 25\gamma_4^{-5T_p}, \end{bmatrix} \end{aligned} \tag{3.42}$$

with the fixed point of this mapping being

$$-\begin{bmatrix} x_1^0 \\ x_3^0 \end{bmatrix} = \Xi_1^{+}(T_p(x^0, c_1, c_2), x^0, c_1, c_2),$$

which yields

$$(x_1^0)^\star = -\frac{\left\{\begin{aligned} \gamma_1 + \left(\frac{1}{150}c_1 - \frac{1}{150}c_2 + \frac{1}{15}x_3^0\right) e^{-10T_p} \\ + \left(-\frac{1}{42}c_1 + \frac{1}{42}c_2 - \frac{1}{6}x_3^0\right) e^{-7T_p} \\ + \left(\frac{1}{50}c_1 - \frac{1}{50}c_2 + \frac{1}{10}x_3^0\right) e^{-5T_p} \end{aligned}\right\}}{1 + \frac{7}{3}e^{-10\Delta T} - \frac{25}{3}e^{-7\Delta T} + 7e^{-5\Delta T}},$$

$$(x_3^0)^\star = -\frac{\left\{\begin{aligned} 100\left(-\frac{1}{150}c_1 - \frac{1}{150}c_2 + \frac{7}{3}x_1^0\right) e^{-10T_p} \\ +49\left(\frac{1}{42}c_1 + \frac{1}{42}c_2 - \frac{25}{3}x_1^0\right) e^{-7T_p} \\ +25\left(-\frac{1}{50}c_1 - \frac{1}{50}c_2 + 7x_1^0\right) e^{-5T_p} \end{aligned}\right\}}{1 + \frac{20}{3}e^{-10\Delta T} - \frac{49}{6}e^{-7\Delta T} + \frac{5}{2}e^{-5\Delta T}},$$

where $\Delta T = T_p - T_{sw}$. To complete the design, one needs to provide the set of equations to find c_1 and c_2 in terms of the known parameters T_p and x_1^0. Toward this end, we obtain from the above equations that c_1 and c_2 are the solutions of the following set of equations:

$$c_2 - c_1 = \frac{\left\{\begin{array}{c} -\left(1+\frac{7}{3}e^{-10T_p}-\frac{25}{3}e^{-7T_p}+7e^{-5T_p}\right)(x_1^0)^\star \\ +\left(-\frac{1}{15}e^{-10T_p}+\frac{1}{6}e^{-7T_p}-\frac{1}{10}e^{-5T_p}\right)(x_3^0) \end{array}\right\}}{\frac{1}{350}-\frac{1}{150}e^{-10T_p}+\frac{1}{42}e^{-7T_p}-\frac{1}{50}e^{-5T_p}}, \tag{3.43}$$

$$c_1 + c_2 = \frac{\left\{\begin{array}{c} -\left(1+\frac{20}{3}e^{-10T_p}-\frac{49}{6}e^{-7T_p}+\frac{5}{2}e^{-5T_p}\right)(x_3^0)^\star \\ +\left(-\frac{700}{3}e^{-10T_p}+\frac{1225}{3}e^{-7T_p}-175e^{-5T_p}\right)(x_1^0) \end{array}\right\}}{-\frac{2}{3}e^{-10T_p}+\frac{7}{6}e^{-7T_p}-\frac{1}{2}e^{-5T_p}}. \tag{3.44}$$

Then, for a given period $T_1 + T_2 = 2\pi/\boldsymbol{\Omega}$ and amplitude $x_1^0 = \boldsymbol{A}_1$ we obtain that

$$c_1 = 2.0623 \qquad \text{and} \qquad c_2 = -2.5258. \tag{3.45}$$

Finally, we need to check the orbital stability, i.e., verify if the following condition holds:

$$\begin{aligned} &\left\| \left. \frac{\partial \Xi_1^+((x_1^0)^\star, (x_3^0)^\star, c_1, c_2)}{\partial(x_1^0, x_3^0)} \right|_{(x_1^0)^\star, (x_3^0)^\star} \right\| = \\ &\left\| \begin{bmatrix} \left.\frac{\partial \Xi_{11}^+((x_1^0)^\star,(x_3^0)^\star,c_1,c_2)}{\partial x_1^0}\right|_{(x_1^0)^\star,(x_3^0)^\star} & \left.\frac{\partial \Xi_{11}^+((x_1^0)^\star,(x_3^0)^\star,c_1,c_2)}{\partial x_3^0}\right|_{(x_1^0)^\star,(x_3^0)^\star} \\ \left.\frac{\partial \Xi_{21}^+((x_1^0)^\star,(x_3^0)^\star,c_1,c_2)}{\partial x_1^0}\right|_{(x_1^0)^\star,(x_3^0)^\star} & \left.\frac{\partial \Xi_{21}^+((x_1^0)^\star,(x_3^0)^\star,c_1,c_2)}{\partial x_3^0}\right|_{(x_1^0)^\star,(x_3^0)^\star} \end{bmatrix} \right\| < 1, \end{aligned} \tag{3.46}$$

where

$$\begin{aligned} &\left. \frac{\partial \Xi_{11}^+((x_1^0)^\star, (x_3^0)^\star, c_1, c_2)}{\partial x_1^0} \right|_{(x_1^0)^\star, (x_3^0)^\star} \\ &\qquad = \left(-10\gamma_2 e^{-10T_p} - 7\gamma_3 e^{-7T_p} - 5\gamma_4 e^{-5T_p}\right) \frac{\partial T_p}{\partial x_1^0} \\ &\qquad\quad + \frac{7}{3}e^{-10T_p} - \frac{25}{3}e^{-7T_p} + 7e^{-5T_p} \\ &\qquad \approx 0.0374, \end{aligned} \tag{3.47}$$

$$
\begin{aligned}
&\left.\frac{\partial \varXi_{11}^{+}((x_1^0)^\star,(x_3^0)^\star,c_1,c_2)}{\partial x_3^0}\right|_{(x_1^0)^\star,(x_3^0)^\star} \\
&\qquad = \left(-10\gamma_2 e^{-10T_p} - 7\gamma_3 e^{-7T_p} - 5\gamma_4 e^{-5T_p}\right)\frac{\partial T_p}{\partial x_3^0} \\
&\qquad\quad + \frac{1}{15}e^{-10T_p} - \frac{1}{6}e^{-7T_p} + \frac{1}{10}e^{-5T_p} \\
&\qquad \approx 5.0153\times 10^{-4},
\end{aligned}
\tag{3.48}
$$

$$
\begin{aligned}
&\left.\frac{\partial \varXi_{21}^{+}((x_1^0)^\star,(x_3^0)^\star,c_1,c_2)}{\partial x_1^0}\right|_{(x_1^0)^\star,(x_3^0)^\star} \\
&\qquad = \left(-1000\gamma_2 e^{-10T_p} - 343\gamma_3 e^{-7T_p} - 125\gamma_4 e^{-5T_p}\right)\frac{\partial T_p}{\partial x_1^0} \\
&\qquad\quad + \frac{700}{3}e^{-10T_p} - \frac{1225}{3}e^{-7T_p} + 175 e^{-5T_p} \\
&\qquad \approx 0.7997,
\end{aligned}
\tag{3.49}
$$

$$
\begin{aligned}
&\left.\frac{\partial \varXi_{21}^{+}((x_1^0)^\star,(x_3^0)^\star,c_1,c_2)}{\partial x_3^0}\right|_{(x_1^0)^\star,(x_3^0)^\star} \\
&\qquad = \left(-1000\gamma_2 e^{-10T_p} - 343\gamma_3 e^{-7T_p} - 125\gamma_4 e^{-5T_p}\right)\frac{\partial T_p}{\partial x_3^0} \\
&\qquad\quad + \frac{20}{3}e^{-10T_p} - \frac{49}{3}e^{-7T_p} + \frac{5}{2}e^{-5T_p} \\
&\qquad \approx -0.0069.
\end{aligned}
\tag{3.50}
$$

The partial derivatives $\partial T_{sw}/\partial x_1^0$, $\partial T_{sw}/\partial x_3^0$, $\partial T_p/\partial x_1^0$, and $\partial T_p/\partial x_3^0$ are given by

$$
\frac{\partial T_{sw}}{\partial x_1^0} = \frac{\frac{7}{3}z^{-11} - \frac{25}{3}z^{-8} + 7z^{-6} - \frac{7}{3}z^{-1} + \frac{25}{3}z^2 - 7z^4}{10\gamma_1 z^9 + 5\gamma_4 z^4 + 3\gamma_3 z^2 + 5\gamma_4 z^{-6} + 7\gamma_3 z^{-8} + 10\gamma_2 z^{-11}} \approx 2.0123
$$

$$
\frac{\partial T_{sw}}{\partial x_3^0} = \frac{\frac{1}{15}z^{-11} - \frac{1}{6}z^{-8} + \frac{1}{10}z^{-6} + \frac{1}{15}z^{-1} - \frac{1}{6}z^2 - \frac{1}{10}z^4}{10\gamma_1 z^9 + 5\gamma_4 z^4 + 3\gamma_3 z^2 + 5\gamma_4 z^{-6} + 7\gamma_3 z^{-8} + 10\gamma_2 z^{-11}} \approx 0.0593
$$

$$\frac{\partial T_p}{\partial x_1^0} = \frac{1}{z_p} \cdot \frac{\left\{ \begin{array}{l} (-\frac{17}{2}z_p^5 + \frac{35}{2}z_p^3 - 8 + \frac{17}{2}z_p^{-5} - \frac{35}{2}z_p^{-7} + 8z_p^{-10})\frac{\partial x_{2sw}^+}{\partial x_1^0} \\ \quad -(\frac{1}{2}z_p^5 - \frac{7}{6}z_p^3 + \frac{2}{3} - \frac{1}{2}z_p^{-5} + \frac{7}{6}z_p^{-7} - \frac{2}{3}z_p^{-10})\frac{\partial x_{3sw}^+}{\partial x_1^0} \end{array} \right\}}{100\gamma_{2p}z_p^{-11} + 49\gamma_{3p}z_p^{-8} + 25\gamma_{4p}z_p^{-6} + 21\gamma_{3p}z_p^2 + 25\gamma_{4p}z_p^4} + \frac{\partial T_{sw}}{\partial x_1^0} \approx 4.2460$$

$$\frac{\partial T_p}{\partial x_3^0} = \frac{1}{z_p} \cdot \frac{\left\{ \begin{array}{l} (-\frac{17}{2}z_p^5 + \frac{35}{2}z_p^3 - 8 + \frac{17}{2}z_p^{-5} - \frac{35}{2}z_p^{-7} + 8z_p^{-10})\frac{\partial x_{2sw}^+}{\partial x_3^0} \\ \quad -(\frac{1}{2}z_p^5 - \frac{7}{6}z_p^3 + \frac{2}{3} - \frac{1}{2}z_p^{-5} + \frac{7}{6}z_p^{-7} - \frac{2}{3}z_p^{-10})\frac{\partial x_{3sw}^+}{\partial x_3^0} \end{array} \right\}}{100\gamma_{2p}z_p^{-11} + 49\gamma_{3p}z_p^{-8} + 25\gamma_{4p}z_p^{-6} + 21\gamma_{3p}z_p^2 + 25\gamma_{4p}z_p^4} + \frac{\partial T_{sw}}{\partial x_3^0} \approx 0.0521.$$

Using (3.46), we obtain

$$\left\| \left. \frac{\partial \Xi_1^+((x_1^0)^\star, (x_3^0)^\star, c_1, c_2)}{\partial(x_1^0, x_3^0)} \right|_{(x_1^0)^\star, (x_3^0)^\star} \right\| = \left\| \begin{bmatrix} 0.0374 & 5.0153 \times 10^{-4} \\ 0.7997 & -0.0069 \end{bmatrix} \right\| = 0.8007,$$

where $\|A\| = \sqrt{\lambda_{\max}\{A^T A\}}$. Therefore, according to Theorem C.1 it is verified that the periodic solution is asymptotically stable.

3.5 Comments

Poincaré map is a recognized method for analysis of the existence of limit cycles in nonlinear systems. In this chapter, Poincaré maps are used for the controller design, particularly for the TRC gain design/tuning. The advantage of Poincaré maps is that one can obtain sufficient and necessary conditions of the existence of periodic solutions exactly. Application of this method to controller design allows one to produce exact values of the TRC gains that ensure the desired periodic motion. Sufficient conditions of local OAS are given too. Moreover, it should be pointed out that Poincaré maps are normally used for analysis of limit cycles in relay feedback systems, but now Poincaré maps are used as a design method. Poincaré map-based design for the two-relay controller gains is proposed in this chapter. Essentially, we deal with the design of a periodic motion in underactuated mechanical systems via generating a self-excited oscillation of a desired amplitude and frequency by means of the TRC but now using Poincaré maps to find the coefficients c_1 and c_2 of the TRC. Therefore, this tool is appropriate to satisfy the goal defined in Chapter 1. Moreover, Poincaré maps provides the values of the controller parameters ensuring the existence of the locally orbitally stable periodic motions for an arbitrary mechanical plant. Experimental verification of the presented results of TRC design for the inertia wheel pendulum is presented below.

Chapter 4
Self-Oscillation via Locus of a Perturbed Relay System Design (LPRS)

Abstract The Poincaré map considered above is a precise tool to find gains of the TRC. The drawback of this approach is in its complexity, which entails extensive computations. This chapter presents an alternative approach—based on the LPRS method, which in the solution of the analysis problem provides exact values of the parameters of self-excited oscillations and a precise solution of the input–output problem, when the plant is linear. Application of this method involved the use of specific computation formulas available within the LPRS method. Unlike other publications on the LPRS method that were focused on analysis, this chapter provides LPRS-based design of self-excited periodic motions. The experiments with inertia wheel pendulum are presented below to illustrate the results of this design.

4.1 Introduction

In Chapter 2, we reviewed the describing function method and its use for the design of TRC. The describing function provides an approximate approach to finding the values of the controller parameters of the TRC from the requirements to the frequency and amplitude of the output signal. Therefore, exact values of the actual frequency and the amplitude would be different from the desired values, if the TRC is designed through the describing function approach. On the other hand, the Poincaré map-based design, given in the previous chapter, provides an exact value of the parameters, but its computation can be complicated and tedious. The locus of a perturbed relay system (LPRS) method presented in this chapter provides an exact solution of the periodic problem in discontinuous control systems, including finding exact values of the amplitude and the frequency of the self-excited oscillation.

Section 4.2 gives introduction to the LPRS and its use for analysis of a system with TRC. Section 4.3 provides the infinite series version of the LPRS analysis for the two-relay controller. In Section 4.4 we solve the inverse problem, that is, the final formulas to compute the gains of the TRC are provided. An example for the inertia wheel pendulum is provided in Section 4.5. In Section 4.6 the linearized Poincaré map-based analysis of orbital stability is given. We conclude the chapter with comments in Section 4.7.

L.T. Aguilar et al., *Self-Oscillations in Dynamic Systems*, Systems & Control: Foundations & Applications, DOI 10.1007/978-3-319-23303-1_4

4.2 LPRS-Based Analysis of a System with TRC

The LPRS method was developed in [13] as a method of analysis and design of relay feedback systems. This method cannot be applied to the system with TRC directly, since the two-relay control assumes a four-level relay control versus two levels of the conventional relay system. However, after some modifications, the methodology of [14] can be used in the considered case too.

The LPRS proposed in [13] provides an exact solution of the periodic and input–output problems in a relay feedback system having a plant

$$\begin{array}{l}\dot{x} = Ax + Bu \\ y = Cx\end{array}, \qquad x \in \mathbb{R}^n, \quad y \in \mathbb{R} \tag{4.1}$$

and the control given by

$$u = \text{sign}(r - y),$$

where $r \in \mathbb{R}$ is the set point (input signal).

Because the subject of our research is self-excited oscillation, we can assume $r = 0$ and disregard for a while input–output properties of the system. Also, the control law under TRC is given as a sum of two discontinuous components:

$$u = -c_1 \,\text{sign}(y) - c_2 \,\text{sign}(\dot{y}). \tag{4.2}$$

We can extend the coverage of the LPRS method in comparison with its original formulation [13] considering the following features of the system. The control provided by TRC can be represented as a sum of two relay controls, and the output of the system can be considered as a superposition of the system reaction to these two relay controls—due to the linear character of the plant. Therefore, as an auxiliary step, let us find the Poincaré map and its fixed point in the system with one relay. Assume that the control is

$$u = -\,\text{sign}(y). \tag{4.3}$$

Then for the part of the period for which $u = 1$, the state vector changes according to

$$x(t) = e^{At}\xi_p + A^{-1}(e^{At} - I)B, \tag{4.4}$$

where ξ_p is the initial value of the state vector.

Assume that a symmetric periodic process of period T occurs in the system (4.1), (4.3). Then at time $t = T/2$ the state vector is

$$x(T/2) = e^{AT/2}\xi_p + A^{-1}(e^{AT/2} - I)B, \tag{4.5}$$

which must be equal to $-\xi_p$ to provide a fixed point of the Poincaré map for the symmetric motion. Therefore, the solution of the equation $-\xi_p = x(T/2)$, where $x(T/2)$ is given by (4.5), provides the fixed point

$$\xi_p = (I + e^{AT/2})^{-1}A^{-1}(I - e^{AT/2})B. \tag{4.6}$$

Now let us introduce a function, which would provide the value of the system output in a periodic motion of the frequency $\omega = 2\pi/T$ at the time $t = \gamma T$, where $t = 0$ corresponds to the control $u(t)$ switch from -1 to $+1$, and $\gamma \in [-1/2; 1/2]$, subject to the control amplitude being $\pi/4$ (this value of the amplitude, which is the ratio between the amplitude of the first harmonic of the square pulse signal and the amplitude of the pulses, is used to comply with the LPRS method [13]). Taking into account (4.4) and (4.5), let us define this function as follows:

$$\begin{aligned} L(\omega, \gamma) &= \frac{\pi}{4}C\{e^{A\gamma T}\xi_p + A^{-1}\left(e^{A\gamma T} - I\right)B\} \\ &= \frac{\pi}{4}C\Big\{e^{A\gamma\frac{2\pi}{\omega}}\left(I + e^{A\frac{\pi}{\omega}}\right)^{-1}A^{-1}\left(I - e^{A\frac{\pi}{\omega}}\right) \\ &\quad + A^{-1}\left(e^{A\gamma\frac{2\pi}{\omega}} - I\right)\Big\}B. \end{aligned} \tag{4.7}$$

Parameter γ is related to θ_1 and θ_2, from the previous chapter, in the following way:

$$\theta_1 = \gamma T$$

and

$$\theta_2 = T/2 - \theta_1 = (0.5 - \gamma)T.$$

Now consider periodic control $u(t)$ as a sum of two periodic square pulse controls $u_1(t)$ and $u_2(t)$ of amplitudes c_1 and c_2, respectively. Assume that control $u_2(t)$ leads with respect to $u_1(t)$ by time $t = \gamma T$, where $\gamma \in [-0.5; 0.5]$. Then for the system output $y(t)$ at the time of the switch from $-c_1$ to $+c_1$ of the control $u_1(t)$, with $y(t)$ being the system response to the periodic control $u(t)$ of frequency $\boldsymbol{\Omega}$, we can write the following formula, which is a superposition of the responses to the two controls:

$$y(0) = \frac{4c_1}{\pi}L(\boldsymbol{\Omega}, 0) + \frac{4c_2}{\pi}L(\boldsymbol{\Omega}, \gamma). \tag{4.8}$$

In the same way, we can write the formula for the derivative of the system output at the time of the switch of the control $u_2(t)$ from $-c_2$ to $+c_2$:

$$\dot{y}(-\gamma T) = \frac{4c_1}{\pi}L_1(\boldsymbol{\Omega}, -\gamma) + \frac{4c_2}{\pi}L_1(\boldsymbol{\Omega}, 0), \tag{4.9}$$

where function L_1 would correspond to the linear plant for the output being the derivative of $y(t)$ and given by $\dot{y} = C\dot{x} = CAx$.

Considering the equations of the closed-loop system (4.1), (4.2), one would notice that the condition $y(0) = 0$ represents the switching condition for the first relay, and the condition $\dot{y}(-\gamma T) = 0$ represents the switching condition for the second relay, which are equations (3.8). Therefore, the fixed point of the Poincaré map for the system (4.1), (4.3) can be written as a set of two algebraic equations with two unknowns $\boldsymbol{\Omega}$ and γ as follows:

$$c_1 L(\boldsymbol{\Omega}, 0) + c_2 L(\boldsymbol{\Omega}, \gamma) = 0 \tag{4.10}$$

$$c_1 L_1(\boldsymbol{\Omega}, -\gamma) + c_2 L_1(\boldsymbol{\Omega}, 0) = 0. \tag{4.11}$$

Representing the periodic solution in the format of the LPRS can simplify the solution of equations (4.10), (4.11). This simplification comes from a specific transformation of the system: we shall consider that the feedback through $\dot{y}(t)$ is closed and the feedback through $y(t)$ is open, thus giving a SISO plant, and find the response of this plant to the discontinuous control of frequencies from a certain frequency range in the same way as it was done for a linear plant. A methodology of analysis similar to the one of [13] can now be used. With this approach, at the step of computation of LPRS, the frequency $\boldsymbol{\Omega}$ is known, which reduces the problem to the solution of one nonlinear algebraic equation for γ. At the second step, after LPRS is computed, the actual frequency $\boldsymbol{\Omega}$ is determined via finding the point of intersection of the LPRS with the real axis (because the relay does not have hysteresis). Considering the definition of LPRS [13] as a function of ω, let us write an expression for the imaginary part of the LPRS as follows:

$$\operatorname{Im} J(\omega) = L(\omega, 0) + \frac{c_2}{c_1} L(\omega, \gamma). \tag{4.12}$$

The value of γ in (4.12) is found from equations (4.10), (4.11), which are reduced to one equation (ω is fixed):

$$\Upsilon(\gamma) = L(\omega, 0) L_1(\omega, -\gamma) - L(\omega, \gamma) L_1(\omega, 0) = 0 \tag{4.13}$$

that can be solved via simple numeric algorithms.

In the present analysis, the real part of LPRS is not used in calculations, as it reflects the transfer properties of relay feedback systems [13], which are not being analyzed. The LPRS analysis of the system would include the steps of finding the value of parameter γ and computing the LPRS point for every frequency ω from the range of interest, plotting the LPRS in the complex plane and finding the point of its intersection with the real axis.

Since function $L(\omega, \gamma)$ provides the value of the system output in a periodic motion at time γT, finding the amplitude of the oscillations is equivalent to finding the maximum of L as follows:

$$\boldsymbol{A}_1 = \max_{t\in[0;T]} \left\{ \frac{4c_1}{\pi} L(\boldsymbol{\Omega}, t/T) + \frac{4c_2}{\pi} L(\boldsymbol{\Omega}, \gamma + t/T) \right\}. \tag{4.14}$$

However, the problem of finding the amplitude can be simplified if instead of the true amplitude given by (4.14) the amplitude of the fundamental frequency (first harmonic) can be used. In this case, using the rotating phasor concept, the control can be represented as a sum of two rotating vectors having amplitudes $4c_1/\pi$ and $4c_2/\pi$, with the angle $2\pi\gamma$ between them. The amplitude of the control vector will be

$$a_u = \frac{4}{\pi}\sqrt{c_1^2 + c_2^2 + 2c_1c_2\cos(2\pi\gamma)} \tag{4.15}$$

and the amplitude of the output (with account of only the first harmonic) will be

$$\boldsymbol{A}_1 \approx \frac{4}{\pi}\sqrt{c_1^2 + c_2^2 + 2c_1c_2\cos(2\pi\gamma)} \quad |W(\boldsymbol{\Omega})|, \tag{4.16}$$

where $\boldsymbol{\Omega}$ is the frequency of the periodic motion and $W(s) = C(sI - A)^{-1}B$ is the transfer function of the plant. It should be noted that this approximation based on the first harmonic is more accurate than the standard describing function approach, used in Chapter 2, because the frequency of the oscillations is computed exactly.

The presented LPRS analysis can be used as a foundation for an alternative design of the gains of the TRC given by (4.2).

4.3 Computation of LPRS for the Two-Relay Controller Based on Infinite Series

The LPRS is defined as a characteristic of the response of a linear part to an unequally spaced pulse control of variable frequency in a closed-loop system [13]. This method requires a computational effort but will provide an exact solution. An infinite series formula for LPRS computation for a conventional linear plant was proposed in [14]. For a conventional linear plant having the transfer function $W(s)$, the LPRS can be computed as follows:

$$J(\omega) = \sum_{k=1}^{\infty}(-1)^{k+1}\operatorname{Re}\{W(jk\omega)\} + j\sum_{k=1}^{\infty}\frac{1}{2k-1}\operatorname{Im}\{W[j(2k-1)\omega]\}. \tag{4.17}$$

The frequency of the periodic motion in the system with the conventional relay control (with an ideal relay) as well as in the system with the TRC algorithm (4.2) can be found from the following equation [13] (see Fig. 4.1):

$$\operatorname{Im} J(\boldsymbol{\Omega}) = 0.$$

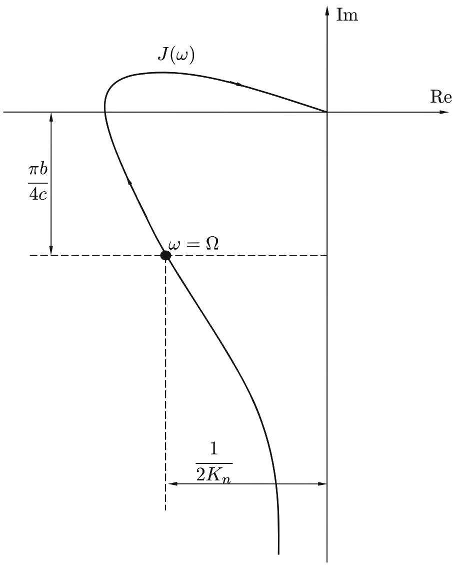

Fig. 4.1 LPRS and oscillation analysis

In fact, we are considering the plant being nonlinear, with the second relay transposed to the feedback in this equivalent plant. Let us rewrite the function $L(\omega)$ that was found instrumental in finding a response of the nonlinear plant to the periodic square-wave pulse control in the format that involves infinite series:

$$\begin{aligned} L(\omega, \gamma) = \sum_{k=1}^{\infty} \frac{1}{2k-1} & (\sin[(2k-1)2\pi\gamma] \operatorname{Re}\{W[(2k-1)\omega]\} \\ & + \cos[(2k-1)2\pi\gamma] \operatorname{Im}\{W[(2k-1)\omega]\}). \end{aligned} \tag{4.18}$$

The function $L(\omega, \gamma)$ denotes a linear plant output (with a coefficient) at the instant $t = \gamma T$ (with T being the period: $T = 2\pi/\omega$) if a periodic square-wave pulse signal of unity amplitude is applied to the plant

$$L(\omega, \gamma) = \left. \frac{\pi y(t)}{4c} \right|_{t=2\pi\gamma/\omega}$$

with $\gamma \in [-0.5, 0.5]$ and $\omega \in [0, \infty]$, where $t = 0$ corresponds to the control switch from -1 to $+1$.

With $L(\omega, \gamma)$ available, we obtain the following expression for $\operatorname{Im}\{J(\omega)\}$ of the equivalent plant:

$$\operatorname{Im}\{J(\omega)\} = L(\omega, 0) + \frac{c_2}{c_1} L(\omega, \gamma). \tag{4.19}$$

The value of the time shift γ between the switching of the first and second relay can be found from the following equation:

$$\dot{y}(\gamma) = 0.$$

As a result, the set of equations for finding the frequency $\boldsymbol{\Omega}$ and the time shift γ is as follows:

$$c_1 L(\boldsymbol{\Omega}, 0) + c_2 L(\boldsymbol{\Omega}, \gamma) = 0 \tag{4.20}$$

$$c_1 L_1(\boldsymbol{\Omega}, -\gamma) + c_2 L_1(\boldsymbol{\Omega}, 0) = 0. \tag{4.21}$$

The amplitude of the oscillations can be found as follows. The output of the system is

$$\begin{aligned} y(t) = \frac{4}{\pi} \sum_{i=1}^{\infty} \{ & c_1 \sin[(2k-1)\boldsymbol{\Omega} + \varphi_L((2k-1)\boldsymbol{\Omega})] \\ & + c_2 \sin[(2k-1)\boldsymbol{\Omega} t + \varphi_L((2k-1)\boldsymbol{\Omega}) \\ & + (2k-1)2\pi\gamma]\} A_L((2k-1)\boldsymbol{\Omega}) \end{aligned} \tag{4.22}$$

where $\varphi_L(\omega) = \arg W(\omega)$, which is a response of the plant to the two square pulse-wave signals shifted with respect to each other by the angle $2\pi\gamma$. Therefore, the amplitude is

$$\boldsymbol{A}_1 = \max_{t \in [0; 2\pi/\omega]} y(t). \tag{4.23}$$

As before, in many situations instead of the true amplitude, we can use the amplitude of the fundamental frequency component (first harmonic) as a relatively precise estimate. In this case, we can represent the input as the sum of two rotating vectors having amplitudes $4c_1/\pi$ and $4c_2/\pi$, with the angle between the vectors $2\pi\gamma$. Therefore, the amplitude of the control signal (first harmonic) is

$$A_u = \frac{4}{\pi} \sqrt{c_1^2 + c_2^2 + 2c_1 c_2 \cos(2\pi\gamma)}, \tag{4.24}$$

and the amplitude of the output (first harmonic) is

$$\boldsymbol{A}_1 = \frac{4}{\pi} \sqrt{c_1^2 + c_2^2 + 2c_1 c_2 \cos(2\pi\gamma)} A_L(\boldsymbol{\Omega}), \tag{4.25}$$

where $A_L(\omega) = |W(j\omega)|$. We should note that despite using approximate value for the amplitude in (4.25), the value of the frequency is exact. Expressions (4.20), (4.25) if considered as equations for $\boldsymbol{\Omega}$ and $\boldsymbol{A}_1$ provide one with mapping F. This mapping is depicted in Fig. 4.2 as curves of equal values of $\boldsymbol{\Omega}$ and $\boldsymbol{A}_1$ in

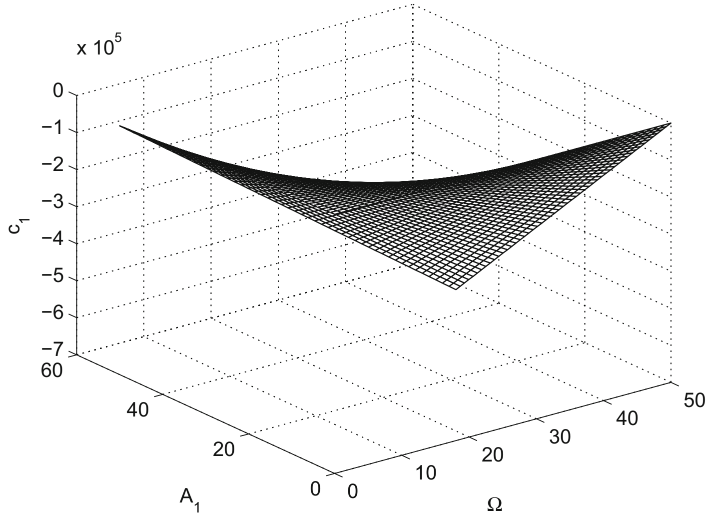

Fig. 4.2 Plot of c_1 vs c_2 for arbitrary frequencies $\boldsymbol{\Omega}_1 < \boldsymbol{\Omega} < \boldsymbol{\Omega}_5$ and amplitudes $a_1 < \boldsymbol{A}_1 < a_{10}$

the coordinates c_1. From (4.20), one can see that the frequency of the oscillations depends only on the ratio $c_2/c_1 = \xi$. Therefore, $\boldsymbol{\Omega}$ is invariant with respect to c_2/c_1: $\boldsymbol{\Omega}(\lambda c_1, \lambda c_2) = \boldsymbol{\Omega}(c_1, c_2)$. It also follows from (4.25) that there is the following invariance for the amplitude: $\boldsymbol{A}_1(\lambda c_1, \lambda c_2) = \lambda \boldsymbol{A}_1(c_1, c_2)$. Therefore, $\boldsymbol{\Omega}$ and $\boldsymbol{A}_1$ can be manipulated independently in accordance with mapping G considered below.

4.4 LPRS as Design Method

It follows from formulas (4.10) and (4.11) that the frequency of the self-excited periodic motions in the two-relay controller is invariant to the ratio c_1/c_2. Therefore, for the desired value of the oscillation frequency $\boldsymbol{\Omega}$, coefficients c_1 and c_2 cannot be determined from (4.10), (4.11) uniquely. Using ξ as the notation for this ratio and applying the desired frequency of oscillations $\boldsymbol{\Omega}$ instead of generic frequency ω, we can rewrite (4.12) as an equation for ξ:

$$\operatorname{Im} J(\boldsymbol{\Omega}) = L(\boldsymbol{\Omega}, 0) + \xi L(\boldsymbol{\Omega}, \gamma) = 0, \tag{4.26}$$

where γ is found from (4.13) at $\omega = \boldsymbol{\Omega}$. With γ computed numerically and

$$\xi = -\frac{L(\boldsymbol{\Omega}, 0)}{L(\boldsymbol{\Omega}, \gamma)}, \tag{4.27}$$

the necessary values of the relay amplitudes that provide the desired frequency $\boldsymbol{\Omega}$ and amplitude $\boldsymbol{A}_1$ of the oscillations are computed as

$$c_1 \approx \frac{\pi}{4} \frac{\boldsymbol{A}_1}{|W(j\boldsymbol{\Omega})|} \frac{1}{\sqrt{1 + 2\xi \cos(2\pi\gamma) + \xi^2}}, \tag{4.28}$$

$$c_2 \approx \frac{\pi}{4} \frac{\boldsymbol{A}_1}{|W(j\boldsymbol{\Omega})|} \frac{\xi}{\sqrt{1 + 2\xi \cos(2\pi\gamma) + \xi^2}}. \tag{4.29}$$

The approximate nature of formulas (4.28) and (4.29) is due to the use of the amplitude of the first harmonic instead of the true amplitude. This approach is acceptable in many applications, as was discussed above.

4.5 The Inertia Wheel Pendulum: Gain Tuning Based on LPRS Design

Let us consider now an inertia wheel pendulum as a plant in the system with TRC algorithm to illustrate the use of the formulas based on the LPRS method. As in the previous chapters, the goal of our design is to compute the values of parameters c_1 and c_2 of the TRC algorithm (4.2). However, this time the design is based on formulas (4.28) and (4.29). Let us start from the linearized model of the IWP (3.27):

$$\begin{bmatrix} \dot{x}_1 \\ \dot{x}_2 \\ \dot{x}_3 \end{bmatrix} = \begin{bmatrix} 0 & 1 & 0 \\ 0 & 0 & 1 \\ -a_0 & -a_1 & -a_2 \end{bmatrix} \begin{bmatrix} x_1 \\ x_2 \\ x_3 \end{bmatrix} + \begin{bmatrix} 0 \\ 0 \\ 1 \end{bmatrix} u, \tag{4.30}$$

$$\dot{p}_1 = -\frac{K}{J_1} p_1 + \frac{1}{J_1} y, \qquad y = \begin{bmatrix} 1 & 0 & 0 \end{bmatrix} x \tag{4.31}$$

where $p_1 = q_1 - \pi + J_1^{-1} J_2 q_2$ and $x_1 = J_1 \dot{q}_1 + J_2 \dot{q}_2 + K p_1$. We select the following desired parameters of the self-excited periodic motion of the pendulum: $\boldsymbol{\Omega} = 2$ rad/s and $\boldsymbol{A}_1 = 0.007$ being the frequency and amplitude, respectively. The constant parameters are $a_0 = 350$, $a_1 = 155$, $a_2 = 22$, $K = 1 \times 10^{-4}$, $J_1 = 4.572 \times 10^{-3}$, and $J_2 = 2.495 \times 10^{-5}$. The corresponding transfer function of the linearized model presented above is

$$W(s) = \frac{1}{s^3 + 22s^2 + 155s + 350}.$$

Figure 4.3 illustrates the LPRS for the linearized model of the inertia wheel pendulum (4.30) highlighting the location of $J(\boldsymbol{\Omega}) = 0.0014 - j0.0022$. We now solve the set of equations (4.12) and (4.13) for the given Ω considering c_2/c_1 and

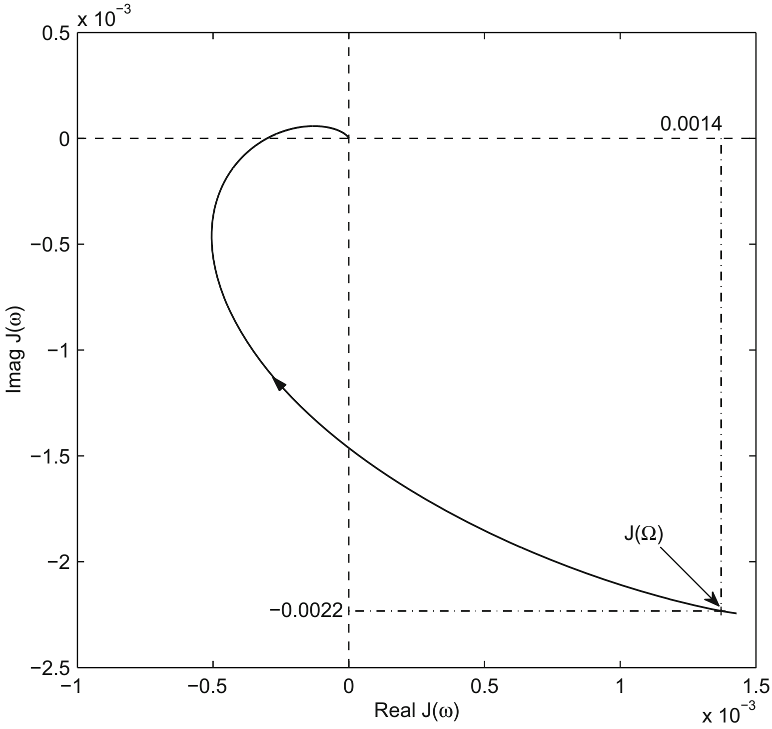

Fig. 4.3 The LPRS for the linearized model of the inertia wheel pendulum

γ as unknown variables. We obtain $\gamma = 0.328$, and using Eq. (4.7), we compute $L(\boldsymbol{\Omega}, 0) = -0.0022$ and $L(\boldsymbol{\Omega}, \gamma) = 0.0021$. Finally, using (4.27)–(4.29), we get

$$c_1 = 2.0626, \quad c_2 = 2.2037. \tag{4.32}$$

4.6 Linearized Poincaré Map-Based Analysis of Orbital Stability

Let us now proceed with the analysis of orbital stability of periodic motions in a system with the TRC algorithm, based on the exact approach provided by the LPRS method. Similar to the results of Chapters 3 and 4, necessary and sufficient conditions for orbital exponential stability of the limit cycle are derived from the analysis of the linearized Poincaré map.

Let us use (3.6) to analyze the deviation of a trajectory initiated on the surface S_1 at $x(0) = \rho_k = \rho_p + \delta_\rho$ from a periodic trajectory corresponding to ρ_p for sufficiently small initial deviations δ_ρ. Using the equation in (3.6) for η_k, the equation in (3.8) for η_p, and the Taylor expansion $e^{At_1} = e^{A\theta_1} + e^{A\theta_1}A\Delta t + O\left(\Delta t^2\right)$, $\Delta t = t_1 - \theta_1$, one can proceed as follows:

$$\begin{aligned}\eta_k &= e^{At_1}(\rho_p + \delta_\rho) + A^{-1}(e^{At_1} - I)B(c_1 + c_2)\\ &= \left(e^{A\theta_1} + e^{A\theta_1}A\Delta t\right)(\rho_p + \delta_\rho) + O\left(\Delta t^2\right)\\ &+ A^{-1}\left(e^{A\theta_1} + (e^{A\theta_1} - I + I)A\Delta t - I\right)B(c_1 + c_2)\end{aligned}$$

so that

$$\eta_k = e^{A\theta_1}\left(\delta_\rho + A\delta_\rho\Delta t\right) + (I + A\Delta t)\eta_p + B(c_1 + c_2)\Delta t + O\left(\Delta t^2\right).$$

Now, since $CA\eta_k = CA\eta_p = 0$, premultiplying the previous equation by CA yields

$$CAe^{A\theta_1}\left(\delta_\rho + A\delta_\rho\Delta t\right) + CA(A\eta_p + B(c_1 + c_2))\Delta t = O\left(\Delta t^2\right).$$

From this equation, one immediately concludes that $\Delta t = O(\delta_\rho)$ and obtains an estimate for $t_1 = \theta_1 + \Delta t$ that can be substituted back as follows:

$$\eta_k = \eta_p + \delta_\eta = \eta_p + \varphi_1\delta_\rho + O(\delta_\rho^2),$$

where

$$\varphi_1 = \left(I - \frac{v_1 CA}{CAv_1}\right)e^{A\theta_1}, \qquad v_1 = A\eta_p + B(c_1 + c_2). \tag{4.33}$$

Following the second equation in (3.6) and computing t_2 using $C\rho_k^- = C\rho_p = 0$, one, in a similar way, obtains

$$\rho_k^- = -\rho_p + \delta_{\rho-} = -\rho_p + \varphi_2\delta_\eta + O(\delta_\rho^2),$$

where

$$\varphi_2 = \left(I - \frac{v_2 C}{Cv_2}\right)e^{A\theta_2}, \qquad v_2 = A\rho_p + B(c_1 - c_2). \tag{4.34}$$

Following the third equation in (3.6) and computing t_3 using $CA\eta_k^- = CA\eta_p = 0$, one obtains

$$\eta_k^- = -\eta_p + \delta_{\eta-} = -\eta_p + \varphi_3\delta_{\rho-} + O(\delta_\rho^2),$$

where $\varphi_3 = \varphi_1$.

Following the last equation in (3.6) and computing t_4 using $C\rho_{k+1} = C\rho_p = 0$, one obtains

$$\rho_{k+1} = \rho_p + \varphi_4 \delta_{\rho-} + O(\delta_\rho^2),$$

where $\varphi_4 = \varphi_2$.

Finally, for small $\delta_\rho = \rho_k - \rho_p$ we can write the following formula: $\rho_{k+1} - \rho_p = \Phi \cdot (\rho_k - \rho_p) + O(\delta_\rho^2)$, with

$$\Phi = (\varphi_2 \cdot \varphi_1)^2. \tag{4.35}$$

Formula (4.35) provides a linearized Poincaré map. Therefore, the conditions of orbital asymptotic stability of the self-excited periodic motions in the system with the TRC algorithm can be formulated as the following theorem, the proof of which is provided above.

Theorem 4.1. *Suppose that the selected parameters c_1 and c_2 of the TRC algorithm (4.2) result in a closed-loop system that generates a periodic motion of the outputs of the plants (2.33), (2.36). This solution is orbitally exponentially stable if and only if all eigenvalues of the matrix Φ, defined by (4.33), (4.34), and (4.35), are located inside the unit circle.*

4.7 Comments

An LPRS-based analysis of a system with the TRC algorithm is presented in this chapter. The LPRS method is extended to the two-relay control. The presented approach provides exact values of the TRC parameters necessary for generation of the desired self-excited periodic motion, for linear plants. The main advantage of the presented approach over the Poincaré map-based design is that simple explicit and exact formulas for the values of the two-relay controller gains can be derived. These formulas are obtained in the chapter. An example of designing a TRC algorithm for an inertia wheel pendulum is presented.

Part II
Robustification of Self-Oscillations Generated by Two-Relay Controller

Chapter 5
Robustification of the Self-Oscillation via Sliding Modes Tracking Controllers

Abstract In this chapter, a strategy was proposed to generate SO in a nonlinear system operating under uncertain conditions. This strategy involves algorithm generating SO using the TRC for a nominal model of the plant, as external generator of reference trajectories. The objective is to design a robust closed-loop system, via variable structure control, capable of tracking such trajectories. Two robust algorithms are revisited: second-order and high-order sliding mode controllers. Stability proof of the closed-loop system with SOSM is also revisited. Results are illustrated on an IWP.

5.1 Introduction

Maintaining a periodic motion of an underactuated pendulum in the upright position around its unstable equilibrium point is a complex task. We show in Chapters 2 through 4 that the two-relay controller produces oscillations in the scalar output of an underactuated system where the desired amplitude and frequency are reached by choosing the controller gains properly. In these chapters, we assume that the system is free from disturbances and friction; however, those assumptions are not realistic for real physical systems. In this chapter, a reference model is developed, based on the two-relay controller, to generate a set of desired trajectories, particularly for the inertia wheel pendulum. After that, a robust tracking controller is designed. Poincaré-map-based design is used to obtain the corresponding parameter values of the TRC. Then a second-order sliding mode tracking controller is used which is capable of tracking the prescribed reference trajectory.

This idea of reference and tracking is illustrated by designing the tracking control for the inertia wheel pendulum under the presence of disturbances and friction using a second-order sliding mode control. It should be pointed out that the tracking control problem for underactuated systems is different from that for fully actuated mechanical systems, where the reference trajectory can be arbitrarily given in its configuration space, because underactuated systems are not full-state feedback linearizable due to insufficient number of actuators. Therefore, a special attention is required in the selection of the desired trajectory for the systems under study.

L.T. Aguilar et al., *Self-Oscillations in Dynamic Systems*, Systems & Control: Foundations & Applications, DOI 10.1007/978-3-319-23303-1_5

Different ideas have been proposed in the literature as Grizzle *et al.* [41] who demonstrate asymptotic tracking for an unactuated link by finding conditions for the existence of a set of outputs that yields a system with a one-dimensional exponentially stable zero dynamics. In Orlov *et al.* [69] and Santiesteban *et al.* [78], an asymptotic harmonic generator was introduced through a modified Van der Pol equation tested on a friction pendulum to solve the swing-up problem for an inverted pendulum.

We start the chapter by describing the reconfiguration of the closed-loop system and synthesis of a second-order sliding mode controller to ensure robustness against disturbances. Section 5.2 gives motivating material about the importance of robustification in the TRC scheme given in Part I. In Section 5.3, the perturbed dynamic model is described and problem formulation is given. In Section 5.4, the reference model with two-relay controller is introduced to generate a set of desired trajectories for the inertia wheel pendulum which oscillates around the upright position, where the equilibrium point is unstable in the absence of feedback. Poincaré maps will be used to compute the coefficients of the TRC. In Section 5.5, we present a sliding mode controller, with a feedback from the rotor velocity, to achieve finite-time exact tracking controller of the desired output against unmatched perturbation. Finally, Section 5.6 illustrates the performance of the algorithm by experiments, and Section 5.7 presents some comments.

5.2 Idea for Robustification

Let us note that in examples presented in Part I, the self-oscillations were generated in an inertia wheel pendulum through the two-relay controller, without tracking control. Consequently, the closed-loop system becomes sensitive to disturbances and uncertainties of the model. The proposed framework for trajectory generation under the same methodology and the robust state-feedback tracking controller and its experimental verification constitute the scope of the chapter. Here, we assume that the deviation of the frequency and amplitude of the periodic trajectory at the output of the closed-loop structure proposed in Chapter 2 with respect to the desired ones depend on the uncertainties of the parameters of the model because computation formulas for the two values of the two-relay controller (c_1 and c_2) include the inertia, length of the link, and masses, only, while viscous friction level is not considered in the formulas, which however exists in the system. Now, the proposed scheme is robust with respect to the effect of the viscous friction and external disturbances which will be rejected using a second-order sliding mode tracking controller.

5.3 Inertia Wheel Pendulum Under Disturbances and Friction

Let us consider the dynamics of an inertia wheel pendulum augmented with viscous friction and disturbances:

$$\begin{bmatrix} J_1 & J_2 \\ J_2 & J_2 \end{bmatrix} \begin{bmatrix} \ddot{q}_1 \\ \ddot{q}_2 \end{bmatrix} + \begin{bmatrix} h \sin q_1 \\ f_s \dot{q}_2 \end{bmatrix} = \begin{bmatrix} 0 \\ 1 \end{bmatrix} \tau + w. \tag{5.1}$$

In the above equation, $f_s > 0$ is the viscous friction coefficient and $w = [w_1 \;\; w_2]^T$ are the external disturbances affecting the system. An upper bound $M_i > 0$ $(i = 1, 2)$ to the magnitude of the disturbances is supposed to be known a priori

$$\sup_t |w_i(t)| \leq M_i, \qquad i = 1, 2. \tag{5.2}$$

The control objective is to find torque τ such that

$$\lim_{t \to \infty} \|q_{1r}(t) - q_1(t)\| = \lim_{t \to \infty} \|\sigma(t)\| = 0 \tag{5.3}$$

where $\sigma(t) \in \mathbb{R}$ stands for the pendulum position error and $q_{1r}(t)$ is the desired trajectory of the pendulum. The desired trajectory is designed such that $q_r(t)$, $\dot{q}_r(t)$, and $\ddot{q}_r(t) \in \mathbb{R}^2$ exist and are bounded.

5.4 Generation of Nominal Trajectories

In this section, we will find the set of trajectories $q_r(t) \in \mathbb{R}^2$ such that the inertia wheel pendulum can follow around its upright position, that is, $\|q_{r_1} - \pi\| \leq \boldsymbol{A}_1$ where $\boldsymbol{A}_1$ is the desired amplitude of the periodic trajectory of the pendulum (q_{r_1}). Let us start by explaining how to find these trajectories. To begin with, let us consider the dynamics of the wheel pendulum in terms of the reference positions and velocities $(q_r, \dot{q}_r)$ without considering the viscous friction force

$$\begin{bmatrix} J_1 & J_2 \\ J_2 & J_2 \end{bmatrix} \begin{bmatrix} \ddot{q}_{1r} \\ \ddot{q}_{2r} \end{bmatrix} + \begin{bmatrix} h \sin q_{1r} \\ 0 \end{bmatrix} = \begin{bmatrix} 0 \\ 1 \end{bmatrix} \tau_r. \tag{5.4}$$

We need to find the reference torque $\tau_r \in \mathbb{R}$ to produce a set of desired periodic motions of the underactuated link $(y = q_{1r})$ such that the output has a periodic motion with desired frequency and amplitude. As will be shown later, account of viscous friction is not required in the above equation since it acts as a damper which helps to achieve asymptotic stability of the closed-loop system. Throughout this chapter, we confine our research to desired oscillations around the upright position of the pendulum which corresponds to the more difficult case due that the open-loop system has an unstable zero dynamics .

Following the procedure described in Section 2.6, we have

$$\tau_r = H^{-1}(q_{1r})\left(u_r - a_0\eta - a_1\dot{\eta} - a_2\ddot{\eta} - R(q_{1r},\dot{q}_{1r})\right), \tag{5.5}$$

where $H(q_r)$ is nonsingular for the equilibrium point $[q_{1r}^\star \;\; \dot{q}_{1r}^\star]^T = [\pi \;\; 0]^T$ and where a_0, a_1, and a_2 are positive constants. Introducing the new state coordinates $x = [x_1 \;\; x_2 \;\; x_3]^T = [\eta \;\; \dot{\eta} \;\; \ddot{\eta}]^T$, we obtain

$$\begin{bmatrix} \dot{x}_1 \\ \dot{x}_2 \\ \dot{x}_3 \end{bmatrix} = \begin{bmatrix} 0 & 1 & 0 \\ 0 & 0 & 1 \\ -a_0 & -a_1 & -a_2 \end{bmatrix} \begin{bmatrix} x_1 \\ x_2 \\ x_3 \end{bmatrix} + \begin{bmatrix} 0 \\ 0 \\ 1 \end{bmatrix} u_r, \tag{5.6}$$

$$\dot{p}_1 = -\frac{K}{J_1}p_1 + \frac{1}{J_1}y_r, \qquad y_r = \begin{bmatrix} 1 & 0 & 0 \end{bmatrix} x. \tag{5.7}$$

The following *two-relay controller* is proposed for the purpose of exciting SO in (5.4):

$$u_r = -c_1\,\mathrm{sign}(y_r) - c_2\,\mathrm{sign}(\dot{y}_r) \tag{5.8}$$

where c_1 and c_2 are scalar parameters designed such that the scalar-valued function output $y_r(t)$ has a periodic motion with the desired frequency $\boldsymbol{\Omega}$ and amplitude $\boldsymbol{A}_1$. Let us note that the difference between (5.8) and the second-order sliding mode controller given, for example, in [53] is that c_1 is not constrained to be positive and greater than c_2.

The gains c_1 and c_2 will be found by Poincaré map-based design given in Chapter 3. To verify the existence of the orbit, the following algebraic equations need to be solved

$$\begin{gathered} \begin{bmatrix} x_1^0 \\ x_3^0 \end{bmatrix} - \Xi^+(2\pi/\boldsymbol{\Omega}, \boldsymbol{A}_1, x^\star, c_1, c_2) = 0 \\ x_{2p}^-(2\pi/\boldsymbol{\Omega}, \boldsymbol{A}_1, x^\star, c_1, c_2) = 0 \end{gathered} \tag{5.9}$$

where

$$\Xi^-(2\pi/\boldsymbol{\Omega}, \boldsymbol{A}_1, x^\star, c_1, c_2) = \begin{bmatrix} x_1^-(T_p^-(x^0, c_1, c_2), x^0, c_1, c_2) \\ x_3^-(T_p^-(x^0, c_1, c_2), x^0, c_1, c_2) \end{bmatrix}. \tag{5.10}$$

Here, $T_p^- = 2\pi/\boldsymbol{\Omega}$, $x_1^\star = \boldsymbol{A}_1$, and $x^0 = (x_1^0, 0, x_3^0)$ are the initial conditions. Precisely, the desired periodic solution corresponds to the fixed point of the Poincaré map

$$\begin{bmatrix} x_1^\star \\ x_3^\star \end{bmatrix} - \Xi(T_p^-, x^\star, c_1, c_2) = 0.$$

The orbital stability of (5.4), (5.8) was verified by using Theorem 3.2.

5.5 Tracking of the SO Generated by the TRC

Since the pendulum is influenced by the acceleration of the wheel, it may happen that the wheel velocity saturates after a while. It is thus desirable to try to achieve the dual goals of stabilizing the pendulum around the desired trajectory and to keep the wheel velocity bounded by introducing a feedback from the rotor velocity. In this section, we will design a feedback law which ensures (5.3) while providing boundedness of $\dot{q}_2(t)$ and attenuating external disturbances where the reference signal $q_r(t) \in \mathbb{R}^2$ is computed online from (5.4), (5.5), and (5.8).

5.5.1 Twisting Tracking Control

The control law is based on the assumption that $q(t) \in \mathbb{R}^2$ and $\dot{q}(t) \in \mathbb{R}^2$ are measurable. Let the tracking error be given by

$$\begin{aligned} \sigma(t) &\triangleq q_{1r}(t) - q_1(t) \\ \dot{\tilde{q}}_2(t) &\triangleq \dot{q}_{2r}(t) - \dot{q}_2(t). \end{aligned} \tag{5.11}$$

Due to (5.1)–(5.8), the error dynamics are then governed by

$$\begin{aligned} \ddot{\sigma} &= \ddot{q}_{1r} + \frac{J_2}{\Delta}\Big(h\sin(q_{1r}-\sigma) - f_s(\dot{q}_{2r} - \dot{\tilde{q}}_2)\Big) - \frac{J_2}{\Delta}(w_1 - w_2) + \frac{J_2}{\Delta}\tau \\ \ddot{\tilde{q}}_2 &= \ddot{q}_{2r} - \frac{J_2}{\Delta}h\sin(q_{1r}-\sigma) + \frac{J_1}{\Delta}f_s(\dot{q}_{2r} - \dot{\tilde{q}}_2) - \frac{1}{\Delta}(J_1 w_2 - J_2 w_1) - \frac{J_1}{\Delta}\tau \end{aligned} \tag{5.12}$$

where $\Delta = (J_1 - J_2)J_2$. Under the following control law,

$$\begin{aligned} \tau = &-\frac{\Delta}{J_2}\Big(\alpha_1 \operatorname{sign}(\sigma) + \alpha_2 \operatorname{sign}(\dot{\sigma}) + \beta_1\sigma + \beta_2\dot{\sigma} - \gamma\operatorname{sign}(\dot{\tilde{q}}_2)\Big) \\ &- h\sin(q_{1r}-\sigma) + f_s(\dot{q}_{2r} - \dot{\tilde{q}}_2) - \frac{\Delta}{J_2}\ddot{q}_{1r} \end{aligned} \tag{5.13}$$

with parameters such that

$$\alpha_1 > \alpha_2 > 2MJ_2\Delta^{-1} + \gamma, \qquad \beta_1, \beta_2, \gamma > 0, \tag{5.14}$$

and using the identity $J_1\ddot{q}_{1r} + J_2\ddot{q}_{2r} = -h\sin(q_{1r})$, the error dynamics (5.12) are feedback transformed to

$$\ddot{\sigma} = -\alpha_1\,\text{sign}(\sigma) - \alpha_2\,\text{sign}(\dot{\sigma}) - \beta_1\sigma - \beta_2\dot{\sigma} + \gamma\,\text{sign}(\dot{\tilde{q}}_2) - \frac{J_2}{\Delta}(w_1 - w_2) \tag{5.15}$$

$$\begin{aligned}\ddot{\tilde{q}}_2 &= \frac{h}{J_2}\sin(q_{1r} - \sigma) - \frac{h}{J_2}\sin(q_{1r}) - \frac{1}{\Delta}(J_1 w_2 - J_2 w_1) \\ &\quad + \frac{J_1}{J_2}\left(\alpha_1\,\text{sign}(\sigma) + \alpha_2\,\text{sign}(\dot{\sigma}) + \beta_1\sigma + \beta_2\dot{\sigma} - \gamma\,\text{sign}(\dot{\tilde{q}}_2)\right).\end{aligned} \tag{5.16}$$

In Theorem 5.1, we will revise that $\|\dot{\tilde{q}}_2\|$ is uniformly bounded. Throughout this chapter, solutions of above system are defined in the sense of Filippov [34] as that of a certain differential inclusion with a multivalued right-hand side.

To verify that $[\sigma^e \;\; \dot{\sigma}^e \;\; \dot{\tilde{q}}_2^e]^T = 0 \in \mathbb{R}^3$ is an equilibrium point of the unperturbed closed-loop system, note from (5.15) that

$$\gamma\,\text{sign}(\dot{\tilde{q}}_2) = \alpha_1\,\text{sign}(\sigma) + \alpha_2\,\text{sign}(0) + \beta_1\sigma.$$

since $\dot{\sigma}^e = 0$. Substituting the above equation into (5.16) together with $\ddot{\tilde{q}}_2 = 0$, we find that $\sigma^e = 0$. Figure 5.1 shows the block diagram of the two-relay controller for real-time trajectory generation for orbital stabilization of inertia wheel pendulum.

Theorem 5.1. *The controller introduced in (5.13) subject to parameters tuning rule (5.14) ensures local asymptotic stability of the equilibrium point* $\varphi^e = [\sigma^e \;\; \dot{\sigma}^e \;\; \dot{\tilde{q}}_2^e]^T = 0 \in \mathbb{R}^3$.

Proof. We break the proof into two steps.
1. Boundedness of trajectories. First, we need to prove that $\dot{\tilde{q}}_2$ does not escape to infinity in finite time. To this end, let us represent (5.15)–(5.16) in the following form:

$$\dot{\varphi} = A\varphi + g(\varphi, w) \tag{5.17}$$

where $\varphi = [\sigma \;\; \dot{\sigma} \;\; \dot{\tilde{q}}_2]^T$ and

$$A = \begin{bmatrix} 0 & 1 & 0 \\ -\beta_1 & -\beta_2 & 0 \\ \frac{J_1}{J_2}\beta_1 & \frac{J_1}{J_2}\beta_2 & 0 \end{bmatrix}, \tag{5.18}$$

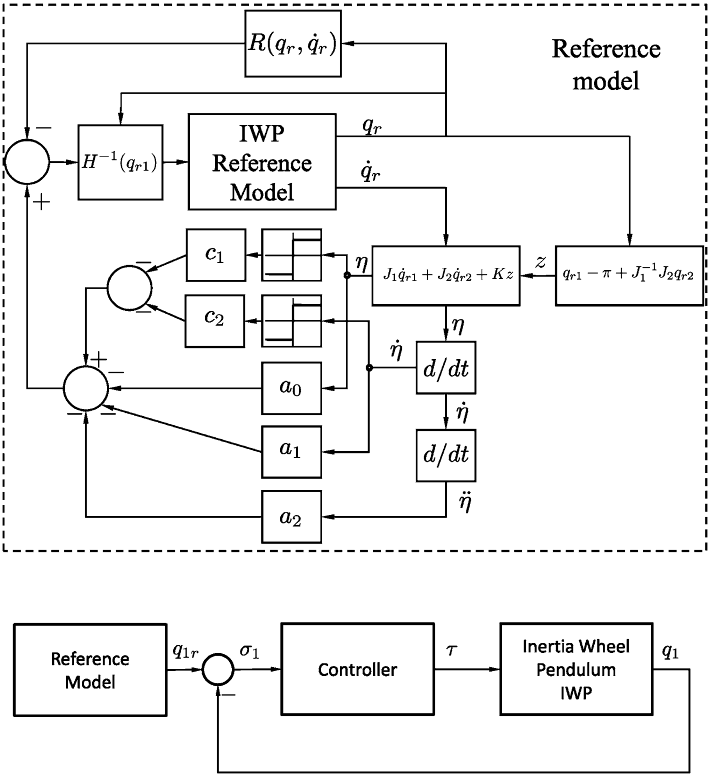

Fig. 5.1 Block diagram of the two-relay controller for real-time trajectory generation for orbital stabilization of inertia wheel pendulum

$$g(\varphi, w) =$$

$$\begin{bmatrix} 0 \\ -\alpha_1 \operatorname{sign}(\sigma) - \alpha_2 \operatorname{sign}(\dot{\sigma}) + \gamma \operatorname{sign}(\dot{\tilde{q}}_2) \\ \frac{h}{J_2}[\sin(q_{1r} - \sigma) - \sin(q_{1r})] + \frac{J_1}{J_2}(\alpha_1 \operatorname{sign}(\sigma) + \alpha_2 \operatorname{sign}(\dot{\sigma}) - \gamma \operatorname{sign}(\dot{\tilde{q}}_2)) \end{bmatrix}$$

$$-\begin{bmatrix} 0 \\ \frac{J_2}{\Delta}(w_1 - w_2) \\ \frac{1}{\Delta}(J_1 w_2 - J_2 w_1) \end{bmatrix}. \qquad (5.19)$$

Consider the following similarity transformation

$$\xi = T^{-1}\varphi \qquad (5.20)$$

where T is any invertible matrix such that $T^{-1}AT$ is a diagonal matrix whose elements are the eigenvalues of A. Substituting (5.17) into the time derivative of (5.20), we obtain

$$\dot{\xi} = \underbrace{T^{-1}AT}_{\overline{A}}\xi + T^{-1}g(T\xi, w) \tag{5.21}$$

where

$$\overline{A} = \begin{bmatrix} -\lambda_1 & 0 & 0 \\ 0 & -\lambda_2 & 0 \\ 0 & 0 & 0 \end{bmatrix}, \qquad T = \begin{bmatrix} -\frac{\lambda_2}{\beta_1} & -\frac{\lambda_1}{\beta_1} & 0 \\ 1 & 1 & 0 \\ -\frac{J_1}{J_2} & -\frac{J_1}{J_2} & 1 \end{bmatrix} \tag{5.22}$$

where

$$\lambda_{1,2} = \frac{1}{2}\beta_2 \mp \frac{1}{2}\sqrt{\beta_2^2 - 4\beta_1}$$

are positive for any positive value of β_1 and β_2. It follows from (5.2) that

$$\frac{J_2}{\Delta}(w_1 - w_2) \leq \frac{J_2}{\Delta}\|w_1 - w_2\| \leq 2\frac{J_2}{\Delta}M$$
$$\frac{1}{\Delta}(J_1w_2 - J_2w_1) \leq \frac{1}{\Delta}\|J_1w_2 - J_2w_1\| \leq 2\frac{J_1}{\Delta}M,$$

therefore, the following upper bound for $g(T\xi)$ is obtained as follows:

$$\|g(T\xi, w)\| \leq \underbrace{\frac{2h}{J_2} + \frac{J_1}{J_2}(\alpha_1 + \alpha_2 + \gamma) + \frac{2J_1}{\Delta}M}_{\varepsilon_0}. \tag{5.23}$$

Note that ε_0 depends on the choice of α_1, α_2, and γ. Consider now the following Lyapunov function

$$V = \frac{1}{2}\xi^T\xi. \tag{5.24}$$

The time derivative of V along the solution of the closed-loop system (5.21)–(5.22) yields

$$\dot{V} = \xi^T\dot{\xi} = \xi^T\overline{A}\xi + \xi^TT^{-1}g(T\xi, w). \tag{5.25}$$

Since $\overline{A}$ is negative semidefinite, we have

$$\dot{V} \leq \|T^{-1}\|\|g(T\xi, w)\|\|\xi\| \leq \varepsilon_0\|T^{-1}\|\|\xi\|. \tag{5.26}$$

Let $W(t)$ be a solution of the differential equation

$$\dot{W} = \varepsilon_0 \|T^{-1}\| \sqrt{2W},\ W(0) = \frac{1}{2}\|\xi(0)\|^2,\ \Rightarrow W(t) = \left(\frac{\sqrt{2}}{2}\varepsilon_0\|T^{-1}\|t + W(0)\right)^2. \tag{5.27}$$

The comparison lemma [49] will be essential in the proof and reads as follows.

Lemma 5.1 (Comparison Lemma). *Consider the scalar differential equation*

$$\dot{u} = f(t,u), \quad u(t_0) = u_0 \tag{5.28}$$

where $f(t,u)$ is continuous in t and locally Lipschitz in u, for all $t \geq 0$ and all $u \in J \subset R$. Let $[t_0, T)$ (T could be infinity) be the maximal interval of existence of the solution $u(t)$, and suppose $u(t) \in J$ for all $t \in [t_0, T)$.Let $v(t)$ be a continuous function whose upper right-hand derivative $D^+v(t)$ satisfies the differential inequality

$$D^+v(t) \leq f(t, v(t)), \quad v(t_0) \leq u_0 \tag{5.29}$$

with $v(t) \in J$ for all $t \in [t_0, T)$. Then, $v(t) \leq u(t)$ for all $t \in [t_0, T)$.

Then, by the comparison lemma, the solution $\varphi(t)$ is defined during the time interval from 0 to t_s and satisfies

$$\|\varphi(t)\| \leq \|T\|\|\xi(t)\| \leq \|T\|\sqrt{2V} \leq \underbrace{\|T\|\left(\varepsilon_0\|T^{-1}\|t_s + \sqrt{2}W(0)\right)}_{\mu}. \tag{5.30}$$

We can conclude that $\varphi(t)$ does not escape to infinity in finite time.
2. Finite-time convergence of $(\sigma, \dot{\sigma})$ to the origin. Now, we will demonstrate that $(\sigma, \dot{\sigma})$ reach the origin asymptotically. To this end, we consider the Lyapunov function

$$V_1 = \frac{1}{2}(\beta_1 + \varepsilon\beta_2)\sigma^2 + \varepsilon\sigma\dot{\sigma} + \frac{1}{2}\dot{\sigma}^2 + \alpha_1|\sigma|$$

which is positive definite and radially unbounded almost everywhere if the constant ε satisfies

$$\frac{1}{2}\beta_2 - \frac{1}{2}\sqrt{\beta_2^2 + 4\beta_1} < \varepsilon < \frac{1}{2}\beta_2 + \frac{1}{2}\sqrt{\beta_2^2 + 4\beta_1}. \tag{5.31}$$

It is straightforward to show that

$$\begin{aligned} \dot{V}_1 \leq & -\varepsilon\beta_1\sigma^2 - (\beta_2 - \varepsilon)\dot{\sigma}^2 - (\alpha_2 - \gamma - 2J_2\Delta^{-1}M)|\dot{\sigma}| \\ & - \varepsilon(\alpha_1 - \alpha_2 - \gamma - 2J_2\Delta^{-1}M)|\sigma|. \end{aligned} \tag{5.32}$$

The function $\dot{V}_1$ will be negative definite provided that (5.14) and $\beta_2 - \varepsilon > 0$ are satisfied. Then, by invoking [67, Th. 4.4] with parameters given in (5.14), it is concluded that (5.3) is reached in finite-time t_s.

Finally, we will prove that $\dot{\tilde{q}}_2$ tends to the origin on the interval $[t_s, \infty)$. To this end, note that the remaining dynamics of the velocity error of the wheel is

$$\ddot{\tilde{q}}_2 = -J_1 J_2^{-1} \gamma \operatorname{sign}(\dot{\tilde{q}}_2).$$

For the Lyapunov function $V_2(\dot{\tilde{q}}_2) = J_1^{-1} J_2 |\dot{\tilde{q}}_2|$, we have

$$\dot{V}_2(\dot{\tilde{q}}_2) = -\gamma.$$

Therefore $\dot{V}_2(\dot{\tilde{q}}_2)$ will be negative definite for all $t \geq t_s$. This completes the proof.

5.5.2 HOSM Tracking Controller

Our goal is to design a controller that ensures exact tracking of q_{1r} in spite of the uncertainty and disturbances present in the real plant with respect to the reference model. Due to some structural properties noted in [41], the inertia wheel pendulum (IWP) model can be transformed to the strict-feedback form. Thus the design algorithm reported in [28] can be applied. Following [41], the strict-feedback form of the IWP model is

$$\begin{aligned}
\dot{z}_1 &= -h \sin(q_1) \\
\dot{q}_1 &= J_1^{-1} z_1 - J_1^{-1} J_2 z_2 \\
\dot{z}_2 &= \frac{h \sin(q_1)}{J_1 - J_2} + \frac{J_1}{J_2(J_1 - J_2)} \tau
\end{aligned} \tag{5.33}$$

where $\dot{q}_2 = z_2$.

The design procedure given in [28, 29] is based on the so-called quasi-continuous HOSM (QC-HOSM) algorithms [54]. The main advantage of these algorithms is that they allow to reduce the gain of the discontinuous control as compared with their direct application. The gain reduction is achieved by constructing virtual controls in which part of the equivalent control is included. It is done through the use of the known nominal part of the system. Due to uncertainties and disturbances, the exact construction of the equivalent control is impossible; nevertheless, a QC-HOSM is also introduced in each virtual control in order to reject those unknown terms. Each virtual control requires some degree of smoothness, determined by its relative degree with respect to the control input, which is achieved via introduction of the discontinuous term through a proper number of integrators which in turn define the order of the QC-HOSM used. For the IWP, the design starts from the state z_2 in

(5.33) as a virtual controller, $\phi_1(q_1)$, for the state q_1, which has relative degree two, of the system (5.33). Since the desired tracking signal is q_{1r}, it has a smooth second derivative and fulfills the smoothness condition for the hierarchic design.
Step 1: The first sliding surface is chosen as $\sigma_1(t) \triangleq q_1(t) - q_{1r}(t)$. The 2-sliding homogeneous quasi-continuous controller is included in $\phi_1(q_1)$

$$\begin{aligned} \phi_1(q_1) &= J_1 J_2^{-1}\{J_1^{-1} z_1 + u_{1,1}\} \\ \dot{u}_{1,1} &= -\alpha_1 \frac{\dot{\sigma}_1 + |\sigma_1|^{1/2}\operatorname{sign}(\sigma_1)}{|\dot{\sigma}_1| + |\sigma_1|^{1/2}}. \end{aligned} \tag{5.34}$$

The derivative $\dot{\sigma}_1$ is calculated by means of the following robust differentiator [53]:

$$\begin{aligned} \dot{s}_0 &= -\lambda_2 L^{1/2}|s_0 - \sigma_1|^{1/2}\operatorname{sign}(s_0 - \sigma_1) + s_1 \\ \dot{s}_1 &= -\lambda_1 L \operatorname{sign}(s_1 - \dot{s}_0). \end{aligned} \tag{5.35}$$

Step 2: Now for state z_2, $\sigma_2 \triangleq z_2 - \phi_1(q_1)$

$$\begin{aligned} \tau &= J_2 J_1^{-1}\{h\sin(q_1) + (J_1 - J_2)u_{2,1}\} \\ u_{2,1} &= -\alpha_2 \operatorname{sign}(\sigma_2). \end{aligned} \tag{5.36}$$

Remark 5.1. Note that in the sliding mode

$$\dot{q}_2 = z_2 = J_1 J_2^{-1}\left\{J_1^{-1} z_1 + \int \dot{u}_{1,1}(s)ds\right\},$$

and due to chattering analysis [55], it can be proved that the term inside the integral is bounded due to the absolute continuity of the desired trajectory. Thus it can be proved that $\dot{q}_2$ remains bounded; nevertheless, the bound depends on the initial conditions $q_1(t_0),\ \dot{q}_1(t_0)$.

5.6 Experimental Study

5.6.1 Experimental Setup

In this section, we present experimental results using the laboratory inertia wheel pendulum manufactured by Quanser Inc., depicted in Figure 2.4 where $J_1 = 4.572\times 10^{-3}$, $J_2 = 2.495 \times 10^{-5}$, and $h = 0.3544$ (see [7]). The viscous friction coefficient $f_s = 8.80 \times 10^{-5}$ was identified by applying the procedure from [48]. The controller was implemented using MATLAB/Simulink® 2007 running on a personal computer with AMD A4-3400, 2.70 GHz, 2 GB processor. The resolution of each encoder is 1000 counts/rev. The PCI Multifunction I/O board *Sensoray 626* from Sensoray was used for the real-time control system, and it consists of four channels of 14-bit D/A outputs and six quadrature 24-bit encoders. The resolution of each encoder is 1000 counts/rev. The amplifier of the motor accepts a control input from the D/A converter in the range of ± 10 V. The sampling time was 1×10^{-3} s.

5.6.2 Experimental Results

Experiments were carried out to achieve the orbital stabilization of the unactuated link (pendulum) q_1 around the equilibrium point $q^{\star} = [\pi \;\; 0]^T$. The parameters of the linearized systems are $K = 1 \times 10^{-4}$, $a_0 = 350$, $a_1 = 155$, and $a_2 = 22$ that were chosen to have a matrix A, in (5.6), (5.7), with negative and real eigenvalues which simplifies analytical computation of the solution for the system of differential equations. Setting $\boldsymbol{\Omega} = 2\pi$ rad/s and $\boldsymbol{A}_1 = 0.07$ as desired frequency and amplitude, respectively, we have $c_1 = 2$ and $c_2 = -2.5$ which have been computed via Poincaré map-based design (5.9). Details on the computation of c_1 and c_2 are given in Chapter 3. The reference signal is shown in Figure 5.2.

The initial conditions for the inertia wheel pendulum, selected for the simulations, were $q_1(0) = 3$ rad and $q_2(0) = 0$ rad, whereas all the velocity initial conditions were set to $\dot{q}_1(0) = \dot{q}_2(0) = 0$ rad/s. The controller gains were selected as follows: $\alpha_1 = 4$, $\alpha_2 = 2$, $\beta_1 = 260$, $\beta_2 = 60$, and $\gamma = 0.15$.

Experimental results for the inertia wheel pendulum, driven by the sliding mode tracking controller (5.13), are presented in Figure 5.3(a) for the disturbance-free case and 5.3(b) for the perturbed case. In order to test the robustness of the orbitally

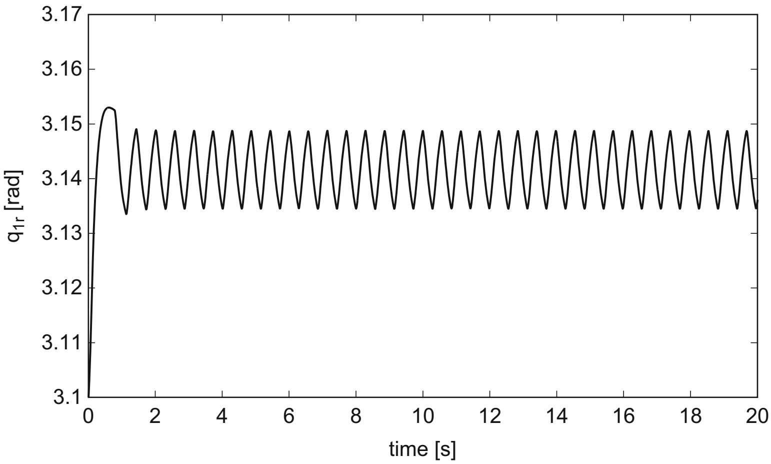

Fig. 5.2 Periodic reference signal at $\boldsymbol{\Omega} = 2\pi$ rad/s and $\boldsymbol{A}_1 = 0.07$ generated by the two-relay controller reference model under the parameters $c_1 = 2$, $c_2 = -2.5$, $K = 1 \times 10^{-4}$, $a_0 = 350$, $a_1 = 155$, and $a_2 = 22$

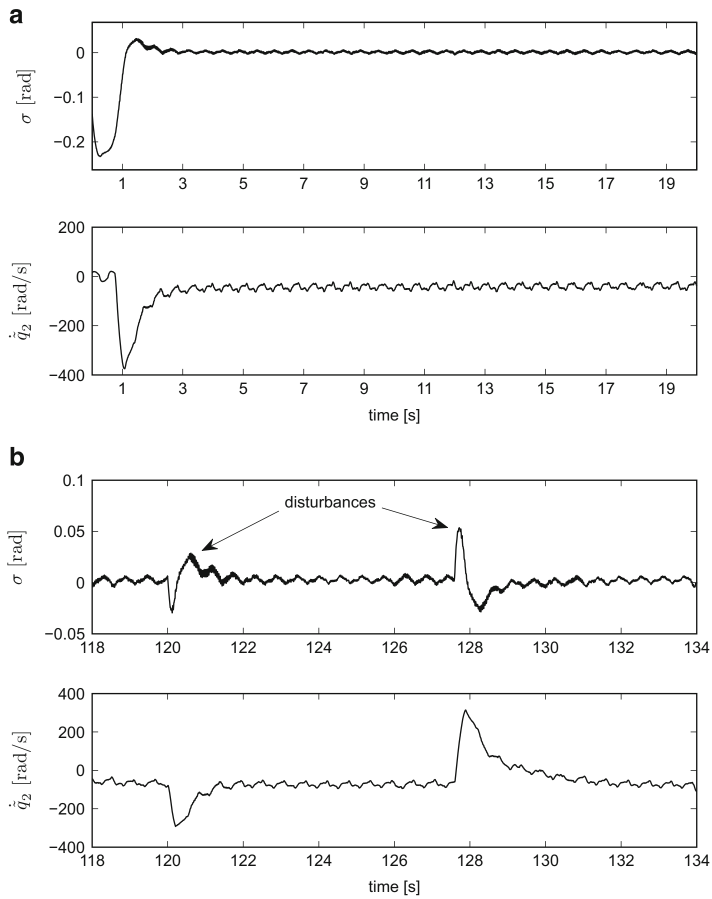

Fig. 5.3 Tracking error of the underactuated link σ and velocity error of the disk ($\dot{\tilde{q}}_2$) without disturbances (**a**) and with random disturbances (**b**)

stabilizing controller (5.13), external disturbances were randomly added by lightly hitting the pendulum at time instants $t_1 \approx 120$ s and $t_2 \approx 128$ s. Figure 5.4 shows the response of the closed-loop system to these disturbances under $\gamma = 0$ where velocity of the motor is higher than 822 rad/s, which is the maximum motor speed.

5.7 Comments and Remarks

A state-feedback sliding mode tracking control problem for underactuated mechanical systems is presented in this chapter. The self-oscillations to be tracked were obtained using TRC for the nominal system. The desired trajectory is of the

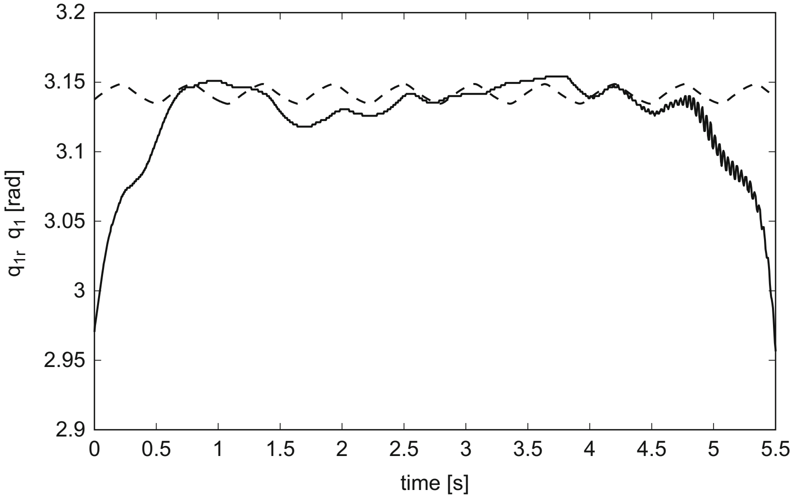

Fig. 5.4 Time response of the underactuated link q_1 around the desired trajectory (dashed) under $\gamma = 0$

pendulum centered at the upright position, where the open-loop plant becomes a non-minimum-phase system. The idea was applied to the IWP in an upright position. The developed sliding mode controllers drive the trajectories of the IWP into a set of inverted desired trajectories which have been generated by a IWP reference model governed by the TRC. The parameters of the controller were found by using Poincaré map-based design. Two important features were obtained: a) the rejection of the viscous friction effects and external disturbances and b) imperfections due to uncertainties in the desired computed self-excited oscillation were avoided since the trajectory was generated for the output of the inertia wheel pendulum reference model plus the two-relay controller dynamics. Stability analysis of the closed-loop system was verified through Lyapunov stability theorems. Experimental verification is implemented for a laboratory prototype. It demonstrates the effectiveness of the developed approach.

Chapter 6
Output-Based Robust Generation of Self-Oscillations via High-Order Sliding Modes Observer

Abstract In this chapter, a high-order sliding mode (HOSM) observer is used to estimate the states of the system and identify the theoretically exact uncertainties/perturbations in finite time. After that, the estimated values of uncertainties are used for compensation. This scheme is used for output-based SO generation considering a TRC and a linearized model of the plant. The proposed scheme ensures robust oscillations with prescribed amplitude and frequency for the real system. The theoretical results are illustrated by simulations in an inverted wheel pendulum.

6.1 Introduction

The approach proposed in Chapters 3–4 is used for the generation of desired self-oscillation in linear time-invariant systems. Some linearization of system in this case is needed. The linearization could be exact as in [41] or local (not exact) [46]. However, all types of linearization strategies rely on the availability of a model which perfectly match the real system. In other words, it cannot deal with uncertainties. Moreover, the aforementioned methods consider that the full state is accessible.

The usage of high-order sliding mode (HOSM) observer allows theoretically exact estimation of the states for strongly observable systems with bounded unknown inputs. Moreover, for the strongly observable systems with Lipschitz uncertainties/perturbations, HOSM observers are able to identify theoretically exactly uncertainties/perturbations [9].

Moreover, the identified values of uncertainties/perturbations when they are matched can be used for robustification of predesigned system trajectory [32].

In this chapter, we will use the HOSM observers for robustification of desired SO designed with methodology of Chapters 3 and 4. Thus, the proposed approach ensures robust generation of self-oscillations with desired frequency and magnitude in the presence of matched uncertainties/perturbations and linearization errors.

L.T. Aguilar et al., *Self-Oscillations in Dynamic Systems*, Systems & Control: Foundations & Applications, DOI 10.1007/978-3-319-23303-1_6

The following methodology is used in this chapter:

- The original model of the system should be linearized.
- The gains of the TRC, tuned by methods of Chapters 3 and 4 to generate nominal SO with desired period and amplitude.
- A theoretically exact and finite-time estimation of the state and identification of the uncertainties/perturbations is carried by means of an HOSM observer.
- The estimated state and identified uncertainties are used to counteract matched uncertainties/perturbations and linearization errors.

This chapter is organized as follows. Section 6.2 is devoted to the presentation of the HOSM observer for the state estimation and unknown inputs identification. This section also motivates the problem about the designed formulas for the TRC (2.14)–(2.15) to obtain the desired frequency and amplitude oscillations based on LPRS methodology for an unperturbed nominal system. Additionally, robust exact compensation-based linearization controller is synthesized. We illustrate the results for the inertia wheel pendulum in Section 6.3. Performance issue of the robust two-relay controller is illustrated in a simulation study in Section 6.4. Finally, in Section 6.5, some concluding remarks are given.

6.2 HOSM Observation and Uncertainties Compensation

Let us consider the nonlinear time-invariant system

$$\begin{aligned} \dot{x} &= f(x) + g(x)(\tau + w) \\ y_m &= h(x) \end{aligned} \tag{6.1}$$

where x is the state, $y_m \in \mathbb{R}^p$ $(p < n)$ is the measured output and it is the only information available for feedback, $\tau \in \mathbb{R}$ is the control input, $w \in \mathbb{R}$ is the disturbance vector, and $f(x)$ is a locally Lipschitz function. Hereinafter, it is assumed that $w(t)$ is uniformly bounded, that is, there exists a constant $w^+ > 0$ such that

$$|w| \leq w^+, \quad |\dot{w}(t)| \leq w^+, \forall t \geq 0. \tag{6.2}$$

It is also assumed that $f(0) = 0$ and $h(0) = 0$.

Due to the criteria for using any method for computing the gains of the TRC, let us consider the linearized system

$$\begin{aligned} \dot{x} &= Ax + B\tau + Bw \\ y &= Cx \end{aligned} \tag{6.3}$$

for the system (6.1) where

$$A = \frac{\partial f}{\partial x}(0), \quad B = g(0), \quad C = \frac{\partial h}{\partial x}(0). \tag{6.4}$$

Here, A, B, and C are matrices with nominal parameters. Let us assume that the triplet (A, C, B) does not contain invariant zeros. Thus an unknown input observer can be constructed (see Bejarano and Fridman [9] for further details).

First, a dynamic auxiliary system is proposed to bound the observation error, i.e., $\dot{\tilde{x}} = A\tilde{x} + Bu + L(y_m - C\tilde{x})$, $\tilde{x} \in \mathbb{R}^n$; the gain L is designed such that $\tilde{A} := A - LC$ is Hurwitz. Let $e = x - \tilde{x}$ whose dynamics follows

$$\dot{e} = \tilde{A}e + Bw \tag{6.5}$$

with $y_e = Ce$.

Now, the error vector will be represented as an algebraic expression of the output and its derivatives. To this aim, a decoupling algorithm is involved in order to get rid of the effects of the unknown input vector w.

Starting with $M_1 := C$ and $J_1 := (M_1B)^{\perp}$, let M_κ be defined in a recursive way in the following form:

$$M_\kappa = \begin{bmatrix} (M_{\kappa-1}B)^{\perp} M_{\kappa-1}\tilde{A} \\ M_1 \end{bmatrix} \;\; J_{\kappa-1} = (M_{\kappa-1}B)^{\perp} \begin{bmatrix} J_{\kappa-2} & 0 \\ 0 & I_p \end{bmatrix}.$$

Due to (A, B, C) does not contain invariant zeros, there exists a unique positive integer $\kappa \leq n$ such that the matrix M_κ generated recursively satisfies the condition $rank(M_\kappa) = n$ (see [9]). Therefore, the following algebraic expression can be constructed:

$$e = \frac{d^{\kappa-1}}{dt^{\kappa-1}} \underbrace{M_\kappa^{+} \begin{bmatrix} J_{\kappa-1} & 0 \\ 0 & I_p \end{bmatrix} \begin{bmatrix} y_e \\ \vdots \\ y_e^{[\kappa-1]} \end{bmatrix}}_{Y} \tag{6.6}$$

where

$$y_e^{[i]} = \int_0^t \cdots \int_0^{\tau_i} y_e d\tau_i \cdots dt.$$

Thus, a real-time HOSM differentiator is used to provide finite time differentiation of Y; see (D.6). It is given by

$$\begin{aligned} \dot{z}_{i,0} &= \lambda_0 \Gamma^{\frac{1}{\kappa}} |z_{i,0} - Y_i|^{\frac{\kappa}{\kappa+1}} \operatorname{sign}(z_{i,0} - Y_i) + z_{i,1} \\ \dot{z}_{i,j} &= \lambda_j \Gamma^{\frac{1}{\kappa-j}} |z_{i,j+1} - \dot{z}_{i,j-1}|^{\frac{\kappa-j}{\kappa}} \operatorname{sign}(z_{i,j} - \dot{z}_{i,j-1}) + z_{i,j+1} \\ \dot{z}_{i,\kappa} &= \lambda_\kappa \Gamma \operatorname{sign}(z_{i,\kappa} - \dot{z}_{i,\kappa-1}) \end{aligned} \tag{6.7}$$

with $j = \overline{1, \kappa - 1}$, κ is the differentiator order. The differentiator input Y_i for $i = \overline{1, n}$ represents the components of Y. The gain Γ is a Lipschitz constant of $Y^{(\kappa)}$, that is, $|\ddot{e}| < \Gamma$.

Hence, the vector e in (6.6) is recovered from the $(\kappa - 1)$-th sliding dynamics, that is, $e = z_{\kappa-1}$ holds for $t \geq T$. Consequently, the next expression holds:

$$\hat{x} := z_{\kappa-1} + \tilde{x} \tag{6.8}$$

where $\hat{x} \in \mathbb{R}^n$ is the estimated value of x for all $t \geq T$.

6.2.1 Generation of SO in a Nominal System

Consider the linearized plant given by

$$\begin{aligned} \dot{x} &= Ax + B(u + w) \\ y_o &= h_o(x) \end{aligned} \tag{6.9}$$

where $x \in \mathbb{R}^n$ is the state vector, $y_o \in \mathbb{R}$ is the oscillating output, and $u \in \mathbb{R}$ is the two-relay input control given by

$$u = -c_1 \operatorname{sign}(y_o) - c_2 \operatorname{sign}(\dot{y}_o). \tag{6.10}$$

Matrices A, B, and C are of appropriated dimensions, and c_1 and c_2 are scalar parameters. Let us assume that matrix A has no eigenvalues at the imaginary axis and the relative degree of (6.9) is greater than one.

The goal is to obtain the values of the gains c_1 and c_2 in the TRC (6.10) to provide a prescribed oscillation at the output of the system with the desired amplitude $\boldsymbol{A}_1$ and frequency $\boldsymbol{\Omega}$ in spite of the existing matched disturbances w. Since the LPRS formulas (4.28)–(4.29) depend on the parameters of the plant, consequently, a deviation in any parameter of the real plant or non-considered dynamics results in discrepancies of the output with respect to the expected frequency and amplitude of the oscillation.

Here, the LPRS-based design from Chapter 4 is performed to specify the TRC parameter values in order to get oscillations of desired amplitude and frequency. In order to obtain the desired amplitude and frequency by means of the LPRS method, it is required a linear model of the plant which is typically nonlinear. For that reason, a robust algebraic observer is designed to estimate the states and identify the discrepancies between the real nonlinear plant and the linearized model.

6.2.2 Uncertainties Compensation

Consider the observation error dynamics (6.5), where $\dot{e}$ can be obtained from the HOSM differentiator (6.7), i.e., the equality $z_\kappa = \dot{e}$ is accomplished for all $t > T$. Hence, working out (6.5), it yields to

$$\hat{w} = B^+(z_\kappa - \tilde{A} z_{\kappa-1}) \tag{6.11}$$

where $\hat{w} \in \mathbb{R}^m$ represents the identified value of w.

Theorem 6.1. *Consider the output-based two-relay controller (6.10) plus a disturbance compensator $\hat{w}$*

$$\tau = -c_1 \operatorname{sign}(y_o) - c_2 \operatorname{sign}(\dot{y}_o) - \hat{w} \tag{6.12}$$

for the nonlinear system (6.1) where $\hat{w}$ is governed by the disturbance observer (6.11). Then, the closed-loop system (6.1), (6.10) has a robust oscillation against matched disturbances.

6.3 Application to the Inertia Wheel Pendulum

We first rewrite the model (5.1) in the state-space form (6.1) with $x(t) = [q_1 \ q_2 \ \dot{q}_1 \ \dot{q}_2]^T$. Hence, by means of Taylor expansion around the upright equilibrium point $x^* = [\pi \ 0 \ 0 \ 0]^T$, it yields to

$$\dot{x} = \underbrace{\begin{bmatrix} 0 & 0 & 1 & 0 \\ 0 & 0 & 0 & 1 \\ \frac{h}{J_1 - J_2} & 0 & 0 & 0 \\ -\frac{h}{J_1 - J_2} & 0 & 0 & 0 \end{bmatrix}}_{A} x + \underbrace{\begin{bmatrix} 0 \\ 0 \\ -\frac{1}{J_1 - J_2} \\ \frac{J_1}{J_2(J_1 - J_2)} \end{bmatrix}}_{B} (\tau + w) \tag{6.13}$$

$$y_m = \underbrace{\begin{bmatrix} 1 & 0 & 0 & 0 \\ 0 & 1 & 0 & 0 \end{bmatrix}}_{C} x. \tag{6.14}$$

The parameters of the IWP are $J_1 = 4.572 \times 10^{-3}$, $J_2 = 2.495 \times 10^{-5}$, and $h = 0.4594$ (see [12]).

Note that the triplet (A, C, B) does not contain invariant zeros and $\kappa = 2$. Therefore, an unknown input observer can be constructed. First, a Luenberger observer is necessary to bound the error trajectories. The observer gain

$$L = \begin{bmatrix} 42 & 0 \\ 0 & 6 \\ 541.0325 & 0 \\ -101.0325 & 8 \end{bmatrix}$$

is such that the eigenvalues of $\tilde{A}$ are $[-4 \ \ -2 \ \ -22 \ \ -20]$.

The system (6.14) has a canonic observability form. That is why the usage of the decoupling algorithm is not needed. This means that the procedure of HOSM observer design is reduced to application of the second-order HOSM differentiator to the Luenberger auxiliary system bounding observation error. As a consequence, the differentiator input $Y(t)$ yields to

$$Y(t) = \begin{bmatrix} 0 & 0 & 1 & 0 \\ 1 & 0 & 25.6 & 0.9 \\ 0 & 0 & 0 & 1 \\ 0 & 1 & 1.06 & 22.3 \end{bmatrix} \begin{bmatrix} y_e \\ \int_0^t y_e(\tau)d\tau \end{bmatrix}.$$

The second-order HOSM differentiator is given by

$$\begin{aligned} \dot{z}_0 &= \lambda_0 \Gamma^{\frac{1}{3}} |z_0 - Y|^{\frac{2}{3}} \operatorname{sign}(z_0 - Y) + z_1 \\ \dot{z}_1 &= \lambda_1 \Gamma^{\frac{1}{2}} |z_1 - \dot{z}_0|^{\frac{1}{2}} \operatorname{sign}(z_1 - \dot{z}_0) + z_2 \\ \dot{z}_2 &= \lambda_2 \Gamma \operatorname{sign}(z_2 - \dot{z}_1). \end{aligned} \tag{6.15}$$

For our case, the HOSM gains are $\Gamma = 83.9 \times 10^3$ and $\lambda_i = \{1.1, 1.5, 2\}$. Theorem 6.1 ensures robustness of the generated SO in the system (6.1), (6.10).

Figure 6.1 shows a block diagram summarizing the proposed method. Starting from the nonlinear model affected by uncertainties, a HOSM observer is designed to estimate the state and perturbations. Such values are involved in the synthesis of a robust exact linearization control law.

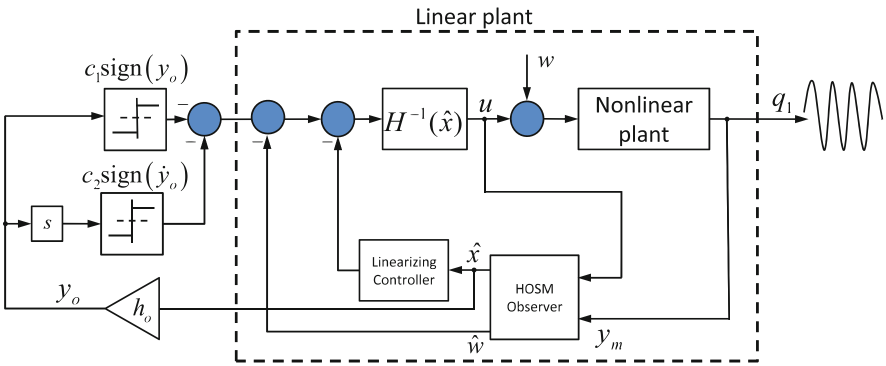

Fig. 6.1 Synthesis of the self-oscillation generation procedure

6.4 Simulation Results

Simulations were carried out to achieve periodic motion in an IWP. We seek for orbital stabilization of the non-actuated link q_1 (pendulum) around the equilibrium point $x^{\star} = [\pi \;\; 0 \;\; 0 \;\; 0]^T$.

Setting $\boldsymbol{\Omega} = 2\pi$ rad/s and $\boldsymbol{A}_1 = 0.07$ as desired frequency and amplitude, respectively, we have $c_1 = 2$ and $c_2 = -2.5$. Figure 6.2 depicts the results when an unknown viscous friction is acting on the actuator. Without identification and compensation of its effects, the oscillation achieved is far from the desired one (dotted line). On the other hand, when the unknown viscous friction $w(t) = 0.1\dot{q}(t)$ is identified and compensated, the output oscillation has the prescribed amplitude and frequency. Figure 6.3 shows self-oscillation generation under a periodic perturbation $w(t) = 0.1\sin(1.3t)$. Dotted line shows the results when a robust linearization technique based on disturbance identification is applied, and solid line shows the oscillation when disturbance is not compensated. It can be noticed in both figures the effectiveness of the disturbance identification via HOSM.

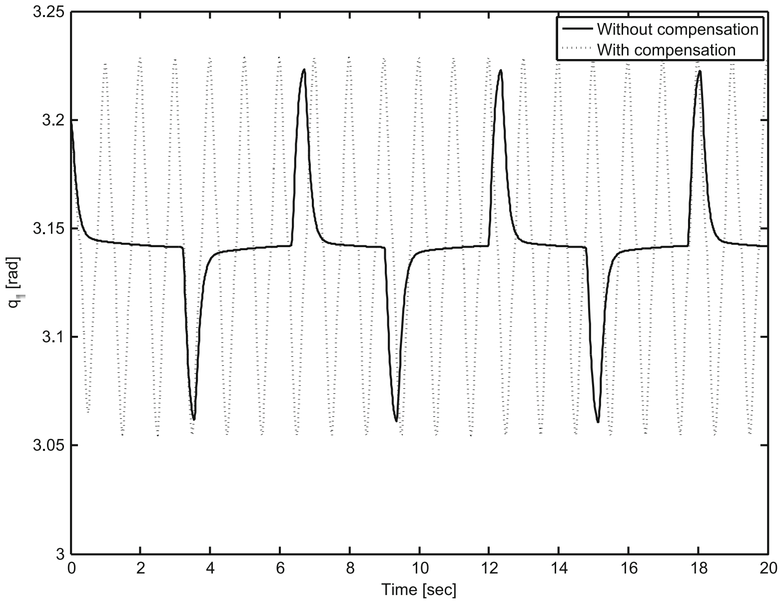

Fig. 6.2 Self-oscillation generation under the presence of viscous friction ($w = 0.1\dot{q}$). Dotted line shows the results when a robust linearization technique based on disturbance identification is applied, and solid line shows the oscillation when the viscous friction is not compensated

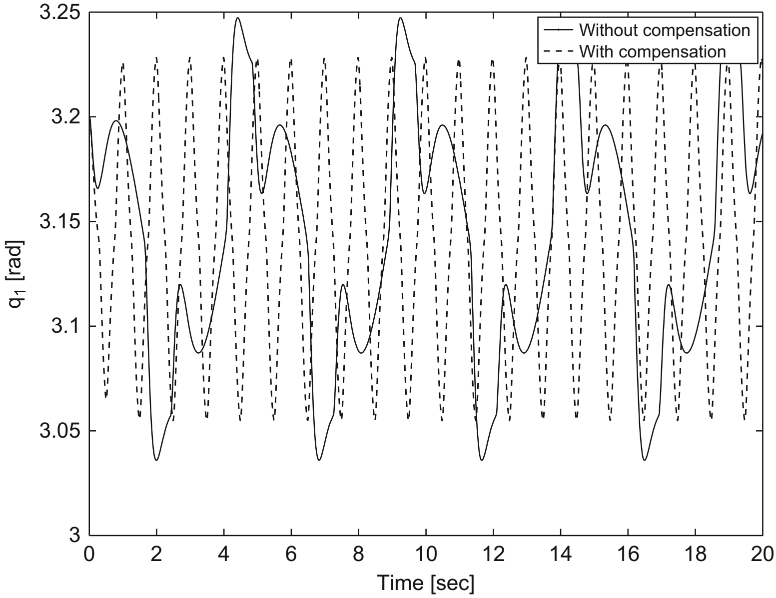

Fig. 6.3 Self-oscillation generation under a periodic perturbation ($w = 0.1\sin(1.3t)$). Dotted line shows the results when a robust linearization technique based on disturbance identification is applied, and solid line shows the oscillation when disturbance is not compensated

6.5 Comments

The problem of robust output-based generation of self-oscillations in nonlinear uncertain underactuated systems is addressed. A high-order sliding mode (HOSM) observer is used to estimate the states of the system and identify the uncertainties/perturbations. Hence, the estimated values of uncertainties are used for compensation. The proposed scheme compensates theoretically exactly the mismatch between the linearized model and the real plant. In this manner, using LPRS method for computation of the TRC gains ensures robust oscillations with prescribed amplitude and frequency.

Part III
Applications

Chapter 7
Generating Self-Oscillations in Furuta Pendulum

Abstract This chapter illustrates the DF, Poincaré maps, and LPRS to obtain the desired amplitude and frequency of SO of an experimental Furuta pendulum. The problem becomes more complicated when oscillations are around an open-loop unstable equilibrium point that corresponds to the upright position of the pendulum. Recalling that TRC design requires linear model of the plant, such linearization was made through Taylor expansion around an unstable equilibrium point. The experimental results illustrate motions at several velocities (frequency) and maximum position (amplitude), and then TRC supply, for generic SO of a wide range of frequencies.

7.1 Introduction

One of the problems that we address in the book is the motion control of underactuated mechanical systems which still remains as an interesting application problem in engineering, mainly when we are dealing with non-minimum-phase systems which are dynamical systems with unstable zero dynamics [49].

Let the underactuated mechanical system, which is a plant in the system where a periodic motion is supposed to occur, be given by the Lagrange equation [85]:

$$M(q)\ddot{q} + H(q, \dot{q}) = B_1 u \tag{7.1}$$

where $q(t) \in \mathbb{R}^n$ is the vector of joint positions; $u(t) \in \mathbb{R}$ is the vector of applied joint torques; $B_1 = [0_{(n-1)} \;\; 1]^T$ is the input that maps the torque input into the joint coordinates space; $M(q) \in \mathbb{R}^{n \times n}$ is the symmetric positive-definite inertia matrix; and $H(q, \dot{q}) \in \mathbb{R}^n$ is the vector that contains the Coriolis, centrifugal, gravity, and friction torques. The TRC (2.2) is proposed for the purpose of exciting a periodic motion where c_1 and c_2 are parameters designed such that the position of a selected link of the plant has a steady periodic motion with the desired frequency and amplitude.

Academic pendulums with rotational links are the class of systems that can be governed by (7.1) (see, e.g., [30]), and those pendulums, without a stabilizing control law, have multiple equilibrium points and they can exhibit a homoclinic orbit. However, under initial conditions close to any equilibrium points or in

L.T. Aguilar et al., *Self-Oscillations in Dynamic Systems*, Systems & Control: Foundations & Applications, DOI 10.1007/978-3-319-23303-1_7

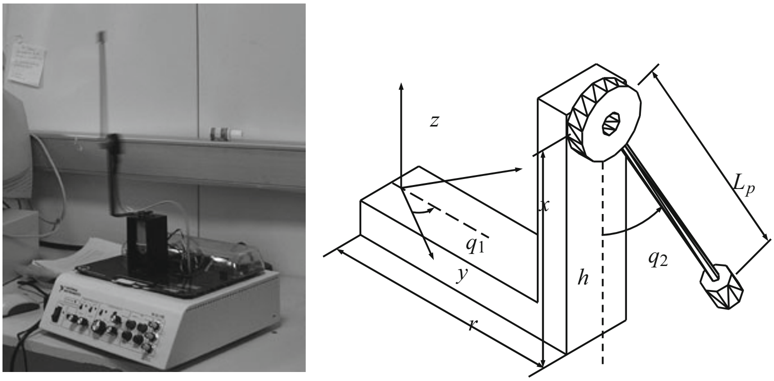

Fig. 7.1 The experimental Furuta pendulum system

the presence of Coulomb and viscous frictions, might exist both the stable and unstable equilibrium points. Typically, inducing a periodic motion around a stable equilibrium point is known as swing-up. Throughout this monograph, we will address three problems: inducing a periodic motion around an unstable equilibrium point, analysis of the periodic orbit, and robustification of the output against matched disturbances.

Let us start with the Furuta pendulum or rotary inverted pendulum, illustrated in Figure 7.1, which consists of a driven arm which rotates in the horizontal plane and a pendulum attached to that arm which is free to rotate in the vertical plane.

In this chapter, we present generation of self-oscillation at the upper position, that is, around the open-loop unstable equilibrium point. Following the same methodology as inertia wheel pendulum, we linearize the nonlinear system but now using Taylor linearization. For practical reasons, we include a stabilizing part to add certain degree of robustness turning out the equilibrium point of the system, without the TRC, locally asymptotically stable. To obtain the gains of the TRC, the DF and LPRS formulas, given in Section 2.4, were applied. We present experimental results in Section 7.4 using the laboratory Furuta pendulum from Quanser Inc.

7.2 Description of the Plant and Problem Formulation

Generally, the equations of motion of the Furuta pendulum described by

$$M(q)\ddot{q} + H(q, \dot{q}) = B\tau \tag{7.2}$$

were specified by applying the Euler–Lagrange formulation [25]. Here, $q = [q_1 \;\; q_2]^T$ is a vector that includes the arm rotation angle (q_1) and the pendulum angle (q_2), and $\tau \in \mathbb{R}$ is the applied torque; $B = [0 \;\; 1]^T$ is the input that maps the torque input to the space of joint coordinates. The matrix $M(q) \in \mathbb{R}^{2\times 2}$ which is symmetric positive definite and $H(q, \dot{q}) \in \mathbb{R}^2$ denoting the vector that contains the Coriolis, centrifugal, and gravity torques are explicitly given by

$$M(q) = \begin{bmatrix} M_{11}(q) & M_{12}(q) \\ M_{12}(q) & M_{22}(q) \end{bmatrix}, \quad H(q, \dot{q}) = \begin{bmatrix} H_1(q, \dot{q}) \\ H_2(q, \dot{q}) \end{bmatrix} \tag{7.3}$$

with

$$M_{11}(q) = J_{eq} + M_p r^2 \cos^2(q_1),$$

$$M_{12}(q) = -\frac{1}{2} M_p r l_p \cos(q_1)\cos(q_2),$$

$$M_{22}(q) = J_p + M_p l_p^2,$$

$$H_1(q, \dot{q}) = -2M_p r^2 \cos(q_1)\sin(q_1)\dot{q}_1^2 + \frac{1}{4} M_p r l_p \cos(q_1)\sin(q_2)\dot{q}_2^2$$

$$H_2(q, \dot{q}) = \frac{1}{2} M_p r l_p \sin(q_1)\cos(q_2)\dot{q}_1^2 + M_p g l_p \sin(q_2)$$

where $M_p = 0.027$ Kg is mass of the pendulum, $l_p = 0.153$ m is the length of pendulum center of mass from pivot, $L_p = 0.191$ m is the total length of pendulum, $r = 0.0826$ m is the length of arm pivot to pendulum pivot, $g = 9.810$ m/s^2 is the gravitational acceleration constant, $J_p = 1.23 \times 10^{-4}$ Kg-m^2 is the pendulum moment of inertia about its pivot axis, and $J_{eq} = 1.10 \times 10^{-4}$ Kg-m^2 is the equivalent moment of inertia about motor shaft pivot axis.

The problem is formulated as follows: find the parameter values c_1 and c_2 in the two-relay controller

$$u = -c_1 \operatorname{sign}(y) - c_2 \operatorname{sign}(\dot{y}), \tag{7.4}$$

following the algorithm provided in Subsection 2.4, such that the output

$$y = q_2 \tag{7.5}$$

of system (7.2), (7.3) has a periodic motion with the desired frequency $\boldsymbol{\Omega}$ and desired amplitude $\boldsymbol{A}_1$. It can be noted that the model of the plant is nonlinear, while the method for gain adjustment requires that the plant be linear; therefore, we will focus in linearization of (7.2), (7.3) in the next subsection.

7.3 Linearization

Self-oscillation was carried out to achieve the orbital stabilization of the unactuated link (the pendulum) $y = q_2$ around the equilibrium point $q^\star = [\pi \;\; 0]^T$. The equation of motion of the Furuta pendulum (7.2), (7.3) is linearized around $q^\star \in \mathbb{R}^2$ and by virtue of the instability of the linearized open-loop system, a state-feedback controller $u_f = -Kx$ and $x = [q - q^\star \;\; \dot{q}]^T \in \mathbb{R}^4$ is designed such that the compensated system has an overshoot of 8 and gain crossover frequency at 10 rad/s (see Bode diagram in Figure 7.2 for the open-loop system); that is, the control input

$$\tau = u_f + u \tag{7.6}$$

is composed of a stabilizing part, adding certain degree of robustness, and the two-relay controller $u(t)$. The purpose of $u_f(t)$ is to give the possibility to initialize the system in any point around the equilibrium point $q^\star$. Thus, the matrices A_{cl}, B, and C of the linear system (2.4) are

$$A_{cl} = \begin{bmatrix} 0 & 0 & 1 & 0 \\ 0 & 0 & 0 & 1 \\ -6.591 & 125.685 & -6.262 & 25.525 \\ 3.031 & -112.408 & 2.879 & -11.737 \end{bmatrix}, \; B = \begin{bmatrix} 0 \\ 0 \\ 56.389 \\ -25.930 \end{bmatrix}, \; C = \begin{bmatrix} 0 \\ 1 \\ 0 \\ 0 \end{bmatrix}^T \tag{7.7}$$

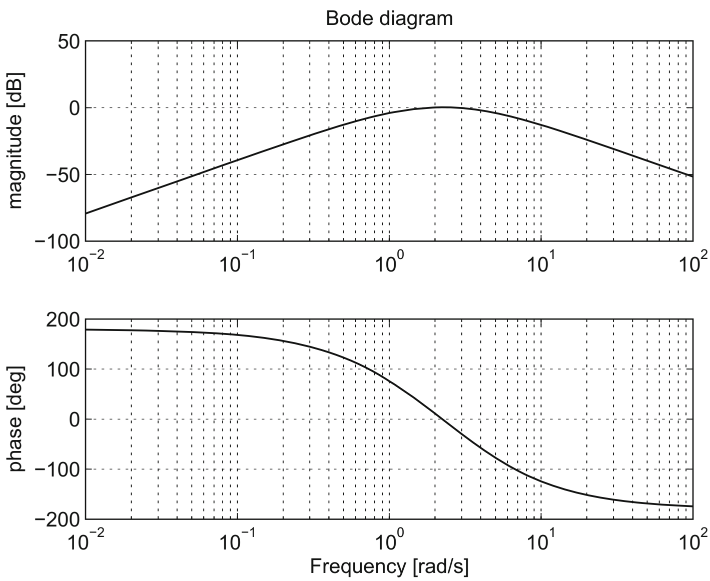

Fig. 7.2 Bode plot of the open-loop system

where $A_{cl} = A - BK$ is Hurwitz. The corresponding transfer function of the linear system (2.4), (7.7) is given by

$$W(s) = \frac{-25.93s^2 - 0.0297s + 0.0104}{s^4 + 18s^3 + 119s^2 + 342s + 360} \qquad s = j\omega. \tag{7.8}$$

The real and imaginary part of the above complex function are

$$\mathrm{Re}\{W(j\omega)\} = \frac{(0.01043 - 25.93\omega^4)(\omega^4 - 119\omega^2 + 359.9)}{(\omega^4 - 119\omega^2 + 359.9)^2 + (119\omega - 18\omega^3)^2} \tag{7.9}$$

$$\mathrm{Im}\{W(j\omega)\} = \frac{(1.776 \times 10^{-14}\omega^3 - 0.02973\omega)(\omega^4 - 119\omega^2 + 359.9)}{(\omega^4 - 119\omega^2 + 359.9)^2 + (119\omega - 18\omega^3)^2}. \tag{7.10}$$

7.4 Experimental Study

7.4.1 Experimental Setup

It consists of a 24-Volt DC motor that is coupled with an encoder and is mounted vertically in the metal chamber. The L-shaped arm, or hub, is connected to the motor shaft and pivots between ±180 degrees. At the end, a suspended pendulum is attached. The pendulum angle is measured by the encoder. As illustrated in Figure 7.1, the arm rotates about z-axis and its angle is denoted by $q_1(t)$, while the pendulum attached to the arm rotates about its pivot and its angle is called $q_2(t)$. The experimental setup includes a PC equipped with an NI-M series data acquisition card connected to the NI Educational Laboratory Virtual Instrumentation Suite (NI-ELVIS®) workstation from National Instrument. The controller was implemented using LabVIEW® programming language allowing debugging, virtual oscilloscope, automation functions, and data storage during the experiments. The sampling frequency for control implementation has been set to 400 Hz.

7.4.2 Experimental Results

For the experiments, we set initial conditions sufficiently close to the equilibrium point $q^\star \in \mathbb{R}^2$. The output $y = q_2(t)$ is driven to a periodic motion for several desired frequencies and amplitudes. The desired frequencies ($\boldsymbol{\Omega}$) and amplitudes ($\boldsymbol{A}_1$) obtained from experiments by using the values of c_1 and c_2 computed by means of the DF and LPRS are given in Tables 7.1 and 7.2, respectively.

Gains computation based on DF: For the selected set of desired frequencies $\boldsymbol{\Omega}$ provided in Table 7.1 we need to compute $\mathrm{Re}\{W(j\boldsymbol{\Omega})\}$ and $\mathrm{Im}\{W(j\boldsymbol{\Omega})\}$ to locate the quadrant of where the desired frequency is located. Figure 7.3 illustrates

Table 7.1 Computed c_1 and c_2 values for several desired frequencies using describing function method

Desired $\boldsymbol{\Omega}$	Desired $\boldsymbol{A}_1$	c_1	c_2	Experimental Ω	Experimental A_1
7	0.10	0.19	0.23	6.28	0.11
8	0.20	0.30	0.61	7.40	0.22
9	0.25	0.25	0.93	8.30	0.20
10	0.30	0.14	1.32	9.00	0.35

Table 7.2 Computed c_1 and c_2 values for several desired frequencies LPRS

Desired $\boldsymbol{\Omega}$	Desired $\boldsymbol{A}_1$	c_1	c_2	Experimental Ω	Experimental A_1
7	0.10	0.1856	0.2001	6.48	0.10
8	0.20	0.2589	0.5269	7.10	0.22
9	0.25	0.2450	0.9796	8.50	0.20
10	0.30	0.1134	1.65	9.20	0.35

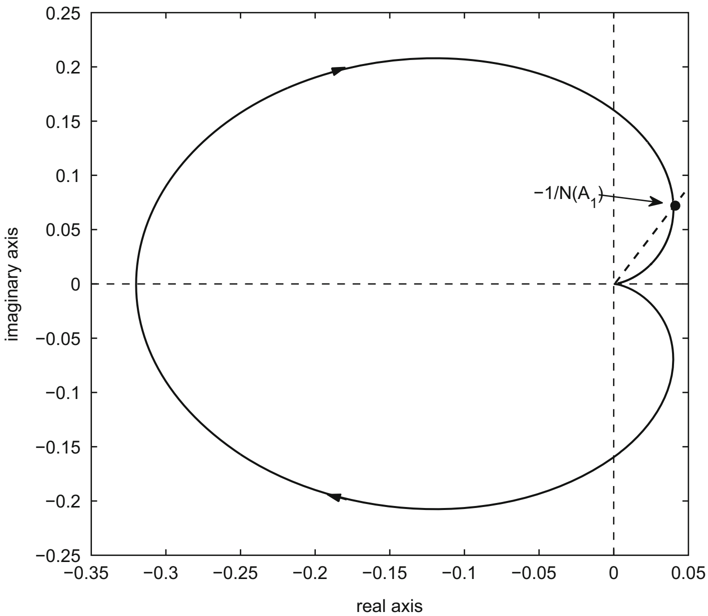

Fig. 7.3 Nyquist plot of the linearized model of Furuta pendulum and describing function in an arbitrary desired frequency ($\boldsymbol{\Omega} = 25$ rad/s)

the Nyquist plot of the linearized model of Furuta pendulum highlighting the describing function. Immediately one can apply equations (2.10), (2.14)–(2.15) to straightforward obtain the gains c_1 and c_2 provided in same Table. Verifying

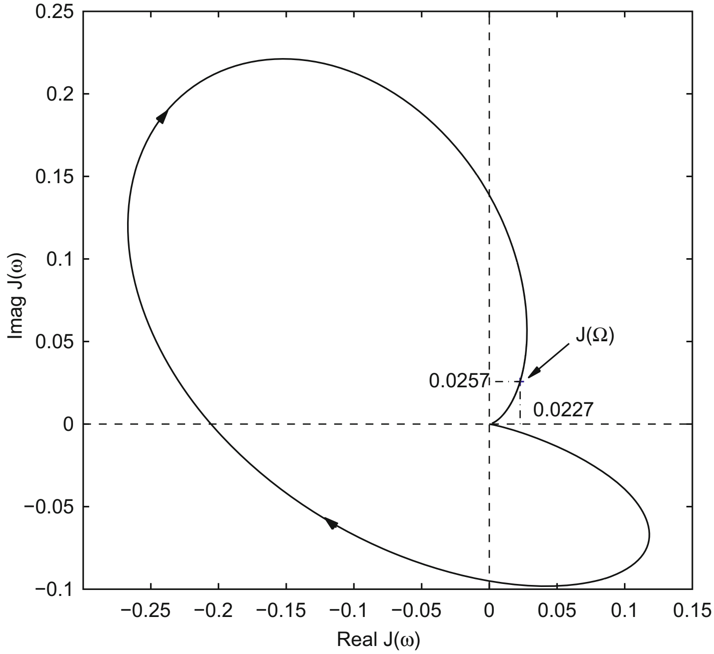

Fig. 7.4 LPRS plot of the linearized model of Furuta pendulum in an arbitrary desired frequency ($\boldsymbol{\Omega} = 25$ rad/s)

conditions of Theorem 2.1, inequality (2.22) holds for the chosen frequencies and amplitudes, thus asymptotical stability of the periodic orbit was established by Theorem 2.1.

Gains computation based on LPRS: For the selected set of desired frequencies $\boldsymbol{\Omega}$ and amplitudes $\boldsymbol{A}_1$ provided in Table 7.1, we need formulas (4.28)–(4.29) to obtain c_1 and c_2, respectively. The TRC gains were obtained under $\gamma = 0.3$. Figure 7.4 shows the LPRS plot of the linearized plant.

In Figure 7.5, experimental oscillations for the output y, for fast ($\boldsymbol{\Omega}_1 = 25$ rad/s) and slow motions ($\boldsymbol{\Omega}_2 = 10$ rad/s), are displayed. Note that certain imperfections appear in the slow motion graphics in Figure 7.5, which are attributed to the Coulomb friction forces, and the dead zone. Also, in some modes, natural frequencies of the pendulum mechanical structure are excited and manifested as higher-frequency vibrations.

7.5 Conclusion and Remarks

A TRC for generation of self-excited oscillations with desired output amplitude and frequencies for the Furuta pendulum is proposed. Values of the controller gains are computed through the DF-based model of periodic motions. Necessary conditions

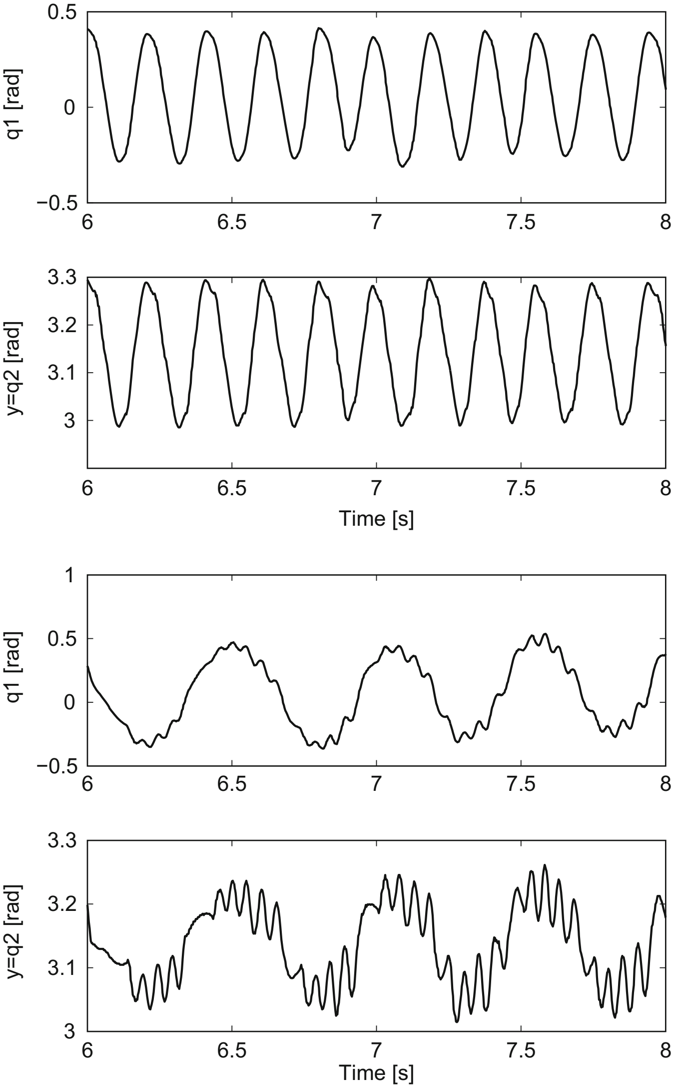

Fig. 7.5 Steady state periodic motion of each joint where (*a*) is the periodic motion at $\boldsymbol{\Omega}_1 = 25$ rad/s and (*b*) is the periodic motion at $\boldsymbol{\Omega}_2 = 10$ rad/s

for the local orbital asymptotic stability of the desired SO are also obtained from the DF-based model. The effectiveness of the proposed design procedures is supported by experiments carried out on the Furuta pendulum from Quanser Inc., for a wide range of frequencies.

Chapter 8
Three Link Serial Structure Underactuated Robot

Abstract This chapter is devoted to generate SO with desired amplitude and frequency in a three-underactuated system with two control inputs. Existence of periodic orbit was also verified. The periodic orbit will be generated at the upper position that is where the open-loop equilibrium point is unstable.

8.1 Introduction

This chapter is devoted to the solution of a periodic balancing problem for a three-link underactuated mechanical manipulator introduced in [41], whose first link is not actuated whereas the second and third joints are actuated (see Fig. 8.1). Taking advantage on results of Boiko [14], demonstrating that if the relative degree of the plant is higher than two, a periodic motion may occur in the system with SOSM controllers. We apply TRC to drive the manipulator to a periodic motion with desired amplitude and frequency. We also analyze the motion that occurs around the equilibrium point of manipulator with the TRC to show the existence of periodic motions. In the forthcoming study, we resort to describing function method to provide the approximate values of periodic and amplitudes of oscillation of the underactuated system driven by the TRC.

The chapter is organized as follows. Section 8.2 gives the dynamic model of the 3-DOF underactuated robot and the problem statement is also defined. In Section 8.3, the linearized model of the plant and procedure to obtain the gains via DF is given. In Section 8.4, the simulation results are given. We conclude the chapter with comments.

8.2 Description of the 3-DOF Underactuated Robot and Problem Statement

Here we will focus in the orbital stabilization of a 3-DOF underactuated robot, depicted in Fig. 8.1, consisting of three point masses connected by three rigid,

L.T. Aguilar et al., *Self-Oscillations in Dynamic Systems*, Systems & Control: Foundations & Applications, DOI 10.1007/978-3-319-23303-1_8

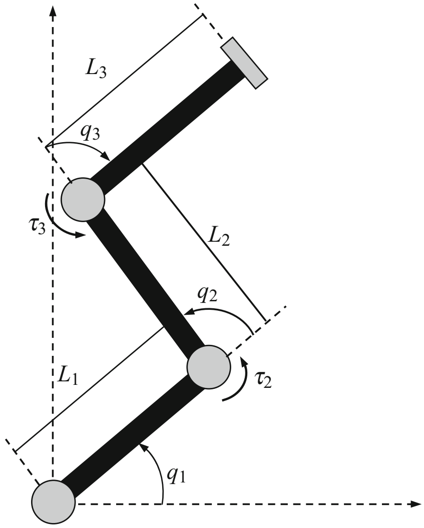

Fig. 8.1 The Three-link serial structure underactuated robot

massless links, with the links joined by an actuated revolute joint. The connection to the pivot is unactuated and frictionless. The equation of motion in such mechanism is given by

$$M(q)\ddot{q} + N(q,\dot{q}) = B\tau \tag{8.1}$$

where $q(t)$ is the 3×1 vector of joint positions; $\tau(t)$ is the 2×1 vector of applied joint torques $(n > m)$, $t \in \mathbb{R}$ is the time, $B = [0\ I]^T$; $M(q)$ is the 3×3 symmetric positive-definite inertia matrix; and $N(q,\dot{q})$ is the 3×1 vector that contains the Coriolis, centrifugal, and gravity torques. We will assume that the measurements of $\dot{q}$ are available.

The equation motion of the three-link serial structure, governed by (8.1), was specified by applying the Euler–Lagrange formulation [25, 41] where

$$M(q) = \begin{bmatrix} m_{11}(q) & m_{12}(q) & m_{13}(q) \\ m_{12}(q) & m_{22}(q) & m_{23}(q) \\ m_{13}(q) & m_{23}(q) & m_{33}(q) \end{bmatrix}, \quad N(q,\dot{q}) = \begin{bmatrix} N_1(q,\dot{q}) \\ N_2(q,\dot{q}) \\ N_3(q,\dot{q}) \end{bmatrix} \tag{8.2}$$

with

$$\begin{aligned}
m_{11}(q) &= (m_1+m_2+m_3)L_1^2 + (m_2+m_3)L_2^2 + m_3L_3^2 + 2(m_2+m_3)L_1L_2\cos(q_2)\\
&\quad + 2m_3L_2L_3\cos(q_3) + 2m_3L_1L_3\cos(q_2+q_3),\\
m_{12}(q) &= (m_2+m_3)L_1L_2\cos(q_2) + (m_2+m_3)L_2^2 + m_3L_3^2 + m_3L_1L_3\cos(q_2+q_3)\\
&\quad + 2m_3L_2L_3\cos(q_3),\\
m_{13}(q) &= m_3L_3^2 + m_3L_1L_3\cos(q_2+q_3) + m_3L_2L_3\cos(q_3),\\
m_{22}(q) &= (m_2+m_3)L_2^2 + m_3L_2^2 + m_3L_2L_3\cos(q_2+q_3) + m_3L_2L_2\cos(q_3),\\
m_{23}(q) &= m_3L_3^2 + m_3L_2L_3\cos(q_3),\\
m_{33}(q) &= m_3L_3^2;\\
N_1(q,\dot q) &= -(m_2+m_3)L_1L_2\sin(q_2)\dot q_2(\dot q_1+\dot q_2) - (m_2+m_3)L_1L_2\sin(q_2)\dot q_1\dot q_2\\
&\quad - m_3L_1L_3\sin(q_2+q_3)(\dot q_2+\dot q_3)^2 - 2m_3L_1L_3\sin(q_2+q_3)\dot q_1(\dot q_2+\dot q_3)\\
&\quad - 2m_3L_2L_3\sin(q_3)(\dot q_1+\dot q_2)\dot q_3 - m_3L_2L_3\sin(q_3)\dot q_3^2 + m_1L_1g\cos(q_1)\\
&\quad + m_2g\cos(q_1) + m_2gL_2\cos(q_1+q_2) + m_3gL_1\cos(q_1)\\
&\quad + m_3gL_2\cos(q_2+q_3) + m_3gL_3\cos(q_1+q_2+q_3),\\
N_2(q,\dot q) &= -(m_2+m_3)L_1L_2\sin(q_2)\dot q_1\dot q_2 - m_3L_1L_3\sin(q_2+q_3)\dot q_1(\dot q_2+\dot q_3)\\
&\quad - m_3L_2L_3\sin(q_2+q_3)(\dot q_1+\dot q_2+\dot q_3)\dot q_3 - m_3L_2L_3\sin(q_2+q_3)\dot q_3\\
&\quad + m_2L_1L_2\sin(q_2)\dot q_1(\dot q_1+\dot q_2) + m_3L_1L_3\sin(q_2+q_3)\dot q_1(\dot q_1+\dot q_2+\dot q_3)\\
&\quad + m_2gL_2\cos(q_1+q_2) + m_3gL_2\cos(q_1+q_2)\\
&\quad + m_3gL_3\cos(q_1+q_2+q_3),\\
N_3(q,\dot q) &= -m_3L_1L_3\sin(q_2+q_3)\dot q_1(\dot q_2+\dot q_3)\\
&\quad - m_3L_2L_3\sin(q_2+q_3)(\dot q_1+\dot q_2)(\dot q_2+\dot q_3)\\
&\quad + m_3L_1L_3\sin(q_2+q_3)(\dot q_1+\dot q_2+\dot q_3)\\
&\quad + m_3L_2L_3\sin(q_2)(\dot q_1+\dot q_2)(\dot q_1+\dot q_2+\dot q_3)\\
&\quad + m_3gL_3\cos(q_1+q_2+q_3).
\end{aligned}$$

Here, $L_1 = L_2 = 0.4\,\text{m}$ and $L_3 = 0.3$ m are the length of the links 1 through 3 starting from the pivot, and $m_1 = 6.4\,\text{Kg}$, $m_2 = 13.6\,\text{Kg}$, and $m_3 = 12.0\,\text{Kg}$ are the point masses of each link.

We first consider the state representation of (8.1) with a dynamic extension [41]:

$$\frac{d}{dt}\underbrace{\begin{bmatrix} q \\ \dot q \\ \vartheta \end{bmatrix}}_{x} = \underbrace{\begin{bmatrix} \dot q \\ -M^{-1}(q)N(q,\dot q) + M^{-1}(q)B\tau(q,\dot q,\vartheta) \\ 0 \end{bmatrix}}_{f(x)} + \underbrace{\begin{bmatrix} 0 \\ 0 \\ 1 \end{bmatrix}}_{g(x)} u \tag{8.3}$$

where $u(t)$ is the variable structure control which is designed such that the scalar-valued function output

$$y = h(q). \tag{8.4}$$

has a steady-state periodic motion with desired frequency and amplitude. The above representation makes possible the linearization of a class of underactuated mechanical systems where the addition of an extra dynamics makes the zero dynamics [46] one-dimensional and exponentially stable [41, 52]; on the other hand, this extra dynamics also can be seen as the influence of an actuator [15].

For the underactuated plant (8.1), we must show the existence of periodic motion and provide the gains of the TRC

$$u(t) = -c_1 \operatorname{sign}(y) - c_2 \operatorname{sign}(\dot{y}) \tag{8.5}$$

to excite dynamics of the non-actuated link with oscillations with certain frequency and amplitude. In the next section, we summarize the DF gain design for the TRC by considering the linearized model of the plant.

8.3 The TRC Gains Computation

The output $y = q_3$ is chosen to produce a periodic motion at the end effector. The procedure to obtain the gains c_1 and c_2 using the DF algorithm in order to excite the output y is as follows.

1. First, the equation of motion of the underactuated robot (8.1) is linearized around the equilibrium point $q^\star = [1.0472\ 1.4522\ -1.4522]^T$ and $\dot{q}^\star = 0 \in \mathbb{R}^3$ [41]. The open loop is unstable, so we design a state-feedback controller to place the eigenvalues arbitrarily at -3. Thus, the linear system, with states $x = [q - q^\star\ \dot{q}\ \vartheta]^T \in \mathbb{R}^7$, is given by (2.4) with

$$A = \begin{bmatrix} 0 & 0 & 0 & 1 & 0 & 0 & 0 \\ 0 & 0 & 0 & 0 & 1 & 0 & 0 \\ 0 & 0 & 0 & 0 & 0 & 1 & 0 \\ -393.026 & -250.587 & -92.341 & -432.856 & -311.502 & -105.683 & 0 \\ 544.519 & 346.565 & 130.977 & 603.491 & 434.430 & 149.424 & 0 \\ -38.806 & -23.563 & -18.230 & -55.616 & -40.413 & -19.774 & 0 \\ 0 & 0 & 0 & 0 & 0 & 0 & 0 \end{bmatrix}$$

$$\begin{aligned} B &= \begin{bmatrix} 0\ 0\ 0\ -0.0034\ -0.0190\ 0.0728\ 1 \end{bmatrix}^T, \\ C &= \begin{bmatrix} 0\ 0\ 1\ 0\ 0\ 0\ 0 \end{bmatrix}. \end{aligned} \tag{8.6}$$

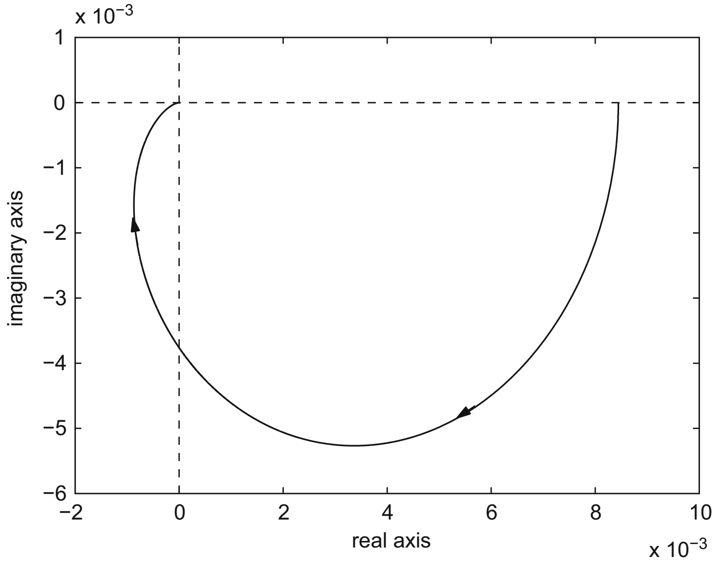

Fig. 8.2 Nyquist plot of the 3-DOF underactuated robot

The corresponding transfer function is

$$W(s) = \frac{0.0728s^5 + 0.8423s^4 + 3.818s^3 + 8.032s^2 + 6.578s + 3.908 \times 10^{-12}}{s(s^6 + 18.2s^5 + 138s^4 + 558.2s^3 + 1270s^2 + 1541s + 778.9)} \tag{8.7}$$

The Nyquist plot of $W(s)$ is shown in Fig. 8.2.

2. Setting the scalars $\boldsymbol{\Omega}$ and $\boldsymbol{A}_1$, the gains c_1 and c_2 can be obtained from equations (2.10) and (2.14)–(2.15) which can be numerically computed using the MATLAB/SIMULINK® CONTROL Toolbox commands `nyquist`, `real`, and `imag`.

8.4 Simulation Results

The initial positions are $q_1(0) = 1.1$ rad, $q_2(0) = 1.42$ rad, and $q_3(0) = -1.8$ rad for the joints 1, 2, and 3, respectively, and $\dot{q}(0) = 0 \in \mathbb{R}^3$ rad/s. For the 3-DOF robot, we select $\boldsymbol{A}_1 = 0.15$ as desired amplitude of oscillations and $\boldsymbol{\Omega} = 5$ rad/s (see Bode diagram in Fig. 8.3 for the open-loop system) as desired frequency.

Two steps for finding c_1 and c_2 via DF given in the previous section are as follows:

1. For the selected frequency $\boldsymbol{\Omega}$, we have $\mathrm{Re}\{W(j\boldsymbol{\Omega})\} = -8.6 \times 10^{-4}$ and $\mathrm{Im}\{W(j\boldsymbol{\Omega})\} = -0.0018$; therefore, $\boldsymbol{\Omega}$ belongs to the third quadrant (Q_3).

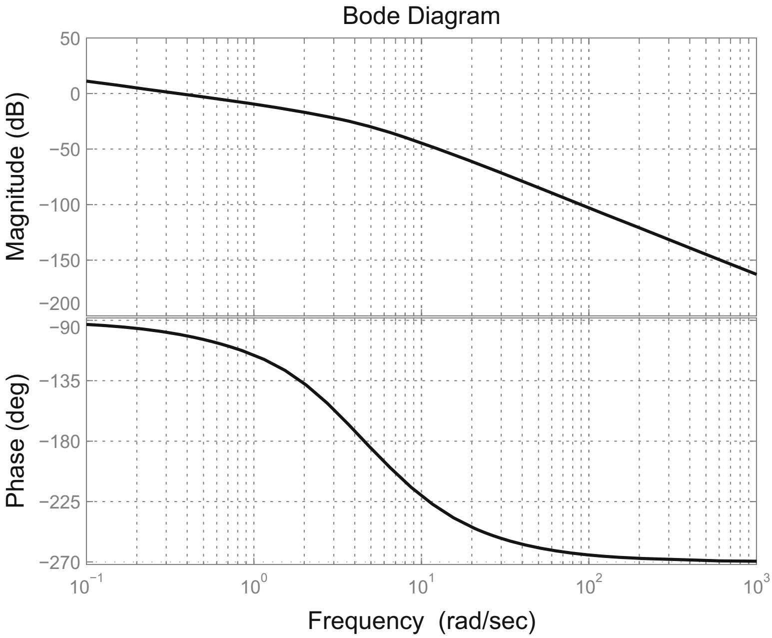

Fig. 8.3 Bode plot of the open-loop system

2. Using (2.10) we have $\xi = -2.0322$. Finally, using (2.14)–(2.15), we obtain $c_1 = 26.59$ and $c_2 = -54.08$.

To check if the periodic solution is stable, find the derivative of the phase characteristic of the plant with respect to the frequency; we need to verify the following inequality:

$$\left.\frac{d \arg W}{d \ln \omega}\right|_{\omega=\Omega} \leq -\frac{c_1 c_2}{\boldsymbol{\Omega}\,(c_1^2 + c_2^2)}. \tag{8.8}$$

Computing the left-hand side (8.8), we have $d \arg W / d \ln \omega = -0.1263$, while the right-hand side is $d \arg W / d \ln \omega = 0.0660$. Therefore, the system is orbitally asymptotically stable.

Figure 8.4 shows the motion of the joint positions for the closed-loop systems using the TRC. Figure 8.5 gives a better picture of the amplitude and frequency of the oscillations by plotting the steady-state output trajectory between 15 and 20 s.

Figure 8.6 shows the input torques for the TRC. The peak torque magnitude on the limit cycle is about 60 N-m that is compatible with the torque of the prototype given in [41]. Finally, Fig. 8.7 illustrates the phase portraits of $(q_3, \dot{q}_3)$ revealing the limit cycle behavior of the closed-loop systems generated for the TRC with initial conditions inside and outside the limit cycle.

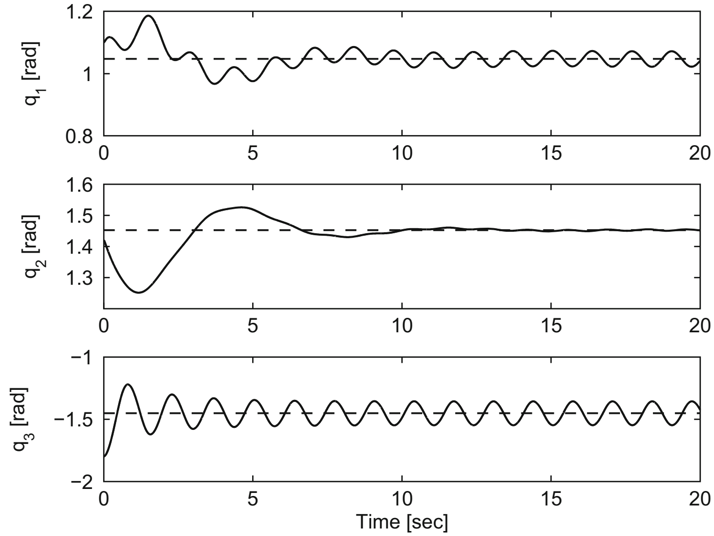

Fig. 8.4 Joint position trajectories

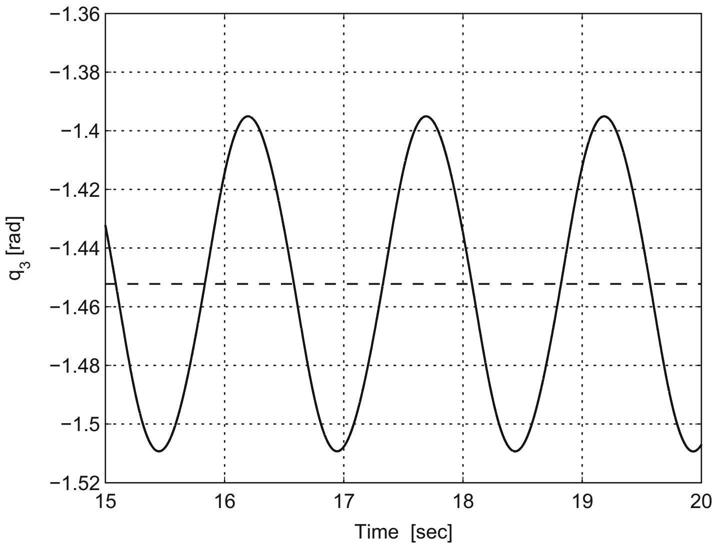

Fig. 8.5 Steady-state output trajectory ($y = q_3$)

8.5 Comments and Remarks

This chapter has addressed the problem of orbital stabilization of a underactuated system around an unstable equilibrium point. The generation of self-oscillations is made through TRC. The transient process converges to a stable limit cycle where

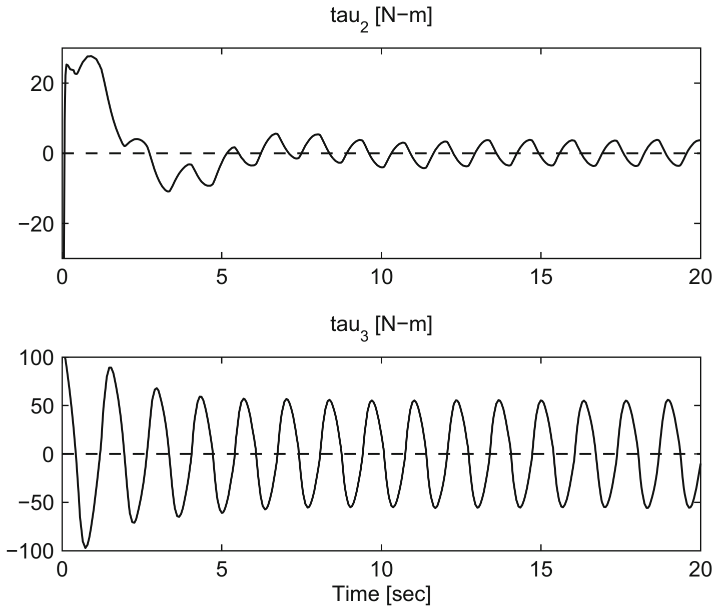

Fig. 8.6 Plot of applied torques

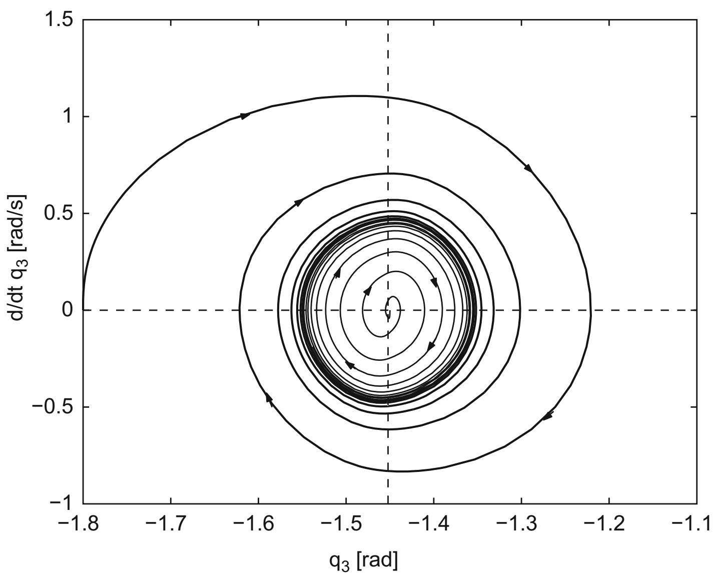

Fig. 8.7 Behavior of $(q_3, \dot{q}_3)$ with initial conditions inside and outside of the limit cycle

the describing function method is used to compute the gain values of the TRC in order to generate SO. It is worth noting that no reference model or periodic desired signal is required to generate the motion of the robot, thus avoiding an extra work in the localization of particular orbits for underactuated mechanical systems. The proposed study can lead to some research topics. Among them is the analysis and generation of SO for more complex systems as the coordinated motion in certain class of legged or walking robots [40, 70] where Poincaré maps play an important role. The problem the model of the plant was taken from the paper of Grizzle et al. [41] with the purpose of solving it via the TRC. The results were identical but required lower computational efforts, which may be attractive for engineers working on the matter.

Chapter 9
Generation of Self-Oscillations in Systems with Double Integrator

Abstract In this chapter, a self-oscillation is generated in a double integrator with application to a 3-DOF experimental helicopter with two control inputs. Two TRCs were used to generate periodic motion at the pitch, roll, and yaw angles. The amplitude and frequency of oscillations depend on the value of the coefficient of the TRC whose formulas were synthesized through the DF method. The performance of the proposed controller, applied to an underactuated 3-DOF helicopter, was verified by simulations.

9.1 Introduction

In the present chapter, we will focus on the SO of a 3-DOF helicopter prototype with two control inputs depicted in Fig. 9.1 which is a class of system with double integrator. Specifically, the prototype under study is a rigid body with a spherical joint at the suspension point. Rotation of the prototype is permitted around the suspension point in any direction. There are two propellers, which are symmetrically attached at the end of the body and which can be actuated individually. A counterweight is installed at the other end so that the gravitational forces become negligible.

Several researcher addressed the regulation problem of similar helicopter prototype (see, e.g., [33, 95] and the references therein); however, few works can be found related to the solution of the tracking or self-oscillations problem. For instance, Meza *et al*. [61] and Westerberg *et al*. [92] solve the tracking control problem of the 3-DOF helicopter prototype, operating under uncertain conditions, where virtual constraints approach [80] is applied for planning of periodic motions. It is important to mention that there are many research works related with the tracking control problem for another class of helicopters, for example, the tracking control problem for small-scale unmanned helicopters [73] and the takeoff and landing problem of scaled helicopter where a specified trajectory is defined with respect to a fixed reference frame [65].

The present chapter presents the capability of the two-relay controller to generate self-oscillations in the 3-DOF helicopter under study. These oscillations may be used as a part of a maneuvering motion (we figured out that the tracking principle may be unusable for this purpose). The TRC is a variable structure system consisting

L.T. Aguilar et al., *Self-Oscillations in Dynamic Systems*, Systems & Control: Foundations & Applications, DOI 10.1007/978-3-319-23303-1_9

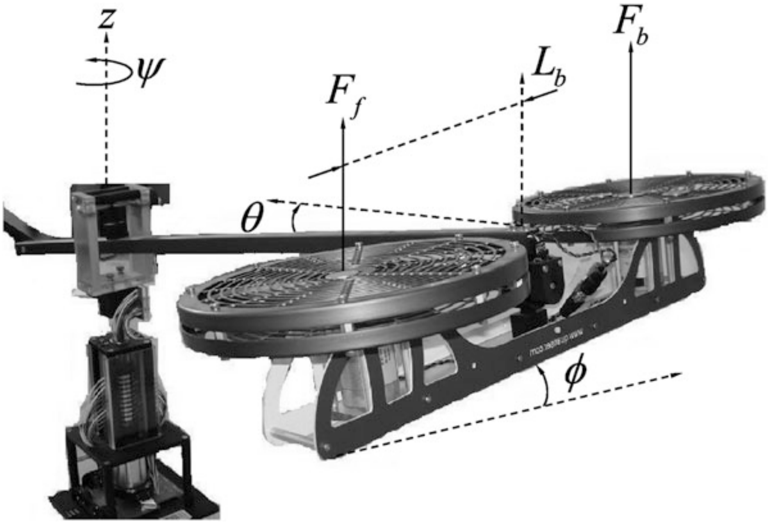

Fig. 9.1 3-DOF helicopter prototype

of two relays that depend on the output and its time derivative and two coefficients whose values are related with the amplitude and frequency of oscillations.

The chapter is structured as follows. Section 9.2 presents the dynamic model of the 3-DOF helicopter and the problem statement is defined. In Section 9.3, double two-relay controllers are applied—one is used to generate a periodic motion at the elevation angle and the other is for the rotation and direction angles. Effectiveness of the proposed method was verified by simulations in Section 9.4. Finally, conclusions are provided in Section 9.5.

9.2 Dynamic Model of 3-DOF Helicopter and Problem Statement

The mathematical model of the laboratory prototype of the 3-DOF helicopter drawn from the user's manual [71] is given by

$$J_e\ddot{\theta} = K_f(F_f + F_b)L_b - F_gL_b \tag{9.1}$$

$$J_d\ddot{\phi} = K_f(F_f - F_b)L_h \tag{9.2}$$

$$J_t\ddot{\psi} = -K_p\sin(\phi)L_b \tag{9.3}$$

where $\theta(t) \in \mathbb{R}$ is the elevation angle, $\phi(t) \in \mathbb{R}$ is the direction angle, $\psi(t) \in \mathbb{R}$ is the rotation angle, J_e is the moment of inertia of the system about the elevation axis,

Table 9.1 Parameter values of the experimental 3-DOF helicopter

Parameter	Value	Units
L_b	0.66	m
L_h	0.177	m
J_e	0.91	Kg–m^2
J_d	0.0364	Kg–m^2
J_t	0.91	Kg–m^2
K_f	0.5	N/V
K_p	0.686	N
F_g	0.686	N

J_d is the moment of the helicopter inertia about the pitch or directional axis, J_t is the moment of the helicopter inertia about the travel or rotation axis, the manipulated variables used for control are forces exerted by the DC motors denoted as $F_f(t)$ and $F_b(t)$, respectively; K_f is the force constant of the motor/propeller combination, L_b is the distance from the pivot point to the helicopter body, F_g is the gravitational force, L_h is the distance from the pitch axis to the either motor, and K_p is the force required to maintain the helicopter in flight. The parameters of the helicopter, taken from Quanser, Inc., 3-DOF helicopter manual, are given in Table 9.1.

For the purpose of decomposing the 3-DOF underactuated system (9.1)–(9.3) into two subsystems, actuated independently, let us introduce the control inputs $u'_1 = F_f + F_b$ and $u'_2 = F_f - F_b$. Then, setting $\theta_1 = \theta$, $\theta_2 = \dot{\theta}$, $\phi_1 = \phi$, $\phi_2 = \dot{\phi}$, $\psi_1 = \psi$, $\psi_2 = \dot{\psi}$, and $a = K_f L_b J_e^{-1}$, $b = L_b F_g J_e^{-1}$, $c = K_f L_h J_d^{-1}$, $d = K_p L_b J_t^{-1}$, system (9.1)–(9.3) takes the form

$$\dot{\theta}_1 = \theta_2, \qquad \dot{\theta}_2 = -b + au'_1 \tag{9.4}$$

$$\dot{\phi}_1 = \phi_2, \qquad \dot{\phi}_2 = cu'_2 \tag{9.5}$$

$$\dot{\psi}_1 = \psi_2, \qquad \dot{\psi}_2 = -d\sin(\phi_1). \tag{9.6}$$

In the design, we will take into account the dynamics of each DC motors whose transfer function is given by

$$W_a(s) = \frac{k}{Js + 1} \tag{9.7}$$

where k and J are positive nominal parameters and it is assumed that its values are the same in each motor.

The objective is to induce a periodic motion at the output $y = [\theta_1 \;\; \phi_1 \;\; \psi_1]^T$ of the system (9.4)–(9.6), with desired amplitude $\boldsymbol{A}_1$ and frequency $\boldsymbol{\Omega}$ using the two-relay controller.

Let us recall that is not possible to generate SO in a system with double integrator as $W(s) = 1/s^2$ since isolated point of intersection between the Nyquist plot and the describing function does not exist. However, for a system with double integrator plus the actuator dynamics as

$$W(s) = \frac{1}{s^2(s+1)} \tag{9.8}$$

it is possible to generate SO using the TRC

$$u = -c_1 \operatorname{sign}(y) - c_2 \operatorname{sign}(\dot{y}) \tag{9.9}$$

Figure 9.2 shows the Nyquist plot and the DF of system using the TRC. Notice now that intersection of the DF with the Nyquist plot can occur; therefore, oscillations now can be induced as illustrated in same figure.

9.3 Main Result

9.3.1 *Periodic Motion of the Elevation Angle*

Equations (9.4), (9.7), describing the pitch dynamics, constitute an independent subsystem. For the design, notice that

$$u_1' = F_f + F_b = W_a(s)(V_f + V_b) = W_a(s)u_1 \tag{9.10}$$

where V_f and V_b stand for the armature voltages applied to the front and back motors.

The following two-relay controller

$$u_1 = -\alpha_1 \operatorname{sign}(\theta_1) - \alpha_2 \operatorname{sign}(\theta_2) \tag{9.11}$$

is proposed to generate self-oscillations at the output $y_\theta = \theta_1$. Here, α_1 and α_2 are scalar parameters that must be computed according to the procedure provided in Section 2.4.

To begin with, Nyquist plot of the open-loop system (see Fig. 9.3) involving the elevation and actuator dynamics is presented in Fig. 9.4(a). This Nyquist plot, generated using the *linear analysis tool* from MATLAB/SIMULINK®, illustrates that plot is found in the third quadrant only.

The linear model considered for design purposes is

$$W_\theta(s) = \frac{ak}{s^2(Js+1)}. \tag{9.12}$$

The real and imaginary parts of the above transfer function are

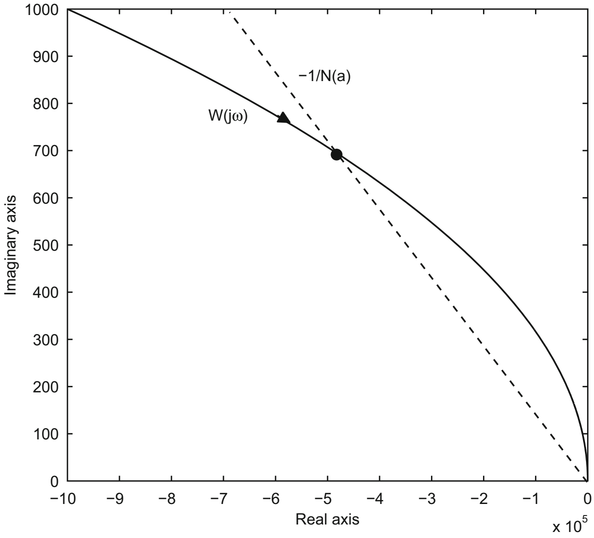

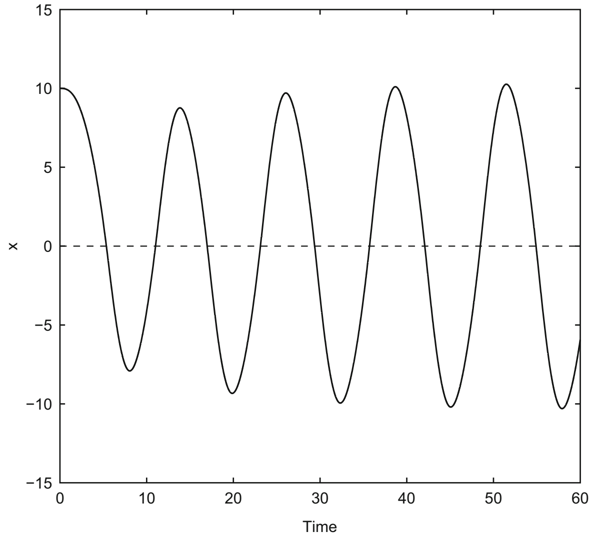

Fig. 9.2 Nyquist plot, DF, and time response of system with double integrator $W(s) = 1/s^2(s+1)$ and using two-relay controller

$$\begin{aligned}
\mathrm{Re}\{W_\theta(j\omega)\} &= \frac{ak}{\omega^2}\left(\frac{1}{1+J^2\omega^2}\right) \\
\mathrm{Im}\{W_\theta(j\omega)\} &= \frac{ak}{\omega^2}\left(\frac{J\omega}{1+J^2\omega^2}\right).
\end{aligned} \tag{9.13}$$

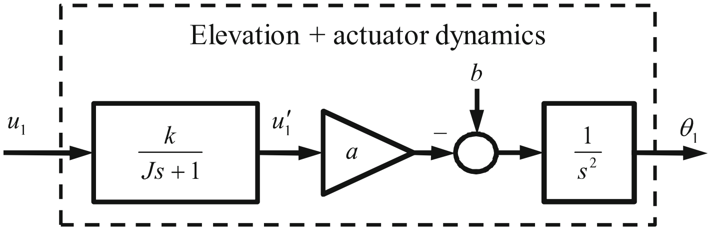

Fig. 9.3 Block diagram of the open-loop system involving the actuator and the elevation dynamics

The straightforward formulas to compute α_1 and α_2, derived from (2.14)–(2.15), are

$$\begin{aligned}\alpha_1 &= \frac{\pi}{4}\boldsymbol{A}_\theta \frac{\boldsymbol{\Omega}_\theta^2}{ak},\\ \alpha_2 &= J\boldsymbol{\Omega}_\theta \alpha_1\end{aligned} \tag{9.14}$$

where $\boldsymbol{A}_\theta$ and $\boldsymbol{\Omega}_\theta$ are the desired elevation amplitude and frequency, respectively.

We shall consider that the harmonic balance condition still holds for small perturbations of the amplitude and the frequency with respect of the periodic motion. In this case the oscillation can be described as a damped one. If the damping parameter will be negative at a positive increment of the amplitude and positive at a negative increment of the amplitude, then the perturbation will vanish and the limit cycle will be asymptotically stable.

From Theorem 2.1, the condition to guarantee that periodic solution is orbitally asymptotically stable, for the system under study, is

$$\left.\frac{d \arg W_\theta}{d \ln \omega}\right|_{\omega=\boldsymbol{\Omega}} \leq -\left(\frac{\pi}{4}\boldsymbol{A}_\theta \frac{\boldsymbol{\Omega}_\theta^2}{ak}\right)\frac{J\boldsymbol{\Omega}_\theta}{1+J\boldsymbol{\Omega}_\theta}. \tag{9.15}$$

Note that for any $\boldsymbol{\Omega}_\theta$ and $\boldsymbol{A}_\theta$ the condition of orbital stability holds.

9.3.2 Periodic Motion of Rotation and Direction Angles

The next goal is to induce self-oscillation at the rotation and direction angles. We can now proceed analogously to the previous subsection if we consider the direction dynamics. First, note that

$$u_2' = F_f - F_b = W_a(s)(V_f - V_b) = W_a(s)u_2. \tag{9.16}$$

The following control input is proposed to generate periodic motion at the direction angle

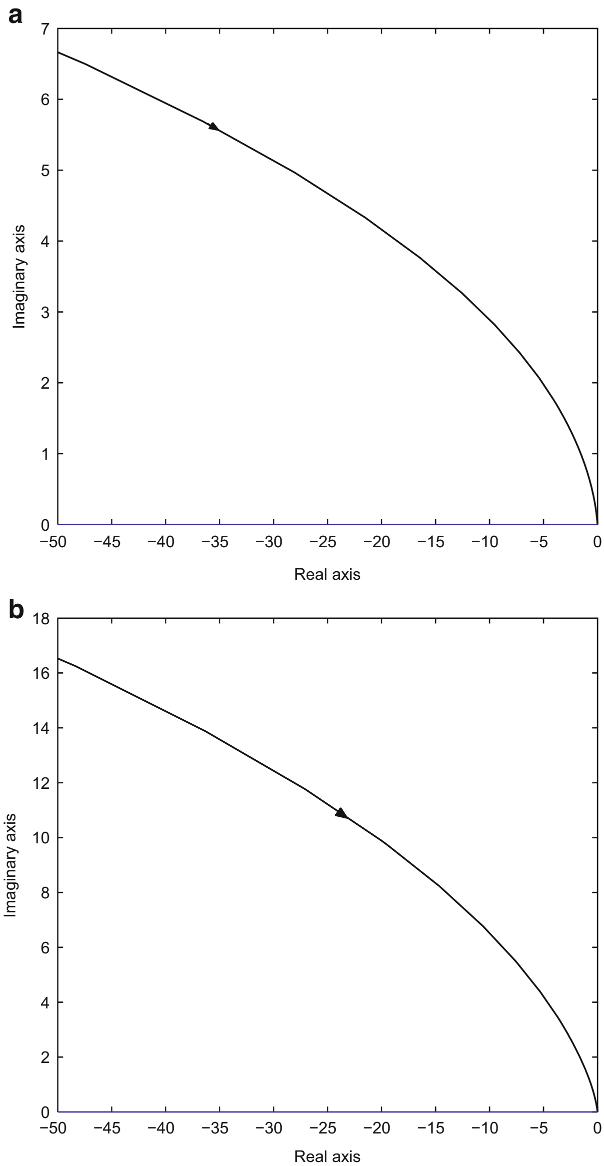

Fig. 9.4 (**a**) Nyquist plot of the elevation plus actuator dynamics and (**b**) Nyquist plot of the rotation plus actuator dynamics

$$u_2 = -\beta_1 \,\mathrm{sign}(\phi_1) - \beta_2 \,\mathrm{sign}(\phi_2) \tag{9.17}$$

where β_1 and β_2 are the scalar coefficients of the TRC to be tuned according to (2.14) and (2.15).

The linear model, involving the direction and actuator dynamics, considered for design purposes is

$$W_\phi(s) = \frac{ck}{s^2(Js+1)}. \tag{9.18}$$

The Nyquist plot of the open-loop system is also presented in Fig. 9.4(b). Therefore, the formulas to compute β_1 and β_2 are

$$\begin{aligned} \beta_1 &= \frac{\pi}{4}\boldsymbol{A}_\phi \frac{\boldsymbol{\Omega}_\phi^2}{ck}, \\ \beta_2 &= J\boldsymbol{\Omega}_\phi \beta_1 \end{aligned} \tag{9.19}$$

where $\boldsymbol{A}_\phi$ and $\boldsymbol{\Omega}_\phi$ are the desired elevation amplitude and frequency, respectively. Of course, the condition to guarantee that periodic solution is orbitally asymptotically stable, for the subsystem under study, is

$$\operatorname{Re} \left.\frac{d \arg W_\phi}{d \ln \omega}\right|_{\omega=\boldsymbol{\Omega}} \leq -\left(\frac{\pi}{4}\boldsymbol{A}_\phi \frac{\boldsymbol{\Omega}_\phi^2}{ck}\right) \frac{J\boldsymbol{\Omega}_\phi}{1+J\boldsymbol{\Omega}_\phi}. \tag{9.20}$$

9.4 Simulation Results

The periodic motion of each axis of the helicopter was verified in simulation by applying the two-relay controller presented in Section 2.4. The constant parameters of the motors are $J = 0.5$ and $k = 10$. The initial conditions of each angle were set to $\theta_1(0) = 0.2$ rad, $\phi_1(0) = 0.01$ rad, and $\psi_1(0) = 0.8$ rad while the initial velocity conditions were set to $\theta_2(0) = \psi_2(0) = \phi_2(0) = 0$ rad/s. For the simulation, we chose $\boldsymbol{A}_\theta = 0.8$ and $\boldsymbol{A}_\phi = 1$ as desired amplitudes and $\boldsymbol{\Omega}_\theta = 1.5$ rad/s and $\boldsymbol{\Omega}_\phi = 0.5$ rad/s as desired frequencies.

The constant $\alpha_1 = 4.873$ $\alpha_2 = 3.655$ and $\beta_1 = 3.23$ $\beta_2 = 1.62$ were obtained from formulas (9.14) and (9.19), respectively.

Figure 9.5 shows the periodic motion of the elevation θ, direction ϕ, and rotation ψ angles of the 3-DOF helicopter prototype. Figure 9.6 illustrates the real control inputs $V_f = (u_1 + u_2)/2$ and $V_b = (u_1 - u_2)/2$.

9.5 Conclusions

In this chapter we propose the two-relay control method to induce SO in a double integrator with an actuator dynamics. Particularly, we find application in 3-DOF underactuated helicopter where dynamics of the actuators have an important influence on the system. Generation of the SO at **each** degree of freedom at the same time is considered. The framework is a two-stage procedure involving periodic motion. The first stage allows us to select a feasible periodic motion for the elevation angle by using the reduced-order dynamics. The second stage implies an self-oscillation of the direction angle. It should be pointed out that rotation angle φ has a natural period motion consisting in the rotation of the body around the axis. Generation of self-oscillation at different frequencies and amplitudes for each angle is a complex problem because of the coupling between models. Our results show how the simple proposed control algorithm, known as two-relay controller, solves the mentioned problem. The effectiveness of the proposed method is demonstrated by numerical simulations.

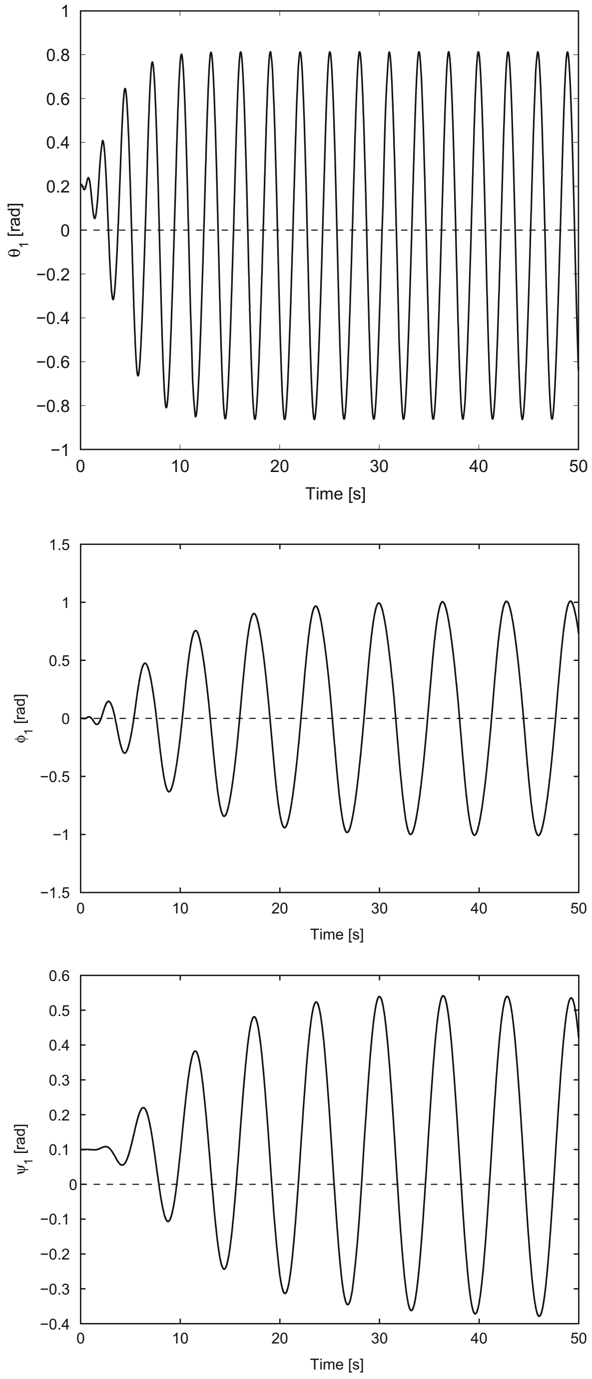

Fig. 9.5 Oscillatory responses of each output of the 3-DOF underactuated helicopter

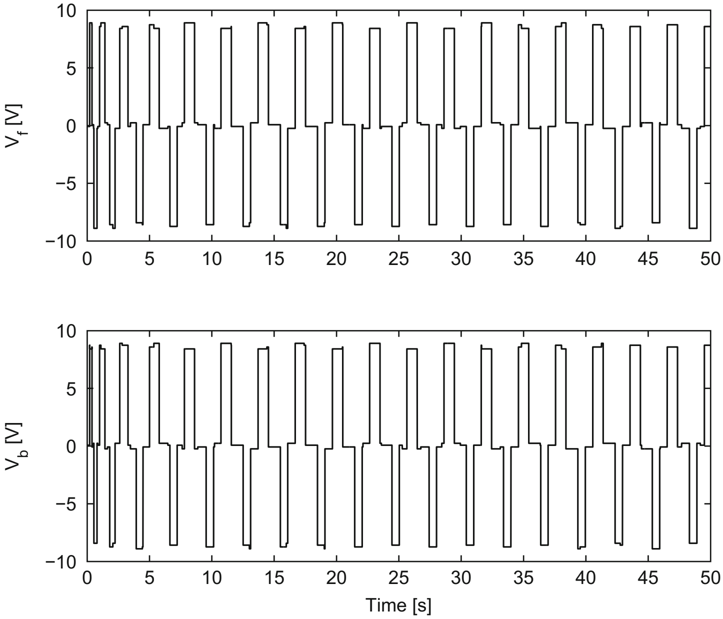

Fig. 9.6 Control inputs $V_f = (u_1 + u_2)/2$ and $V_b = (u_1 - u_2)/2$

Chapter 10
Fixed-Phase Loop (FPL)

Abstract There exist a number of applications in which oscillations must be produced at a certain phase shift with respect to a reference signal. Phase-lock loop (PLL) is widely used for this purpose. PLL uses a closed-loop control principle for tracking the required phase shift. Another solution, which uses an open-loop control principle for the phase angle, can be realized on the TRC considered in this book. This solution is named here a fixed-phase loop (FPL). FPL is an oscillator consisting of a TRC and a low-pass (LP) filter that generates a periodic voltage signal of the frequency corresponding to a certain specified phase lag of the LP filter. Regardless of the LP filter connected in a loop with the TRC, oscillations are always produced at the same phase lag value. Two different circuits are considered: without and with an additional integrator. The purpose of the considered self-oscillating circuit is to produce a periodic reference signal at the output of the filter with desired frequency and amplitude. Sufficient conditions for orbital asymptotic stability of the closed-loop system is verified through the Poincaré map. The two FPL circuits are illustrated by simulations and experiments.

10.1 Introduction

In electronics, the idea of using self-oscillating circuits is used in many applications. In dc–dc inverters [59], self-oscillating principle is used because of nearly zero sensitivity to load changes and high performance. Such inverters are attractive to operate in dc–ac converters where two buck–boost dc–dc inverters are commonly used. Several topologies have been proposed to design these converters, for example, Sanchis *et al*. [77] design a buck–boost dc–ac inverter using a double-loop control for the buck–boost dc–dc converter. Youssef and Jain [94] present a self-sustained oscillating controller for power factor correction circuits. Several circuit topologies for nonconventional dc–ac inverters are illustrated in J. Lai [51]. Recently, Albea *et al*. [3] designed an autonomous oscillator using energy-shaping methodology for a nonlinear boost inverter whose topology was originally presented by Cáceres and Barbi [19]. Very often in these and other applications, oscillations must be produced at a certain phase shift with respect to a reference signal. Phase-lock loop (PLL) is widely used for this purpose. PLL uses a closed-loop control principle for tracking the required phase shift. Another solution, which

L.T. Aguilar et al., *Self-Oscillations in Dynamic Systems*, Systems & Control: Foundations & Applications, DOI 10.1007/978-3-319-23303-1_10

uses an open-loop control principle for the phase angle, can be realized on the TRC considered in this book. This solution is named here a fixed-phase loop (FPL). FPL is an oscillator consisting of a TRC and a low-pass (LP) filter that generates a periodic voltage signal of the frequency corresponding to a certain specified phase lag of the LP filter. Regardless of the LP filter connected in a loop with the TRC, oscillations are always produced at the same phase lag value.

Analysis of the TRC interconnected with a second-order linear plant, for example, to induce low voltage at the output of the plant is unsuitable for dc–ac power conversion purposes due to the limitations of linear amplifiers configured as relays and differentiators. In this chapter, we use the first approach in the application of the two-relay controller [1] in dc–ac power converters. We start our investigation by using a buck converter topology interconnected with a bridge-type circuit which is used to obtain the sinusoidal output voltage. Reference signal will be injected through the output of the interconnection between the TRC and a linear or nonlinear plant, which will be referred to as a two-relay system.

The chapter is devoted to the design of an FPL and organized as follows. At first gain synthesis, upper bound estimate, and sufficient conditions for orbital asymptotic stability are presented in Section 10.2 for the TRC. TRC design formulas are produced in Section 10.2.1. Experimental study of an FPL is given in Section 10.2.3. After that, analogue realization, including design formulas, is given in Section 10.3. Finally, Section 10.4 presents some conclusions.

10.2 Design of TRC for FPL

Assume that linear dynamics in the FPL is of second order. Consider the stable second-order transfer function

$$W(s) = \frac{1}{\frac{s^2}{\omega_0^2} + \frac{2\zeta s}{\omega_0} + 1} \tag{10.1}$$

interconnected with a two-relay controller

$$u = -c_1 \operatorname{sign}(y) - c_2 \operatorname{sign}(\dot{y}) \tag{10.2}$$

where $\zeta > 0$ is the damping factor, $\omega_0 > 0$ is the natural frequency, $s = j\omega$ is the complex variable, and c_1 and c_2 are scalar coefficients designed such that the output of the system $y(t)$ has a steady periodic motion voltage with desired frequency $\boldsymbol{\Omega}$ and amplitude $\boldsymbol{A}_1$.

Contrary to Chapters 7–9, the TRC (10.2) is considered in this section as a device for generating a periodic voltage signal. The desired amplitude and frequency of the signal at the output of the filter $W(s)$ are produced through tuning c_1 and c_2. However, there is a possibility of obtaining excessively large required values of c_1

and c_2. This may result in the necessity of a very high amplitude of the switched control $u(t)$. To avoid this, we need to account for natural physical limits on the produced voltage and choose the desired $\boldsymbol{A}_1 \in [0, \boldsymbol{A}_1^{\max}(u^{\max})]$ such that

$$\sup_{t\geq 0} |u(t)| \leq u^{\max} \tag{10.3}$$

where $u^{\max} > 0$ is the maximum control input level.

10.2.1 Synthesis of TRC under Input Saturation

We now proceed with analyzing the FPL with a two-relay controller under input saturation. The reason for this is the necessity of avoiding unrealistic selection of c_1 and c_2 which would correspond to high required amplitude values of the output voltage.

The right-hand sides of formulas

$$c_1 = \begin{cases} \frac{\pi}{4}\frac{\boldsymbol{A}_1}{|W(j\boldsymbol{\Omega})|}\left(\sqrt{1+\xi^2}\right)^{-1} & \text{if } \boldsymbol{\Omega} \in Q_3 \\ -\frac{\pi}{4}\frac{\boldsymbol{A}_1}{|W(j\boldsymbol{\Omega})|}\left(\sqrt{1+\xi^2}\right)^{-1} & \text{if } \boldsymbol{\Omega} \in Q_4 \end{cases} \tag{10.4}$$

$$c_2 = \xi \cdot c_1, \tag{10.5}$$

with

$$\xi = \frac{c_2}{c_1} = -\frac{\mathrm{Im}\{W(j\boldsymbol{\Omega})\}}{\mathrm{Re}\{W(j\boldsymbol{\Omega})\}}, \tag{10.6}$$

can be expressed in terms of the parameters of the filter natural frequency ω_0 and damping ζ and the required $(\boldsymbol{A}_1, \boldsymbol{\Omega})$. Here, Q_3 and Q_4 are defined as the third and fourth quadrants of the complex plane, respectively. We express the real and imaginary part of (10.1) in terms of the desired frequency, damping, and natural frequency which are given by

$$\mathrm{Re}\{W(j\boldsymbol{\Omega})\} = \frac{(\omega_0^2 - \boldsymbol{\Omega}^2)w_0^2}{\omega_0^4 + 2\Omega^2(2\zeta^2 - 1)\omega_0^2 + \boldsymbol{\Omega}^4} \tag{10.7}$$

$$\mathrm{Im}\{W(j\boldsymbol{\Omega})\} = -\frac{2\zeta\boldsymbol{\Omega}\omega_0^3}{w_0^4 + 2\boldsymbol{\Omega}^2(2\zeta^2 - 1)\omega_0^2 + \boldsymbol{\Omega}^4} \tag{10.8}$$

where the denominator of the above equations are positive since the transfer function $W(s)$ is stable. The magnitude of $W(j\omega)$ at the desired frequency $\boldsymbol{\Omega}$ is

$$\|W(j\boldsymbol{\Omega})\| = \frac{\omega_0^2}{\sqrt{(\omega_0^2 - \boldsymbol{\Omega}^2)^2 + 4(\zeta \boldsymbol{\Omega} \omega_0)^2}}. \tag{10.9}$$

Therefore, coefficients c_1 and c_2 can be computed from (10.4)–(10.9) as follows:

$$c_1 = \frac{\pi}{4} A_p \cdot \left(\frac{\boldsymbol{\Omega}^2 - \omega_0^2}{\omega_0^2} \right) \tag{10.10}$$

$$c_2 = -\frac{\pi A_p \zeta \boldsymbol{\Omega}}{2\omega_0} \tag{10.11}$$

where the Nyquist quadrant identification is no longer required.

10.2.2 Upper Bound Estimates

Let us now solve the inverse problem and determine the upper bound estimate for the generated signal amplitude $\boldsymbol{A}_1^{\max}$. To this end, note from (10.2) that inequality (10.3) is equivalent to

$$|c_1| + |c_2| \leq u^{\max}. \tag{10.12}$$

It follows from (10.10)–(10.12) that

$$|u| = |c_1| + |c_2| = \frac{\pi}{4} \frac{|\omega_0^2 - \boldsymbol{\Omega}^2|}{\omega_0^2} \boldsymbol{A}_1 + \frac{\pi \zeta \boldsymbol{\Omega}}{2\omega_0} \boldsymbol{A}_1 \leq u^{\max}, \tag{10.13}$$

and therefore, by setting $|c_1| + |c_2| = u^{\max}$, we have

$$\boldsymbol{A}_1^{\max} = \frac{4}{\pi} \left(\frac{\omega_0^2}{|\omega_0^2 - \boldsymbol{\Omega}^2| + 2\zeta \omega_0 \boldsymbol{\Omega}} \right) u^{\max}. \tag{10.14}$$

Moreover, one can conclude that if the closed-loop system (10.1)–(10.2) is orbitally asymptotically stable then

$$\sup \|y_{ss}(t)\| \leq \boldsymbol{A}_1^{\max} \tag{10.15}$$

where $y_{ss}(t)$ is the steady state response of the output $y(t)$. We can now summarize our investigation into the possibility of providing necessary amplitudes of the generated oscillation as the following two statements.

Theorem 10.1. *Suppose that the closed-loop system, consisting of a stable second-order transfer function* (10.1) *and the two-relay controller* (10.2)*, is orbitally asymptotically stable. Then for any* $\boldsymbol{A}_1 \in [0, \boldsymbol{A}_1^{max}]$*, where* $\boldsymbol{A}_1^{max} \in \mathscr{A} \subset \mathbb{R}$ *is given by* (10.14)*, there exists a positive constant* $u^* \leq u^{max}$ *such that* $\sup_{t \geq 0} |u(t)| \leq u^*$.

Theorem 10.2. *Suppose that the coefficients c_1 and c_2 of the TRC produce a FPL that induces a periodic trajectory, i.e.,* (10.1)–(10.2)*. This periodic solution is orbitally exponentially stable if and only if all the eigenvalues of the matrix Φ, defined by* (4.33)–(4.35)*, are located inside the unit circle.*

Proof. The proof is given in Subsection 4.6 and it is therefore omitted here.

Let us illustrate the above theorem by applying it to the system (10.1) whose state-space representation is

$$\frac{d}{dt}\begin{bmatrix} x_1 \\ x_2 \end{bmatrix} = \underbrace{\begin{bmatrix} 0 & 1 \\ -\omega_0^2 & -2\zeta\omega_0 \end{bmatrix}}_{A} \underbrace{\begin{bmatrix} x_1 \\ x_2 \end{bmatrix}}_{x} + \underbrace{\begin{bmatrix} 0 \\ \omega_0^2 \end{bmatrix}}_{B} u \tag{10.16}$$

$$y = \underbrace{\begin{bmatrix} 1 & 0 \end{bmatrix}}_{C} \begin{bmatrix} x_1 \\ x_2 \end{bmatrix} \tag{10.17}$$

where A is Hurwitz without eigenvalues on the imaginary axis. Introduce

$$\varphi_1 = \frac{1}{2\sqrt{\xi^2 - 1}} \begin{bmatrix} p_{11} - \frac{v_{1,1}}{v_{1,2}} p_{21} & p_{12} - \frac{v_{1,1}}{v_{1,2}} p_{22} \\ 0 & 0 \end{bmatrix} \tag{10.18}$$

$$\varphi_2 = \frac{1}{2\sqrt{\xi^2 - 1}} \begin{bmatrix} 0 & 0 \\ q_{21} - \frac{v_{2,2}}{v_{2,1}} q_{11} & q_{22} - \frac{v_{2,2}}{v_{2,1}} q_{12} \end{bmatrix} \tag{10.19}$$

where

$$\begin{aligned}
v_1 &= \begin{bmatrix} v_{1,1} \\ v_{1,2} \end{bmatrix} = \begin{bmatrix} 0 \\ \omega_0^2 |\eta_{p1}| + \omega_0^2 (c_1 + c_2) \end{bmatrix} \\
v_2 &= \begin{bmatrix} v_{2,1} \\ v_{2,2} \end{bmatrix} = \begin{bmatrix} \rho_{p2} \\ 2\zeta\omega_0 |\rho_{p2}| + \omega_0^2 (c_1 - c_2) \end{bmatrix} \\
p_{11} &= \left(-\zeta + \sqrt{\zeta^2 - 1}\right) e^{\lambda_1 \theta_1} + \left(\zeta + \sqrt{\zeta^2 - 1}\right) e^{\lambda_2 \theta_1} \\
p_{12} &= -e^{\lambda_1 \theta_1} + e^{\lambda_2 \theta_1} \\
p_{21} &= -\omega_0 p_{12} \\
p_{22} &= \left(\zeta + \sqrt{\zeta^2 - 1}\right) e^{\lambda_1 \theta_1} + \left(-\zeta + \sqrt{\zeta^2 - 1}\right) e^{\lambda_2 \theta_1} \\
q_{11} &= \left(-\zeta + \sqrt{\zeta^2 - 1}\right) e^{\lambda_1 \theta_2} + \left(\zeta + \sqrt{\zeta^2 - 1}\right) e^{\lambda_2 \theta_2} \\
q_{12} &= -e^{\lambda_1 \theta_2} + e^{\lambda_2 \theta_2} \\
q_{21} &= -\omega_0 q_{12} \\
q_{22} &= \left(\zeta + \sqrt{\zeta^2 - 1}\right) e^{\lambda_1 \theta_2} + \left(-\zeta + \sqrt{\zeta^2 - 1}\right) e^{\lambda_2 \theta_2}.
\end{aligned}$$

The parameters $\lambda_1 = -\zeta\omega_0 - \omega_0\sqrt{\zeta^2 - 1}$ and $\lambda_2 = -\zeta\omega_0 + \omega_0\sqrt{\zeta^2 - 1}$ are the eigenvalues of A. Conditions given in (3.8) were taken into account in v_1 and v_2, i.e., $\eta_{p1} < 0$, $\eta_{p2} = 0$, $\rho_{p1} = 0$, and $\rho_{p2} < 0$. Substituting (10.18)–(10.19) into (4.35) yields

$$\Phi = \frac{1}{16(\zeta^2 - 1)^2}\begin{bmatrix} \Phi_{11} & \Phi_{12} \\ 0 & 0 \end{bmatrix} \tag{10.20}$$

whose eigenvalues are 0 and $\Phi_{11}/16(\zeta^2 - 1)^2$ where

$$\begin{aligned} &\Phi_{11} \\ &= -\left(\omega_0 + \frac{v_{2,2}}{v_{2,1}}\lambda_2\right)e^{\lambda_1 T/2} + \left(\omega_0 + \frac{v_{2,2}}{v_{2,1}}\lambda_1\right)e^{\lambda_1\theta_1 + \lambda_2\theta_2} \\ &\quad + \left(\omega_0 + \frac{v_{2,2}}{v_{2,1}}\lambda_2\right)e^{\lambda_1\theta_2 + \lambda_2\theta_1} - \left(\omega_0 + \frac{v_{2,2}}{v_{2,1}}\lambda_1\right)e^{\lambda_2 T/2}. \end{aligned} \tag{10.21}$$

Finally, according to Theorem 10.2, if $16(\zeta^2 - 1)^2 > \|\Phi_{11}\|$, then the orbit of the closed-loop system (10.1)–(10.2) will be asymptotically stable. Under the assumption that $\lambda_i < 0$, $i = 1, 2$ are real, the following upper bound holds

$$\begin{aligned} \|\Phi_{11}\| &\le 2\left|\omega_0 + \frac{v_{2,2}}{v_{2,1}}\lambda_1\right| + 2\left|\omega_0 + \frac{v_{2,2}}{v_{2,1}}\lambda_2\right| \\ &\le 4\omega_0\left(1 + (\zeta + \sqrt{\zeta^2 - 1})\left|\frac{v_{2,2}}{v_{2,1}}\right|\right). \end{aligned} \tag{10.22}$$

10.2.3 Experimental Results

The experimental setup for the FPL includes a second-order filter, which is realized as the unity-gain Sallen–Key low-pass filter [58]. Its transfer function is given by

$$W(s) = \frac{1}{\omega_c^2 R_1 R_2 C_1 C_2 s^2 + \omega_c C_1(R_1 + R_2)s + 1}, \tag{10.23}$$

where ω_c is the cutoff frequency. Therefore, it follows from (10.1) that

$$\omega_0 = \frac{1}{\omega_c\sqrt{R_1 R_2 C_1 C_2}} \text{ and } \zeta = \frac{C_1(R_1 + R_2)}{2\sqrt{R_1 R_2 C_1 C_2}}. \tag{10.24}$$

Our *objective*, at this stage, is to induce a periodic voltage signal at the output of the filter $y(t)$ with $\boldsymbol{A}_1 = 10$ V and $\boldsymbol{\Omega} = 60$ Hz as desired voltage and frequency, respectively. Simulation and experimental results were obtained using

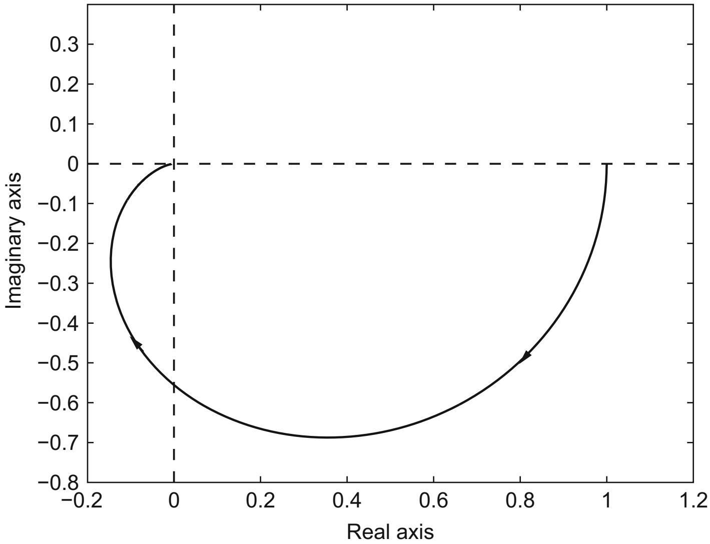

Fig. 10.1 Nyquist plot of the second-order filter

MATLAB/SIMULINK® and National Instruments MULTISIM 10.0® software packages.

For the simulations, we choose $\zeta = 0.9$, $\omega_0 = 150$, and $\omega_c = 500$ rad/s to realize the second-order transfer function (10.1). By selecting $\boldsymbol{\Omega} = 377$ rad/s and $u^{\max} = 80$, we find from (10.14) that the maximum amplitude is $\boldsymbol{A}_1^{\max} = 10.3507$. For the experiments, we choose $\boldsymbol{A}_1 = 10$ V. Selecting $R_1 = R_2 = 1$ MΩ and using equations (10.24), we find that $C_1 = 12$ pF and $C_2 = 15$ pF.

Now, following the procedure given in Section 10.2.1 to compute c_1 and c_2, we first find, by plotting the Nyquist plot of the second-order filter (10.1), that the desired frequency belongs to the third quadrant, i.e., $\Omega \in Q_3$ (see Fig. 10.1). Since $\mathrm{Re}\{j377\} = -0.1091$ and $\mathrm{i}\{j377\} = -0.0928$ and by using (10.4), (10.5), we find that $c_1 = 41.7584$ and $c_2 = -35.5314$.

Figure 10.2 shows the output voltage $y(t)$ of the filter demonstrating that the required amplitude and frequency can be realized.

10.3 Analogue Realization of Fixed-Phase Loop (FPL)

Phase-lock loops (PLL) [4] are used in many applications for tracking periodic signals with a specified phase shift. Usually PLL is a circuit synchronizing an output signal, generated by an oscillator, with a reference or input signal in frequency as well as in phase [11]. PLLs are particularly found in communications, control, power electronics, servo-systems, and digital signal processors.

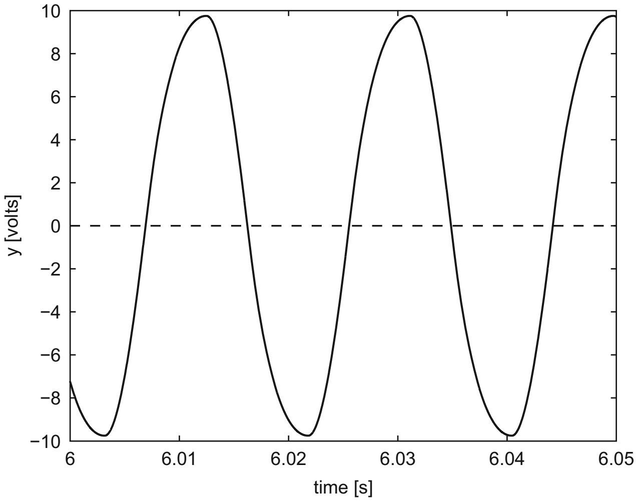

Fig. 10.2 Simulation of the output of the second order filter

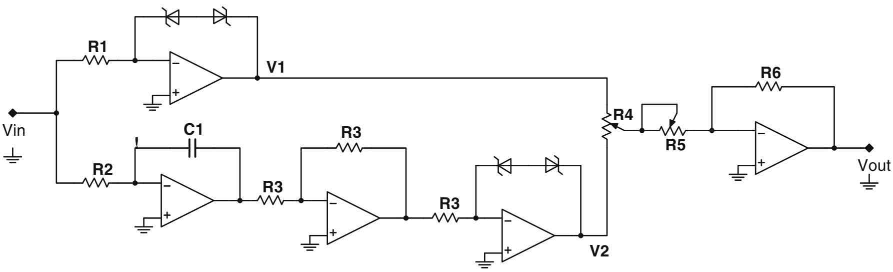

Fig. 10.3 Electric circuit diagram for TRC (non-inverting)

As shown in the previous section, a circuit having similar to PLL functionality can be produced by using the TRC in combination with an LP filter. It was named an FPL. However, having in mind an analogue realization of an FPL, one can notice that the differentiator implementation may be problematic due to amplification of the noise component. A better option in this respect would be the use of the serially connected TRC and an integrator. In fact, this serial connection transforms into a parallel connection of an integrator and a relay and a relay. A few schematics of this design are presented below that were experimentally tested, simulated and found suitable as realizations of the FPL.

The first TRC schematic is given in Fig. 10.3.

Its working principle can be described as follows. The first relay is implemented on the first operational amplifier having two Zener diodes in the feedback. The integrator is implemented on the second operational amplifier; the integral time constant is R_2C. Amplifier on Opamp 3 is necessary to invert the voltage. It should be noted that this inverting amplifier is necessary only if the frequency of the self-exited oscillation needs to be generated in the third quadrant of the Nyquist plot of the plant (LP filter). In this case, the signals from the first Opamp and the fourth Opamp are summed. If the inverter is not used, then the output signal of the fourth Opamp is subtracted from the output of the first Opamp, and oscillations are generated in the fourth quadrant of the Nyquist plot of the plant (LP filter). The second relay is realized on the fourth Opamp. Potentiometer R_4 is used as a voltage divider between the outputs of the two relays: V_1 and V_2. To find the model of the divider circuit, one should take into account the fact that the inverting input of the fifth amplified is at zero potential. Therefore, the three resistances: the part of R_4 from the tap point to the upper terminal (denoted below as R_8), the part of R_4 from the tap point to the bottom terminal (denoted below as R_7), and R_5 have a Y-connection. Equating the sum of currents arriving at the tap point of R_4 to zero, we find the following relationship:

$$V_3 = \frac{\frac{V_1}{R_8} + \frac{V_2}{R_7}}{\frac{1}{R_8} + \frac{1}{R_7} + \frac{1}{R_5}} \tag{10.25}$$

and the output of TRC:

$$V_{\text{out}} = -V_3 \cdot \frac{R_6}{R_5} = -\frac{\frac{V_1}{R_8} + \frac{V_2}{R_7}}{\frac{R_5}{R_8} + \frac{R_5}{R_7} + 1} \cdot R_6. \tag{10.26}$$

Considering that $R_8 = \alpha R_4$ and $R_2 = (1-\alpha)R_4$, with $\alpha \in [0, 1]$ being the potentiometer position (assuming linear characteristic), we rewrite the expression for output voltage as

$$\begin{aligned} V_{out} &= \left(\frac{V_1}{\alpha R_4} + \frac{V_2}{(1-\alpha)R_4}\right) \cdot \frac{-R_6}{R_5\left(\frac{1}{\alpha R_4} + \frac{1}{(1-\alpha)R_4}\right) + 1} \\ &= \frac{1}{R_4}\left(\frac{V_1}{\alpha} + \frac{V_2}{1-\alpha}\right) \cdot \frac{-R_6}{\frac{R_5}{R_4}\left(\frac{1}{\alpha} + \frac{1}{1-\alpha}\right) + 1} \\ &= \left(\frac{V_1}{\alpha} + \frac{V_2}{1-\alpha}\right) \cdot \frac{-R_6}{R_5\left(\frac{1}{\alpha} + \frac{1}{1-\alpha}\right) + R_4}. \end{aligned} \tag{10.27}$$

If R_4 is small ($R_4 \ll R_5$), then the potentiometer works as a linear voltage divider:

$$\begin{aligned} V_{out} &\approx -\left(\frac{V_1}{\alpha} + \frac{V_2}{1-\alpha}\right)\alpha(1-\alpha)\frac{R_6}{R_5} \\ &= -\left((1-\alpha)V_1 + \alpha V_2\right) \cdot \frac{R_6}{R_5}. \end{aligned} \tag{10.28}$$

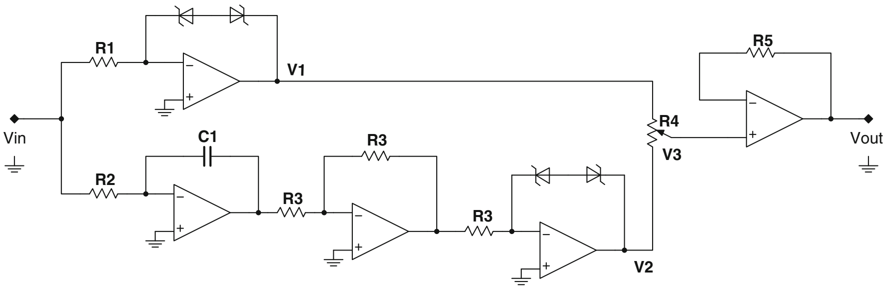

Fig. 10.4 Electric circuit diagram for TRC (inverting)

Another schematic of TRC is presented in Fig. 10.4. It has a non-inverting voltage repeater built on operational amplifier 5. Because of the high input resistance, the output voltage is simply V_3:

$$V_{out} = V_3. \tag{10.29}$$

And since the current through R_4 is $i = \frac{V_1 - V_2}{R_4}$, the TRC output voltage is

$$\begin{aligned} V_{out} = V_3 = V_2 + i(1-\alpha)R_4 &= V_2 + \frac{V_1 - V_2}{R_4}(1-\alpha)R_4 \\ &= V_2 + (1-\alpha)V_1 - (1-\alpha)V_2 \\ &= (1-\alpha)V_1 + \alpha V_2. \end{aligned} \tag{10.30}$$

If the amplitudes of V_1 and V_2 are equal to c, then

$$c_1 = (1-\alpha)c \tag{10.31}$$

and

$$c_2 = \alpha c. \tag{10.32}$$

The describing function of the controller is

$$N(a) = -\frac{h}{\pi a}(c_1 - jc_2) = -\frac{hc}{\pi a}(1 - \alpha - j\alpha). \tag{10.33}$$

The minus in (10.33) is due to inverting.

The phase shift provided by the circuit in Fig. 10.4 (disregarding inversion) is

$$\Psi = -\arctan\left(-\frac{\alpha}{1-\alpha}\right). \tag{10.34}$$

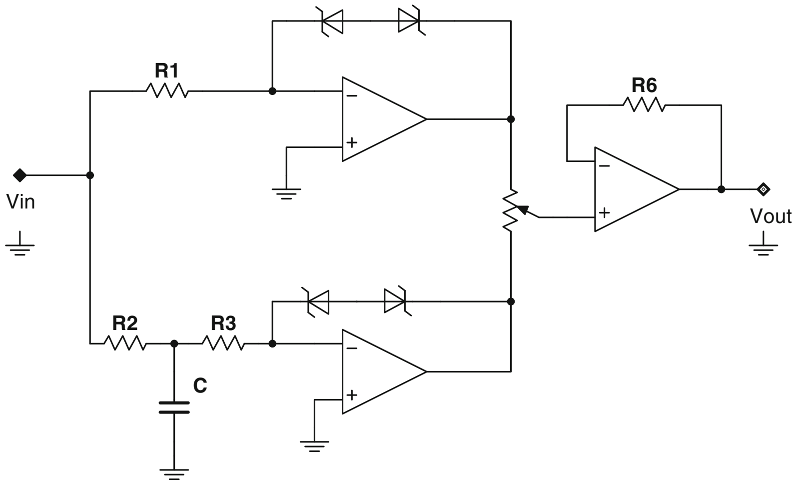

Fig. 10.5 Simplified TRC circuit (inverting)

The total phase shift (including inversion) is

$$\Psi = -\pi - \arctan\left(\frac{\alpha}{1-\alpha}\right). \tag{10.35}$$

Therefore, the phase shift can be regulated by the potentiometer R_4, which will not result in a change of any other parameter. The value of the phase shift is determined only by the position of R_4 and will be the same for every circuit connected in the loop with the controller: the frequency of oscillations will be different, but it will correspond to a specific (determined by position of R_4) phase.

A simplified circuit is provided in Fig. 10.5. The circuit given by R_2 and C is not an integrator, but a first-order low-pass filter with transfer function

$$W_f(s) = \frac{1}{R_2Cs + 1}.$$

If the frequency of the input signal (of the oscillations in the loop) is high enough, so that $R_2C\omega \gg 1$, then this circuit would act as an integrator with $W_f(s) \approx 1/R_2Cs$.

It can be noted that the LP filter included in the loop with TRC to form an FPL circuit must be inverting for the non-inverting TRC and non-inverting for the inverting TRC to ensure proper phase relationship necessary for generating an oscillation. Therefore, for the circuit Fig. 10.3, the LP filter can be built on one inverting operational amplifier. An example of this circuit is given in Fig. 10.6.

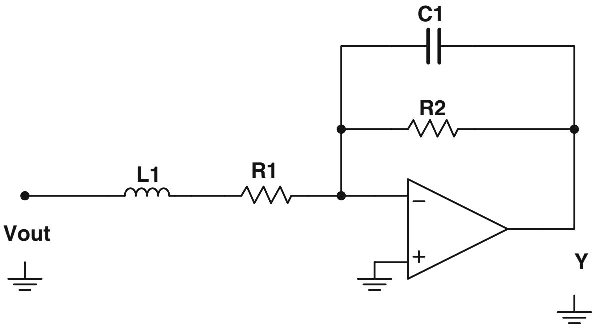

Fig. 10.6 Second-order filter circuit used as plant

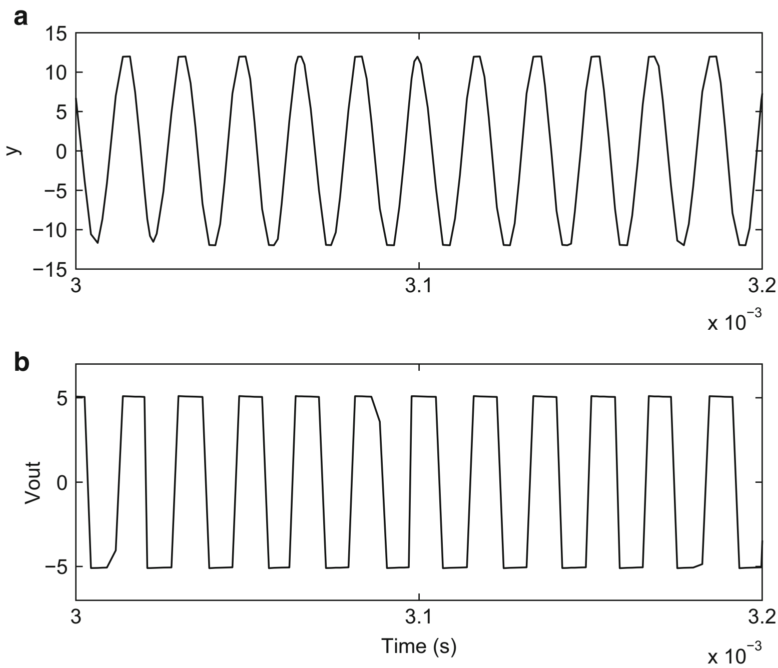

Fig. 10.7 Output voltage responses for circuit of Fig. 10.5 coupled to circuit of Fig. 10.6: (a) voltage at the output of the plant and (b) voltage signal at the output of the TRC

10.3.1 Simulations and Experiments

PSpice simulations of circuits Fig. 10.5 and Fig. 10.6 connected in a loop are presented in Fig. 10.7.

Realization of the circuit Fig. 10.3, having parameters $R_1 = R_2 = R_3 = R_4 = R_5 = R_6 = 10\,\mathrm{k}\Omega$, $C_1 = 1\,\mu\mathrm{F}$, $R_7 = 100\,\mathrm{k}\Omega$, $R_8 = 51\,\mathrm{k}\Omega$, Zener diodes all for 9.1 V, all operational amplifiers LM348N, and of the circuit Fig. 10.6 having parameters

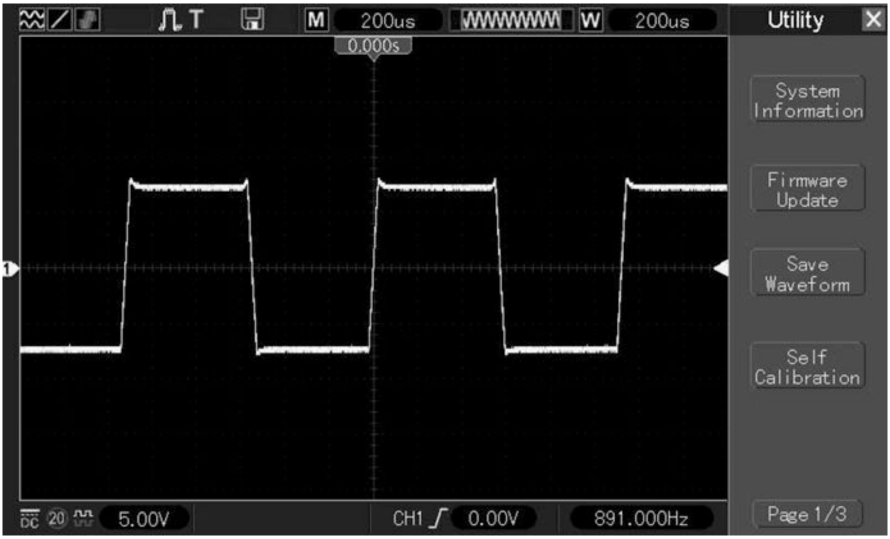

Fig. 10.8 Output of TRC in FPL; lowest position of potentiometer R_4

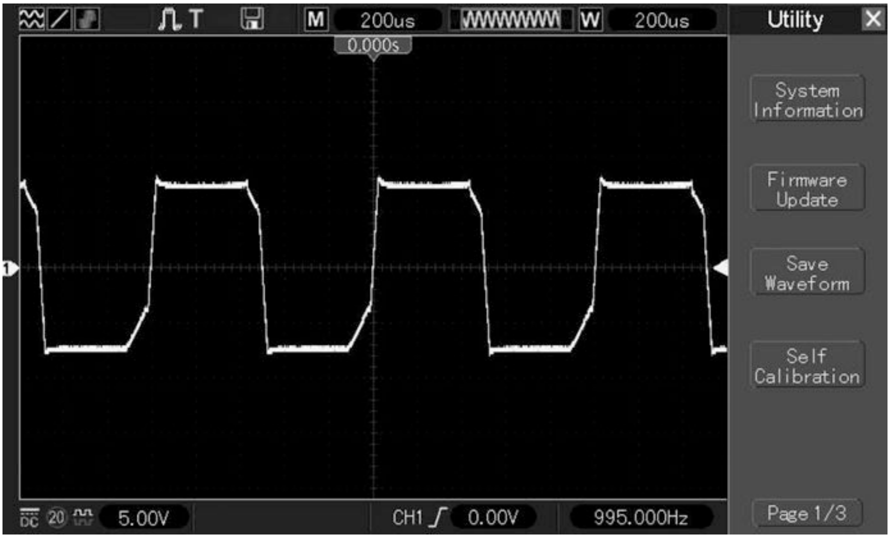

Fig. 10.9 Output of TRC in FPL; lower-intermediate position of potentiometer R_4

$R_1 = 10\ \mathrm{k}\Omega$, $L_1 = 10\ \mathrm{mH}$, $R_2 = 10\ \mathrm{k}\Omega$, $C_1 = 1\ u\mathrm{F}$ was done to produce a FPL. The results of experimental testing of this FPL are given in Figs. 10.8, 10.9, 10.10, 10.11.

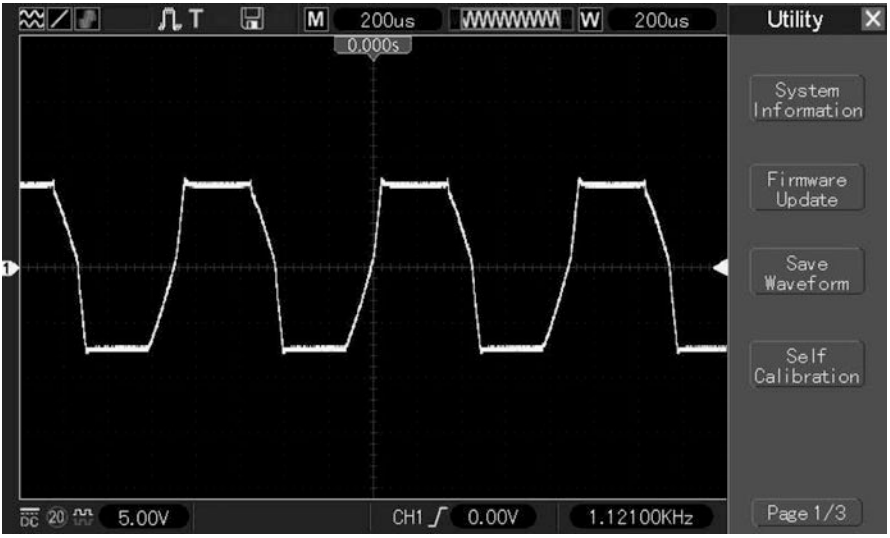

Fig. 10.10 Output of TRC in FPL; upper-intermediate position of potentiometer R_4

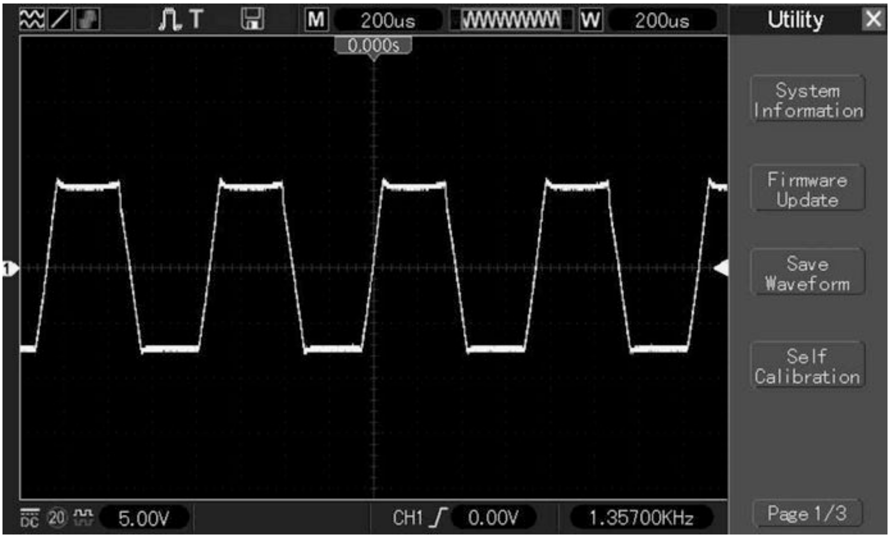

Fig. 10.11 Output of TRC in FPL; upper position of potentiometer R_4

10.4 Conclusions

In this chapter a fixed-phase loop (FPL) is presented. FPL consists of the TRC and an arbitrary plant having low-pass filtering properties (an LP filter). The FPL has the remarkable property of generating oscillations at a fixed (specified) phase lag of the LP filter, so that if the filter is replaced with another one the oscillations will be again generated at the same phase lag of the second PL filter. The authors believe that this property of the FPL can be used in practice.

A few examples of FPL circuits are presented. The circuits are provided with formulas relating the *RLC* elements and the characteristics of the FPL and illustrated by simulations and experiments.

Appendix A
Describing Function

Describing Function (DF) is a classical tool for analyzing the existence of limit cycles in nonlinear systems based in the frequency-domain approach. Although this method is not as general as the analysis for linear system is, it gives good approximated results for relay feedback systems.

The idea of the method using the scheme presented in Fig. A.1 is to obtain the DF of the single-input–single-output control block, which is assumed nonlinear, and according to [39] the definition of DF is the complex fundamental-harmonic gain of a nonlinearity in the presence of a driving sinusoid. Consider the input signal of the control block as $\sigma(t) = A\sin(\omega t)$ and its output signal, presented by its Fourier representation, as

$$u(t) = \frac{a_0}{2} + \sum_{n=1}^{\infty}[a_n\cos(n\omega t) + b_n\sin(n\omega t)].$$

A restriction for this approach is that in the above scheme only one block can be nonlinear, so a common case might be considering the plant to be linear and allowing the control block to be the nonlinear part, covering in such a way a wide variety of real engineering problem like saturation, dead zones, Coulomb friction or backlash. Also linear plant has to be time invariance and regarding the approximation of the output $u(t)$ via its Fourier representation, the analysis is done with null offset ($a_0 = 0$) and taking only the first harmonic ($n = 1$) of the Fourier series of this signal:

$$\frac{u(t)}{\sigma(t)} \simeq \frac{a_1\cos(\omega t) + b_1\sin(\omega t)}{A\sin(\omega t)} \tag{A.1}$$

due to this last consideration, most of the information of $u(t)$ has to be contained in the first harmonic term, otherwise approximation will be extremely poor, for achieving this, the linear element must have low-pass properties (filtering hypothesis), it

L.T. Aguilar et al., *Self-Oscillations in Dynamic Systems*, Systems & Control: Foundations & Applications, DOI 10.1007/978-3-319-23303-1

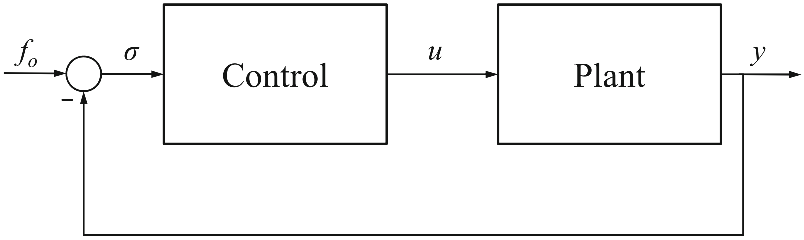

Fig. A.1 Basic scheme for DF analysis

means that

$$|G(j\omega)| \gg |G(jn\omega)| \qquad n = 2, 3, \ldots$$

Using the trigonometric identity $a_1 \cos(\omega t) + b_1 \sin(\omega t) = \sqrt{a_1^2 + b_1^2} \sin(\omega t + \phi)$, where $\phi = \arctan(a_1/b_1)$, in Eq. (A.1), we get

$$\frac{u(t)}{\sigma(t)} \simeq \frac{\sqrt{a_1^2 + b_1^2} \sin(\omega t + \phi)}{A \sin(\omega t)}.$$

According to [39] the describing function $N(A, \omega)$ is defined as the ratio of the phasor representation of output component at frequency ω and the phasor representation of input component at frequency ω, that is

$$N(A, \omega) = \frac{\left(\sqrt{a_1^2 + b_1^2}\right) e^{j(\omega t + \phi)}}{A e^{j\omega t}} = \frac{1}{A}(b_1 + ja_1) \tag{A.2}$$

where the coefficients a_1 and b_1 of the first harmonic of Fourier representation are given by

$$a_1 = \frac{\omega}{\pi} \int_0^{2\pi/\omega} u(t) \cos(\omega t) dt, \qquad b_1 = \frac{\omega}{\pi} \int_0^{2\pi/\omega} u(t) \sin(\omega t) dt.$$

Finally, substituting a_1 and b_1 into (A.2) yields to

$$N(A, \omega) = \frac{\omega}{\pi A} \int_0^{2\pi/\omega} u(t) \sin(\omega t) dt + j \frac{\omega}{\pi A} \int_0^{2\pi/\omega} u(t) \cos(\omega t) dt. \tag{A.3}$$

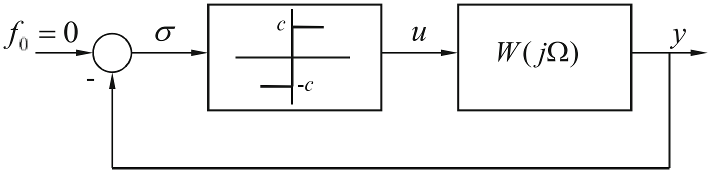

Fig. A.2 Relay feedback using single-relay control

A.1 Describing Function of a Single-Relay

Let us first investigate the existence of periodic solution of a single-relay control given by (see Fig. A.2)

$$u(t) = \begin{cases} -c & \text{if } \frac{\pi}{\omega} < t < 0 \\ c & \text{if } 0 < t < \frac{\pi}{\omega}. \end{cases} \tag{A.4}$$

Using (A.3) yields

$$N(A, \omega) = \frac{4c}{\pi A} \tag{A.5}$$

where A and ω are the amplitude and frequency of the output $y(t)$, respectively.

Appendix B
The locus of a perturbed relay system (LPRS)

B.1 Asymmetric oscillations in relay feedback systems

The *locus of a perturbed relay system* (LPRS) method of analysis is similar from the methodological point of view to the DF method. It is designed to imitate the methodology of analysis used in the DF-based approach. Some concepts (like the notion of the *equivalent gain*) are also similar. However, the LPRS method is exact and the notions that are traditionally used within the DF method are redefined, so that in the LPRS analysis similar notions are used in the exact sense.

Let us consider the SISO relay feedback system, that has a constant input, described by the following equations:

$$\begin{aligned} \dot{\mathbf{x}}(t) &= \mathbf{A}\mathbf{x}(t) + \mathbf{B}u(t) \\ y(t) &= \mathbf{C}\mathbf{x}(t), \end{aligned} \tag{B.1}$$

where $\mathbf{A} \in \mathbb{R}^{n\times n}$, $\mathbf{B} \in \mathbb{R}^{n\times 1}$ and $\mathbf{C} \in \mathbb{R}^{1\times n}$ are matrices, $\mathbf{A}$ is nonsingular, $\mathbf{x} \in \mathbb{R}^{n\times 1}$ is the state vector, $y \in \mathbb{R}^1$ is the system output and $u \in \mathbb{R}^1$ is the control defined as follows:

$$u(t) = \begin{cases} +h & \text{if } e(t) = r_0 - y(t) \geq b \\ & \text{or} \quad e(t) > -b\,,\ u(t-) = h \\ -h & \text{if } e(t) = r_0 - y(t) \leq -b \\ & \text{or} \quad e(t) < b\,,\ u(t-) = -h \end{cases} \tag{B.2}$$

where r_0 is a constant input to the system, e is the error signal, h is the relay amplitude, $2b$ is the hysteresis value of the relay and $u(t-) = \lim\limits_{\epsilon\to 0, \epsilon>0} u(t-\epsilon)$ is the control at the time instant immediately preceding time t. We shall consider that

L.T. Aguilar et al., *Self-Oscillations in Dynamic Systems*, Systems & Control: Foundations & Applications, DOI 10.1007/978-3-319-23303-1

time $t = 0$ corresponds to the time of the error signal becoming equal to the positive half-hysteresis value (subject to $\dot{e} > 0$): $e(0) = b$ and call this time the *time of relay switch from* $-h$ *to* h.

We can also represent the linear part of the relay feedback system (B.1) by the transfer function $W_l(s)$:

$$W_l(s) = \mathbf{C}(\mathbf{I}s - \mathrm{A})^{-1}\mathbf{B}. \tag{B.3}$$

We shall assume that the linear part is strictly proper, i.e., the relative degree of $W_l(s)$ is 1 or higher, which is a valid assumption for all physically realisable systems.

If the input to the system is a constant value $r_0 : r(t) \equiv r_0$, then an asymmetric periodic motion occurs in the relay feedback system, so that each signal has a periodic term with zero mean value and a nonzero constant term: $u(t) = u_0 + u_p(t)$, $y(t) = y_0 + y_p(t)$, $e(t) = e_0 + e_p(t)$, where subscript 0 refers to the constant term, and subscript p refers to the periodic term of the function. The periodic term represents the sum of all periodic terms (harmonics) in the Fourier series expansion for respective signal. The constant term is the averaged value of the signal on the period.

The constant input signal r_0 can be quasi-statically (slowly) slewed from a certain negative value to a positive value, so that at each value of the input signal the system establishes a stable oscillation, and the values of the constant terms of the error signal and of the control signal are measured. Then the constant term of the control signal can be considered as a function of the constant term of the error signal. This dependance would give the *bias function* $u_0 = u_0(e_0)$, which would be not a discontinuous but a smooth function. The described smoothing effect is known as the *chatter smoothing* phenomenon. The derivative of the mean control with respect to the mean error taken in the point of zero mean error $e_0 = 0$ (corresponding to zero constant input) provides the *equivalent gain* of the relay k_n. The *equivalent gain* of the relay can be used as a local approximation of the *bias function*: $k_n = \mathrm{d}u_0/\mathrm{d}e_0|_{e_0=0} = \lim\limits_{r_0 \to 0}(u_0/e_0)$.

B.2 Computation of the LPRS

B.2.1 Computeation of LPRS from matrix state space description

A complex function of frequency ω named the locus of a perturbed relay system (LPRS) was introduced in [13] for analysis of self-excited oscillations in and external signal propagation through the relay system as follows:

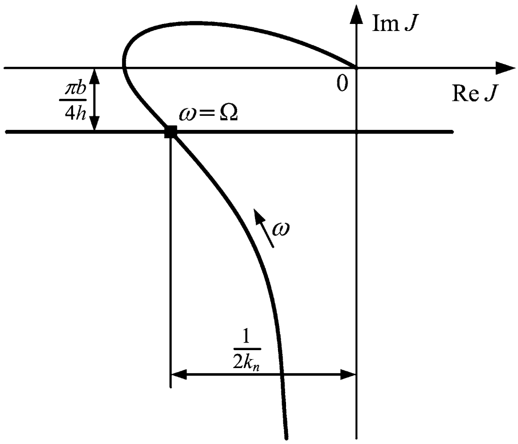

Fig. B.1 LPRS and analysis of relay feedback system

$$J(\omega) = -0.5\mathbf{C}\left[\mathbf{A}^{-1} + \tfrac{2\pi}{\omega}\left(\mathbf{I} - e^{\frac{2\pi}{\omega}\mathbf{A}}\right)^{-1} e^{\frac{\pi}{\omega}\mathbf{A}}\right]\mathbf{B} \\ +j\tfrac{\pi}{4}\mathbf{C}\left(\mathbf{I} + e^{\frac{\pi}{\omega}\mathbf{A}}\right)^{-1}\left(\mathbf{I} - e^{\frac{\pi}{\omega}\mathbf{A}}\right)\mathbf{A}^{-1}\mathbf{B}, \tag{B.4}$$

where $\omega \in [0, \infty)$. An LPRS plot is presented in Fig. B.1.

It was proved in [13] and [14] that the frequency Ω of the self-excited oscillations can be computed through solving the equation:

$$\mathrm{Im}\, J(\Omega) = -\frac{\pi b}{4h}, \tag{B.5}$$

and the equivalent gain k_n, which describes propagation of constant signals (or signals slowly varied with respect to the self excited oscillation) can be computed as:

$$k_n = -\frac{1}{2\mathrm{Re}\, J(\Omega)}. \tag{B.6}$$

Both values provided by formulas (B.5) and (B.6) are exact. LPRS also offers a convenient graphic interpretation of finding the frequency Ω and the equivalent gain k_n (Fig. B.1). The point of intersection of the LPRS and the horizontal line, which lies at the distance of $\pi b/(4h)$ below (if $b > 0$) or above (if $b < 0$) the horizontal axis (line "$-\pi b/4h$"), allows for computation of the frequency of the oscillations and of the equivalent gain k_n of the relay.

B.2.2 Computation of the LPRS from transfer function

A different formula for $J(\omega)$ was derived in [14] for the case of the linear part given by a transfer function. Through application of the Fourier series, it was proved that LPRS can also be computed as the following infinite series:

$$J(\omega) = \sum_{k=1}^{\infty}(-1)^{k+1}\mathrm{Re}W_l(k\omega) + j\sum_{k=1}^{\infty}\frac{1}{2k-1}\mathrm{Im}W_l[(2k-1)\omega]. \tag{B.7}$$

Another technique of LPRS computation is based on the possibility of derivation of analytical formulas for the LPRS of low-order dynamics. It is a result of the additivity property that LPRS possesses, which can be formulated as follows.

Additivity property. If the transfer function $W_l(s)$ of the linear part is a sum of n transfer functions: $W_l(s) = W_1(s) + W_2(s) + \cdots + W_n(s)$ then the LPRS $J(\omega)$ can be calculated as a sum of the n component LPRS: $J(\omega) = J_1(\omega) + J_2(\omega) + \cdots + J_n(\omega)$, where $J_i(\omega)$ $(i = 1, \ldots, n)$ is the LPRS of the relay system with the transfer function of the linear part being $W_i(s)$.

The considered property offers a technique of the LPRS computation based on the expansion of the process transfer function into partial fractions. Therefore, if $W_l(s)$ is expanded into the sum of first and second order dynamics then LPRS $J(\omega)$ can be calculated through the summation of the component LPRS $J_i(\omega)$ corresponding to each of the component transfer functions, subject to analytical formulas for the LPRS of first and second order dynamics. Formulas for $J(\omega)$ of first and second order dynamics were derived in [14]. They are presented in Table B.1.

B.2.3 Some properties of the LPRS

Some important properties of the LPRS as a frequency-domain characteristic are related with the boundary points corresponding to zero frequency and infinite frequency. The initial point of the LPRS (which corresponds to zero frequency) can be found through formula (B.4). It can be noted that the limit of function $J(\omega)$ for ω tending to zero can be found as follows. First the following two limits must be evaluated: $\lim_{\omega\to 0}\left[\frac{2\pi}{\omega}((\mathbf{I} - e^{\frac{2\pi}{\omega}\mathbf{A}})^{-1}e^{\frac{\pi}{\omega}\mathbf{A}}\right] = \mathbf{0}$, $\lim_{\omega\to 0}\left[(\mathbf{I} + e^{\frac{\pi}{\omega}\mathbf{A}})^{-1}(\mathbf{I} - e^{\frac{\pi}{\omega}\mathbf{A}})\right] = \mathbf{I}$. Then the limit for the LPRS can be written as follows:

$$\lim_{\omega\to 0} J(\omega) = \left[-0.5 + j\frac{\pi}{4}\right]\mathbf{CA}^{-1}\mathbf{B} \tag{B.8}$$

The product of matrices $\mathbf{CA}^{-1}\mathbf{B}$ in (B.8) is the negative value of the gain of the transfer function. Therefore, for a *nonintegrating linear part of the relay feedback system, the initial point of the corresponding LPRS is* $(0.5K, -j\pi/4K)$*, where* K *is the static gain of the linear part.*

Table B.1 Formulas of the LPRS $J(\omega)$

Transfer fun. $W(s)$	LPRS $J(\omega)$
$\frac{K}{s}$	$0-j\frac{\pi^2 K}{8\omega}$
$\frac{K}{Ts+1}$	$\frac{K}{2}(1-\alpha\ \mathrm{csch}\alpha)-j\frac{\pi K}{4}\tanh(\alpha/2)$ $\alpha=\pi/(T\omega)$
$\frac{Ke^{-\tau s}}{Ts+1}$	$\frac{K}{2}(1-\alpha e^{\gamma}\ \mathrm{csch}\alpha)+j\frac{\pi K}{4}\left(\frac{2e^{-\alpha}e^{\gamma}}{1+e^{-\alpha}}-1\right)$ $\alpha=\frac{\pi}{T\omega},\ \ \gamma=\frac{\tau}{T}$
$\frac{K}{(T_1 s+1)(T_2 s+1)}$	$\frac{K}{2}[1-T_1/(T_1-T_2)\alpha_1\ \mathrm{csch}\alpha_1-T_2/(T_2-T_1)\alpha_2\ \mathrm{csch}\alpha_2)]$ $-j\frac{\pi K}{4}/(T_1-T_2)[T_1\tanh(\alpha_1/2)-T_2\tanh(\alpha_2/2)]$ $\alpha_1=\pi/(T_1\omega),\ \ \alpha_2=\pi/(T_2\omega)$
$\frac{K}{s^2+2\xi s+1}$	$\frac{K}{2}[(1-(B+\gamma C)/(\sin^2\beta+\sinh^2\alpha)]$ $-j\frac{\pi K}{4}(\sinh\alpha-\gamma\sin\beta)/(\cosh\alpha+\cos\beta)$ $\alpha=\pi\xi/\omega,\ \ \beta=\pi(1-\xi^2)^{1/2}/\omega,\ \ \gamma=\alpha/\beta$ $B=\alpha\cos\beta\sinh\alpha+\beta\sin\beta\cosh\alpha,$ $C=\alpha\sin\beta\cosh\alpha-\beta\cos\beta\sinh\alpha$
$\frac{Ks}{s^2+2\xi s+1}$	$\frac{K}{2}[\xi(B+\gamma C)-\pi/\omega\cos\beta\sinh\alpha]/(\sin^2\beta+\sinh^2\alpha)]$ $-j\frac{\pi K}{4}(1-\xi^2)^{-1/2}\sin\beta/(\cosh\alpha+\cos\beta)$ $\alpha=\pi\xi/\omega,\ \ \beta=\pi(1-\xi^2)^{1/2}/\omega,\ \ \gamma=\alpha/\beta$ $B=\alpha\cos\beta\sinh\alpha+\beta\sin\beta\cosh\alpha,$ $C=\alpha\sin\beta\cosh\alpha-\beta\cos\beta\sinh\alpha$
$\frac{Ks}{(s+1)^2}$	$\frac{K}{2}[\alpha(-\sinh\alpha+\alpha\cosh\alpha)/\sinh^2\alpha-j0.25\pi\alpha/(1+\cosh\alpha)]$ $\alpha=\pi/\omega$
$\frac{Ks}{(T_1 s+1)(T_2 s+1)}$	$\frac{K}{2}/(T_2-T_1)[\alpha_2\ \mathrm{csch}\alpha_2-\alpha_1\ \mathrm{csch}\alpha_1]$ $-j\frac{\pi K}{4}/(T_2-T_1)[\tanh(\alpha_1/2)-\tanh(\alpha_2/2)]$ $\alpha_1=\pi/(T_1\omega),\ \ \alpha_2=\pi/(T_2\omega)$

To find the limit of $J(\omega)$ for ω tending to infinity, the following two limits of the expansion into power series of the exponential function must be considered:

$$\lim_{\omega\to\infty}\exp\left(\frac{\pi}{\omega}\mathbf{A}\right)=\lim_{\omega\to\infty}\sum_{n=0}^{\infty}\frac{(\pi/\omega)^n}{n!}\mathbf{A}^n=\mathbf{I}$$

and

$$\lim_{\omega\to\infty}\left\{\frac{2\pi}{\omega}\left[\mathbf{I}-\exp\left(\frac{2\pi}{\omega}\mathbf{A}\right)\right]^{-1}\right\}=\lim_{\lambda=\frac{2\pi}{\omega}=\to 0}\{\lambda[\mathbf{I}-\exp(\lambda\mathbf{A})]^{-1}\}=-\mathbf{A}^{-1}.$$

These limits show that the end point of the LPRS for $\omega\to\infty$ for nonintegrating linear parts is the origin:

$$\lim_{\omega\to\infty}J(\omega)=0+j0. \tag{B.9}$$

Appendix C
Poincaré map

C.1 Basic concepts in Poincaré maps

Consider a time-invariant system

$$\dot{x} = f(x) \tag{C.1}$$

where $x(t) \in \mathbb{R}^n$ is the state. Let $\bar{x}(t)$ be its T-periodic solution starting from x_0. Introduce a smooth surface S by the equation $s(x) = 0$ where $s : \mathbb{R}^n \mapsto \mathbb{R}$ is a smooth scalar function and assume it intersects the trajectory in x_0 transversely, that is, $s(x_0) = 0$, $\nabla s(x_0)^T F(x) \neq 0$. We will call such a surface the transverse surface or cross-section across x_0. It can be shown that the solution starting from $x \in S = \{x : s(x) = 0\}$ close to x_0 will cross the surface $s(x) = 0$ again at least once. Let $\bar{t}(x)$ be the time of the first return and $P(x) \in S$ be the point of the first return.

Let us recall, that a *periodic orbit* of a nonlinear system $\dot{x} = f(x)$, with a vector state $x(t) \in \mathbb{R}^n$, is an invariant set which is determined by an initial condition x_p and a period T. Here T is defined as the smallest time $T > 0$ for which $\Phi(x_p, T) = x_p$ where $\Phi(x, t)$ stand for the solution operator ([26, p. 49]). A periodic orbit that is isolated (there no exist any other periodic orbit in its neighborhood) is named *limit cycle*.

Definition C.1 (Poincaré map [35]). The mapping $x \mapsto P(x)$ is called Poincaré map or return map.

For later use, the following Theorem for asymptotic orbital stability based on Poincaré maps read as follows.

Theorem C.1. *Let $\bar{x}(t)$ be a T-periodic solution, $x(t_0) = x_0$; S be the smooth cross-section across x_0 and P be the corresponding Poincaré map.*

L.T. Aguilar et al., *Self-Oscillations in Dynamic Systems*, Systems & Control: Foundations & Applications, DOI 10.1007/978-3-319-23303-1

If for any $\varepsilon > 0$ *there exists* $\delta > 0$ *such that* $x(t) \in S$, $|x - x_0| < \delta$ *implies* $|P(x) - x_0| < \varepsilon$, *then* $\bar{x}(t)$ *is orbitally stable. If, in addition,* $P^n(x) \to x_0$ *as* $n \to \infty$, *then* $\bar{x}(t)$ *is AOS.*

If all $n - 1$ *eigenvalues of the linearized Poincaré map* $\xi \mapsto \partial P(\xi)/\partial x$, $\xi \in S$ *have the absolute values less than 1, then* $\bar{x}(t)$ *is asymptotically orbitally stable.*

If the linearized Poincaré map has at least one eigenvalue with an absolute value greater than one then $\bar{x}(t)$ *is orbitally unstable.*

Proof. The proof is provided by Fradkov and Pogromsky [35] and it is therefore omitted.

Readers can review supplementary material and examples about Poincaré maps in [79][Chap. 7].

Appendix D
Output Feedback

D.1 State observer design

To maintain the estimation error bounded, the following linear observer for (6.4), (6.9)

$$\dot{\tilde{x}} = A\tilde{x} + B_2\tau + L(y - \tilde{y}) \tag{D.1}$$

is considered. Here, $\tilde{y} = C\tilde{x}$ and L must be designed such that the matrix $\tilde{A} := (A - LC)$ is Hurwitz. Let $e(t) := x(t) - \tilde{x}(t)$. Thus, $e(t)$ enters to a ball $\mathscr{B}_\delta(E_0)$ centered at the equilibrium point E_0 with radius $\delta > 0$ in finite-time T_e, such that

$$\|e(t)\| \leq e^+ \qquad \text{for all } t > T_e.$$

Now, let us decouple the unknown inputs from the successive derivatives of the output of the linear estimation error system defined as $y_e = y - \tilde{y}$.

Definition D.1 (Strong observability [86]). The system

$$\begin{aligned} \dot{x}(t) &= Ax(t) + B_2u(t), \\ y(t) &= Cx(t) + Du(t), \end{aligned} \tag{D.2}$$

it is called strongly observable if for all $x_0 \in \chi \subseteq \mathbb{R}^n$ and for every input function u, the following holds:

$$y_u(t, x_0) = Ce^{At}x_0 + \int_0^t Ce^{A(t-\tau)}B_2u(\tau)d\tau + Du(t) = 0 \tag{D.3}$$

for all $t \geq 0$ implies $x_0 = 0$.

L.T. Aguilar et al., *Self-Oscillations in Dynamic Systems*, Systems & Control: Foundations & Applications, DOI 10.1007/978-3-319-23303-1

Consider the output distribution matrix C and deriving a linear combination of the output y_e, ensuring that the derivative of this combination is unaffected by the uncertainties, that is,

$$\frac{d}{dt}(CB_1)^{\perp}y_e(t) = (CB_1)^{\perp}C\tilde{A}e(t), \tag{D.4}$$

and construct the extended vector

$$\begin{bmatrix} \frac{d}{dt}(CB_1)^{\perp}y_e \\ y_e \end{bmatrix} = \underbrace{\begin{bmatrix} (CB_1)^{\perp}C\tilde{A} \\ C \end{bmatrix}}_{M} e.$$

Rearranging terms, the following equation is obtained

$$Me = \frac{d}{dt}\begin{bmatrix} (CB_1)^{\perp} & 0 \\ 0 & I_2 \end{bmatrix}\begin{bmatrix} y_e(t) \\ \int y_e(t)dt \end{bmatrix}.$$

Since (A, C, B_2) is strongly observable, the matrix M has full row rank (see Molinari [62]). This implies that the above algebraic equation has an unique solution for $e(t)$, that is

$$e(t) = \frac{d}{dt}\underbrace{M^{+}\begin{bmatrix} (CB_1)^{\perp} & 0 \\ 0 & I \end{bmatrix}\begin{bmatrix} y_e(t) \\ \int y_e(t)dt \end{bmatrix}}_{\theta(t)} \tag{D.5}$$

where $M^{+} := (M^T M)^{-1}M^T$. From the above expression, the reconstruction of $x(t)$ is equivalent to the reconstruction of $e(t)$. Hence, a real time high-order sliding mode differentiator will be used. The HOSM differentiator is given by

$$\begin{aligned}
\dot{z}_0 &= -\lambda_k \Gamma^{\frac{1}{k+1}}|z_0 - \theta|^{\frac{k}{k+1}}\,\mathrm{sign}(z_0 - \theta) + z_1 \\
\dot{z}_1 &= -\lambda_{k-1} \Gamma^{\frac{1}{k}}|z_1 - \dot{z}_0|^{\frac{k-1}{k}}\,\mathrm{sign}(z_1 - \dot{z}_0) + z_2 \\
&\vdots \\
\dot{z}_{k-1} &= -\lambda_1 \Gamma^{\frac{1}{2}}|z_{k-1} - \dot{z}_{k-2}|^{\frac{1}{2}}\,\mathrm{sign}(z_{k-1} - \dot{z}_{k-2}) + z_k \\
\dot{z}_k &= -\lambda_0 \Gamma\,\mathrm{sign}(z_k - \dot{z}_{k-1}).
\end{aligned} \tag{D.6}$$

The values of the parameters $\lambda_0, \lambda_1, \ldots, \lambda_k$ are chosen separately by recursive methods provide for the convergence of the $(k-1)$th-order differentiator commonly obtained by computer simulation [53], obtaining a finite-time T such that the identity

$$z_i(t) = \frac{d^i\theta(t)}{dt^i} \tag{D.7}$$

holds for every $i = 0, 1, \ldots, k$. The parameter Γ is a Lipschitz constant of $\ddot{\theta}(t)$, which is defined as

$$\Gamma \leq \|\tilde{A}\|e^{+} + \|B\|w^{+}. \tag{D.8}$$

The vector $e(t)$ can be reconstructed from the first order sliding dynamics. Thus, we achieve the identity $z_1(t) = e(t)$, and consequently

$$\hat{x}(t) := z_1(t) + \tilde{x}(t) \text{ for all } t \geq T$$

where $\hat{x}(t)$ represents the estimated value of $x(t)$. Therefore, the identity

$$\hat{x}(t) \equiv x(t), \tag{D.9}$$

is achieved for all $t \geq T$.

Definition D.2 ([63]). Given the system:

$$\dot{x}(t) = Ax(t) + Bu(t), \quad y(t) = Cx(t) \qquad x(0) = x_0, \tag{D.10}$$

the invariant zeros of the above system are the set of all the eigenvalues λ such that

$$\begin{bmatrix} \lambda - A & B \\ C & 0 \end{bmatrix} \begin{bmatrix} x \\ u \end{bmatrix} = \begin{bmatrix} 0 \\ 0 \end{bmatrix} \tag{D.11}$$

as a solution for some scalar u and non-zero x.

References

1. Aguilar, L., Boiko, I., Fridman, L., Iriarte, R.: Generating self-excited oscillations via two-relay controller. IEEE Trans. Autom. Control **54**(2), 416–420 (2009)
2. Albea, C., Canudas de Wit, C., Gordillo, F.: Adaptive control of the boost DC-AC converter. In: Proceedings of the IEEE International Conference on Control Applications, pp. 611–616. Singapore (2007)
3. Albea, C., Gordillo, F., Canudas de Wit, C.: Adaptive control design for a boost inverter. Control Eng. Pract. **19**, 32–44 (2011)
4. Appleton, E.: Automatic synchronization of triode oscillators. Proc. Camb. Philos. Soc. **21**(3), 231 (1923)
5. Arimoto, S.: Control Theory of Non-linear Mechanical Systems: A Passivity-Based and Circuit-Theoretic Approach. Oxford Engineering Science Series. Oxford University Press, Oxford (1996)
6. Astashev, V.K., Korendyasev, G.K.: Thermomechanical model of cutter selfoscillation in perpendicular free cutting. J. Mach. Manuf. Reliab. **41**(6), 3–10 (2012)
7. Åström, K., Block, D., Spong, M.: The Reaction Wheel Pendulum. Lecture Notes for the Reaction Wheel Pendulum (Part of the Mechatronics Control Kit). Morgan & Claypool Publisher, San Rafael (2001)
8. Atherton, D.: Nonlinear Control Engineering–Describing Function Analysis and Design. Van Nostrand, Wokingham (1975)
9. Bejarano, F., Fridman, L.: High order sliding mode observer for linear systems with unbounded unknown inputs. Int. J. Robust Nonlinear Control **9**, 1920–1929 (2010)
10. Berkemeier, M., Fearing, R.: Tracking fast inverted trajectories of the underactuated acrobot. IEEE Trans. Robot. Autom. **15**(4), 740–750 (1999)
11. Best, R.: Phase-Locked Loops: Design, Simulation, and Application, 4th edn. McGraw-Hill, New York (1999)
12. Block, D., Astrom, K., Spong, M.: The Reaction Wheel Pendulum. Synthesis Lectures on Control and Mechatronics #1. Morgan & Claypool Publisher, San Rafael (2007)
13. Boiko, I.: Oscillations and transfer properties of relay servo systems – the locus of a perturbed relay system approach. Automatica **41**, 677–683 (2005)
14. Boiko, I.: Discontinuous Control Systems: Frequency-Domain Analysis and Design. Birkhäuser, Boston (2009)
15. Boiko, I., Fridman, L.: Analysis of chattering in continuous sliding-mode controllers. IEEE Trans. Autom. Control **50**(9), 1442–1446 (2005)
16. Boiko, I., Fridman, L.: Frequency domain analysis of second order sliding modes. In: Advances in Variable Structure and Sliding Mode Control, pp. 125–142. Springer, Berlin (2006)

L.T. Aguilar et al., *Self-Oscillations in Dynamic Systems*, Systems & Control: Foundations & Applications, DOI 10.1007/978-3-319-23303-1

17. Boiko, I., Fridman, L., Castellanos, M.: Analysis of second-order sliding-mode algorithms in the frequency domain. IEEE Trans. Autom. Control **49**(4), 946–950 (2004)
18. Boiko, I., Fridman, L., Pisano, A., Usai, E.: Analysis of chattering in systems with second-order sliding modes. IEEE Trans. Autom. Control **52**(11), 2085–2102 (2007)
19. Cáceres, R., Barbi, I.: A boost DC–AC converter: analysis, design, and experimentation. IEEE Trans. Power Electron. **14**(1), 134–141 (1999)
20. Canudas de Wit, C., Espiau, B., Urrea, C.: Orbital stabilization of underactuated mechanical systems. In: Proceedings of the 15th IFAC World Congress. Barcelona (2002)
21. Cardon, S., Iberall, A.: Oscillations in biological systems. Biosystems **3**(3), 237–249 (1970)
22. Chen, F., Liang, T., Lin, R., Chen, J.: A novel self-oscillating, boos-derived DC–DC converter with load regulation. IEEE Trans. Power Electron. **20**(1), 65–74 (2005)
23. Chevallereau, C., Abba, G., Aoustin, Y., Plestan, E., Canudas-de-Wit, C., Grizzle, J.: Rabbit: a testbed for advanced control theory. IEEE Control. Syst. Mag. **23**(5), 57–79 (2003)
24. Choukchou-Braham, A., Cherki, B., Djemaï, M., Busawon, K.: Analysis and Control of Underactuated Mechanical Systems. Springer, Cham (2014)
25. Craig, J.: Introduction to Robotics: Mechanics and Control. Addison-Wesley Publishing, Massachusetts (1989)
26. di Bernardo, M., Budd, C., Champneys, A., Kowalczyk, P.: Piecewise-Smooth Dynamical Systems: Theory and Applications. Applied Mathematical Sciences, vol. 163. Springer, London (2008)
27. Epstein, I.R.: Nonlinear oscillations in chemical and biological systems. Physica D: Nonlinear Phenomena **51**(1–3), 152–160 (1991)
28. Estrada, A., Fridman, L.: Exact compensation of unmatched perturbation via quasi-continuous HOSM. In: 47th IEEE Conference on Decision and Control, pp. 2202–2207. Cancún (2008)
29. Estrada, A., Fridman, L.: Quasi-continuous HOSM control for systems with unmatched perturbations. Automatica **46**(11), 1916–1919 (2010)
30. Fantoni, I., Lozano, R.: Nonlinear Control for Underactuated Mechanical Systems. Springer, London (2001)
31. Fendrich, O.: Describing functions in limit cycles. IEEE Trans. Autom. Control **37**(4), 486–488 (1992)
32. Ferreira, A., Bejarano, F.J., Fridman, L.: Robust control with exact uncertainties compensation: with or without chattering? IEEE Trans. Control Syst. Technol. **19**(5), 969–975 (2011)
33. Ferreira, A., Rios, H., Rosales, A.: Robust regulation for a 3-DOF helicopter via sliding-mode observation and identification. J. Frankl. Inst. **349**(2), 700–718 (2012)
34. Filippov, A.: Differential Equations with Discontinuous Right-Hand Sides. Kluwer Academic Publisher, Dordrecht (1988)
35. Fradkov, A., Pogromsky, A.: Introduction to Control of Oscillations and Chaos. Series on Nonlinear Science, vol. 35. World Scientific, Singapore (1998)
36. Fridman, L.: An averaging approach to chattering. IEEE Trans. Autom. Control **46**(8), 1260–1265 (2001)
37. Fridman, L.: Slow periodic motion in variable structure systems. Int. J. Syst. Sci. **33**(14), 1145–1155 (2002)
38. Fridman, L.: Slow periodic motions with internal sliding modes in the singularly perturbed relay systems. Int. J. Control. **75**(7), 524–537 (2002)
39. Gelb, A., Velde, W.V.: Multiple-Input Describing Functions and Nonlinear Systems Design. McGraw-Hill, New York (1968)
40. Grizzle, J., Abba, G., Plestan, F.: Asymptotically stable walking for biped robots: analysis via systems with impulsive effects. IEEE Trans. Autom. Control **48**(1), 51–64 (2001)
41. Grizzle, J., Moog, C., Chevallereau, C.: Nonlinear control of mechanical systems with an unactuated cyclic variable. IEEE Trans. Autom. Control **50**(5), 559–576 (2005)
42. Hamel, B.: Contribution a l'etude mathematique des systemes de reglage par tout-ou-rien, C.E.M.V. Service Technique Aeronautique **17** (1949)
43. Hara, Y., Jahan, R.A.: Activation energy of aggregation-disaggregation self-oscillation of polymer chain. Int. J. Mol. Sci. **13**, 16281–16290 (2012)

44. Hsu, J., Meyer, A.: Modern Control Principles and Applications. McGraw Hill, New York (1968)
45. Hurmuzlu, Y., Génot, F., Brogliato, B.: Modeling, stability and control of biped robots—a general framework. Automatica **40**, 1647–1664 (2004)
46. Isidori, A.: Nonlinear Control Systems: An Introduction. Springer, Berlin (1989)
47. Isidori, A.: Nonlinear Control Systems, 3rd edn. Springer, London (1995)
48. Kelly, R., Llamas, J., Campa, R.: A measurement procedure for viscous and coulomb friction. IEEE Trans. Instrum. Meas. **49**(4), 857–861 (2000)
49. Khalil, H.: Nonlinear Systems, 3rd edn. Prentice Hall, Upper Saddle River (2002)
50. Koenig, D.R., Weig, E.M.: Voltage-sustained self-oscillation of a nano-mechanical electron shuttle. Appl. Phys. Lett. **101**(213111), 1–5 (2012)
51. Lai, J.: Power conditioning circuit topologies: power conversion from low-voltage dc to high-voltage ac for single-phase grid-tie applications. IEEE Ind. Electron. Mag. **3**(2), 24–34 (2009)
52. Lee, H., Kim, Y., Jeon, H.: On the linearization via restricted class of dynamic feedback. IEEE Trans. Autom. Control **45**(7), 1385–1391 (2000)
53. Levant, A.: High-order sliding modes: differentiation and output feedback control. Int. J. Control **76**(11), 924–941 (2003)
54. Levant, A.: High-order sliding mode controllers. IEEE Trans. Autom. Control **50**(11), 1812–1816 (2005)
55. Levant, A.: Chattering analysis. IEEE Trans. Autom. Control **55**(6), 1380–1389 (2010)
56. Lin, A.T., Lin, C.: Peniotron forward wave self-oscillations. Appl. Phys. Lett. **64**(9), 1088–1090 (1994)
57. Loeb, J.: Frequency response. In: Advances in Nonlinear Servo Theory, pp. 260–268. The Macmillan Company, New York (1956)
58. Mancini, R.: Op Amps For Everyone: Design Reference. Texas Instruments, Dallas (2002)
59. Martínez-Salamero, L., Valderrama-Blavi, H., Giral, R., Alonso, C., Estibals, B., Cid-Pastor, A.: Self-oscillating DC-to-DC switching converters with transformer characteristics. IEEE Trans. Aerosp. Electron. Syst. **41**(2), 710–716 (2005)
60. Melkikh, A.V., Dolgirev, Y.E.: Self-oscillations in oscillating heat pipes. High Temp. **44**(4), 542–547 (2006)
61. Meza, M., Aguilar, L., Shiriaev, A., Freidovich, L., Orlov, Y.: Periodic motion planning and nonlinear H_∞ tracking control of a 3-DOF underactuated helicopter. Int. J. Syst. Sci. **42**(5), 829–838 (2011)
62. Molinari, B.P.: A strong controllability and observability in linear multivariable control. IEEE Trans. Autom. Control **21**, 761–764 (1976)
63. Morris, K., Rebarber, R.: Invariant zeros of siso infinite-dimensional systems. Int. J. Control **83**(12), 2573–2579 (2010)
64. Neĭmark, Y.: The Method of Point Transformations in the Theory of Nonlinear Oscillations. Nauka, Moscow (1972)
65. Oh, S., Pathak, K., Agrawal, S., Pota, H., Garratt, M.: Approaches for a tether-guided landing of an autonomous helicopter. IEEE Trans. Robot. **22**(3), 536–544 (2006)
66. Olivier, J.C., Le Claire, J.C., Loron, L.: An efficient switching frequency limitation process applied to high dynamic voltage supply. IEEE Trans. Power Electron. **23**(1), 153–162 (2008)
67. Orlov, Y.: Discontinuous Systems: Lyapunov Analysis and Robust Synthesis Under Uncertain Conditions. Springer, London (2009)
68. Orlov, Y., Riachy, S., Floquet, T., Richard, J.: Stabilization of the cart-pendulum system via quasi-homogeneous switched control. In: Proceedings of the 2006 International Workshop on Variable Structure Systems, pp. 139–142. Alghero (2006)
69. Orlov, Y., Aguilar, L., Acho, L., Ortiz, A.: Asymptotic harmonic generator and its application to finite time orbital stabilization of a friction pendulum with experimental verification. Int. J. Control **81**(2), 227–234 (2008)
70. Plestan, F., Grizzle, J., Westervelt, E., Abba, G.: Stable walking of a 7-DOF biped robot. IEEE Trans. Robot. Autom. **19**(4), 653–668 (2003)
71. Quanser: 3D helicopter system with active disturbance. Techical report (2004)

72. Rabinovich, M.I.: Self-oscillations of distributed systems. Radiophys. Quantum Electron. **17**(4), 361–385 (1974)
73. Raptis, I., Valavanis, K., Vachtsevanos, G.: Linear tracking control for small-scale unmanned helicopters. IEEE Trans. Control Syst. Technol. **20**(4), 995–1009 (2012)
74. Robinett, III, R., Wilson, D.: What is a limit cycle? Int. J. Control **81**(12), 1886–1900 (2008)
75. Romanov, Y.A., Romanova, Y.Y.: Self-oscillations in semiconductor superlattices. J. Exp. Theor. Phys. **91**(5), 1033–1045 (2000)
76. Sanchis, P., Ursua, A., Gubia, E., Marroyo, L.: Buck-boost DC-AC inverter for a new control strategy. In: 35th Annual IEEE Power Electronics Specialist Conference, pp. 3994–3998. Aachen (2004)
77. Sanchis, P., Ursæa, A., Gubia, E., Marroyo, L.: boost DC–AC inverter: a new control strategy. IEEE Trans. Power Electron. **20**(2), 343–353 (2005)
78. Santiesteban, R., Floquet, T., Orlov, Y., Riachy, S., Richard, J.: Second order sliding mode control for underactuated mechanical system II: orbital stabilization of an inverted pendulum with application to swing up/balancing control. Int. J. Robust Nonlinear Control **18**(4–5), 544–556 (2008)
79. Sastry, S.: Nonlinear Systems: Analysis, Stability, and Control. Springer, New York (1999)
80. Shiriaev, A., Perram, J., Canudas-de-Wit, C.: Constructive tool for orbital stabilization of underactuated nonlinear systems: virtual constraint approach. IEEE Trans. Autom. Control **50**(8), 1164–1176 (2005)
81. Shiriaev, A., Freidovich, L., Robertsson, A., Sandberg, A.: Virtual-holonomic-constraints-based design stable oscillations of furuta pendulum: theory and experiments. IEEE Trans. Robot. **23**(4), 827–832 (2007)
82. Shiriaev, A., Freidovich, L., Manchester, I.: Can we make a robot ballerina perform a pirouette? orbital stabilization of periodic motions of underactuated mechanical systems. Annu. Rev. Control. **32**(2), 200–211 (2008)
83. Shiriaev, A., Freidovich, L., Gusev, S.: Transverse linearization for controlled mechanical systems with several passive degrees of freedom. IEEE Trans. Autom. Control **55**(4), 893–906 (2010)
84. Shtessel, Y., Edwards, C., Fridman, L., Levant, A.: Sliding Mode Control and Observation. Birkhäuser, Boston (2013)
85. Spong, M., Vidyasagar, M.: Robot Dynamics and Control. Wiley, New York (1989)
86. Trentelman, H., Stoorvogel, A., Hautus, M.: Control Theory for Linear Systems. Springer, London (2001)
87. Tsypkin, Y.: Relay Control Systems. Cambridge University Press, Cambridge (1984)
88. Utkin, V.: Sliding Modes in Control Optimization. Springer, Berlin (1992)
89. Utkin, V., Guldner, J., Shi, J.: Sliding Mode Control in Electromechanical Systems. CRC Press, Boca Raton (1999)
90. Varigonda, S., Georgiou, T.: Dynamics of relay relaxation oscillators. IEEE Trans. Autom. Control **46**(1), 65–77 (2001)
91. Weldon, J., Alemán, B., Sussman, A., Gannett, W., Zettl, A.: Sustained mechanical self-oscillations in carbon nanotubes. Nano Lett. **10**, 1728–1733 (2010)
92. Westerberg, S., Mettin, U., Shiriaev, A., Freidovich, L., Orlov, Y.: Motion planning and control of a simplified helicopter model based on virtual holonomic constraints. In: Proceedings of the 14th International Conference on Advanced Robotics, pp. 1–6. Munich (2009)
93. Wiggins, S.: Introduction to Applied Nonlinear Dynamical Systems and Chaos. Text in Applied Mathematics, 2nd edn. Springer, New York (2000)
94. Youssef, M., Jain, P.: A novel single stage AC–DC self-oscillating series-parallel resonant converter. IEEE Trans. Power Electron. **21**(6), 1735–1744 (2006)
95. Zheng, B., Zhong, Y.: Robust attitude regulation of a 3-DOF helicopter benchmark: theory and experiments. IEEE Trans. Ind. Electron. **58**(2), 660–670 (2011)

Index

Symbols
3-DOF helicopter, 109

A
actuator dynamics, 116
asymptotic stability, 72

B
biological systems, 2
biped robots, 1
Bode plot, 7

C
chatter smoothing, 142
chattering, 2
chemical processes, 2
comparison Lemma, 75
Coulomb friction, 92, 97, 137

D
describing function (DF), vii, viii, 2–5, 7, 8, 14, 15, 19–25, 28, 29, 36, 37, 91, 92, 95, 97, 99, 102, 103, 109, 112, 137
double integrator, 4, 9, 10, 14, 15, 109

E
equivalent gain, 141, 142

F
finite-time convergence, 75
fixed point, 41, 46, 49, 54–56, 71
Fixed-Phase Loop, 121, 127
frequency-domain approach, 2
Furuta pendulum, 92

H
harmonic balance equation, 5, 22
homoclinic orbit, 91

I
inertia wheel pendulum (IWP), 30, 31, 35, 36, 46, 61, 69, 76, 80, 85, 87
invariant zeros, 85

L
Lagrange equation, 43, 91
limit cycles, 1, 46, 52, 147
linearization, 31
linearized-Poincaré-map, 62
LPRS, viii, 3, 4, 15, 16, 53–57, 61, 62, 64, 82, 84, 88, 91, 92, 95, 97

M
marginally stable system, 5

N
non-minimum-phase systems, 91
nuclear systems, 2
Nyquist plot, 8, 22

L.T. Aguilar et al., *Self-Oscillations in Dynamic Systems*, Systems & Control: Foundations & Applications, DOI 10.1007/978-3-319-23303-1

O
orbital asymptotic stability, 4, 24, 46, 64, 98, 121, 122, 148
orbital stability, 24
orbital stabilization, 1, 2
orbitally exponentially stable, 64
orbitally unstability, 148

P
periodic orbit, 147
periodic solution, 139
phase crossover frequency, 12
Poincaré map based design, viii, 2, 4, 15, 39, 40, 43, 52, 53, 64, 67, 70, 78, 80
Poincaré maps, 2, 15, 39–41, 46, 52, 147

Q
quasi-continuous (HOSM), 76

R
robustification, 69

S
self-excited oscillations, 5
single-relay system, 139
solid-state electronics, 2
state-space approach, 2
strongly observable, 150

T
Taylor linearization, 92
tracking control, 69
tracking control using HOSM, 76
tracking external signals, 11
transverse surface, 147
twisting tracking controller, 71
two-relay controller (TRC), vii, 2–4, 14, 15, 19–22, 24, 26, 28, 30, 33, 37, 39, 40, 43, 46, 52–54, 57, 61, 62, 64, 67, 68, 70, 71, 79–82, 84, 88, 91, 92, 97, 99, 102, 104, 105, 107, 109, 112, 115, 122, 123

U
underactuated system, 19, 91
underactuation degree, 31
unknown input observer, 85
unknown inputs, 81
unknown inputs identification, 82, 83

V
Van der Pol equation, 3, 6
variable structure controller, 21
virtual constraints, 3
virtual control, 76
viscous friction, 69

Z
zero dynamics, 31, 70, 91